Scuola di Dottorato di Ricerca in Ingegneria Industriale
Indirizzo Ingegneria Chimica
Ciclo XXV

Dipartimento di Ingegneria Industriale
Università degli Studi di Padova

Nicola Gemo

ENGINEERING THE CATALYTIC BATCHWISE SYNTHESIS OF H_2O_2 FROM ITS ELEMENTS

Direttore della Scuola: Ch.mo Prof. Paolo Colombo

Coordinatore d'indirizzo: Ch.mo Prof. Alberto Bertucco

Supervisore: Ch.mo Prof. Paolo Canu

Sede Amministrativa: Università degli Studi di Padova

Dipartimento di Ingegneria Industriale (DII)

SCUOLA DI DOTTORATO DI RICERCA IN: Ingegneria Industriale
INDIRIZZO: Ingegneria Chimica
CICLO XXV

ENGINEERING THE CATALYTIC BATCHWISE SYNTHESIS OF H_2O_2 FROM ITS ELEMENTS

Direttore della Scuola: Ch.mo Prof. Paolo Colombo
Coordinatore d'indirizzo: Ch.mo Prof. Alberto Bertucco
Supervisore: Ch.mo Prof. Paolo Canu

Dottorando: Nicola Gemo

Preface

The present work was carried out at the Dipartimento di Principi ed Impianti di Ingegneria Chimica (DIPIC), Università di Padova, between 2009 and 2012. Financial support from the Cariparo Foundation is gratefully acknowledged. This research would not have been possible without the supervision and guidance of Prof. Paolo Canu, to whom my deepest esteem goes. His clever ideas and stimulating scientific discussions were, and still are, sincerely appreciated. Experimental studies were also performed at the Laboratory of Industrial Chemistry and Reaction Engineering, Department of Chemical Engineering at Åbo Akademi University, Finland, under the guidance of Academy Prof. Tapio Salmi, whose support and precious advices were fundamental to this work. Financial support during the period spent in Finland from Åbo Akademi Foundation (Johan Gadolin Scholarship) is gratefully acknowledged.

This project was only possible thanks to the valuable help and advices of many people, particularly: Prof. Jyri-Pekka Mikkola (Åbo Akademi University), Dr. Kari Eränen (Åbo Akademi University), Prof. Francesco Pinna (Università Ca' Foscari, Venezia), Dr. Federica Menegazzo (Università Ca' Foscari, Venezia), Dr. Pierdomenico Biasi (Università di Padova), Prof. Marco Zecca (Università di Padova), Dr. Paolo Centomo (Università di Padova), Dr. Stefano Sterchele (Università di Padova).

I am forever in debt with all my family for their love and infinite, unconditional support throughout the years. In the same spirit, my warmest appreciation goes to all my friends in Italy and up there in the land of ice for the good times together and the better to come.

Last but not least, I would like to thank Sabrina for her immense patience and support.

Abstract

Hydrogen peroxide is a versatile oxidizing agent with several industrial applications. It is also one of "greenest", since its oxidation by-product is only water. The global demand of the peroxide is increasing, due to its recent usage in new large scale oxidation processes, such as the epoxidation of propylene to propylene oxide and the synthesis of caprolactam. Nowadays most of the world production of H_2O_2 is carried out by the anthraquinone autoxidation process. Though very safe (H_2 and O_2 are never in direct contact), the costs related to the high energy consumption for the extraction and purification of the peroxide produced, together with the usage and periodic replacement of toxic and expensive solvents, stimulated the interest in new production paths. Among the several alternatives proposed, the most fascinating one is the direct synthesis (DS) from H_2 and O_2. It is a environmentally friendly process that would be economically profitable for an in-situ production, requiring lower investments and operating costs. During the last thirty years this system has been under intensive study both by industries as well as academia. However, it has not been commercialized yet, mainly because of poor selectivity and safety concerns.

While most of the efforts on improving DS must address the catalyst, there are reaction engineering aspects that deserve attention. DS is frequently carried out in solvents other than water, both to improve H_2 solubility and isolate the undesired product (H_2O). Further, CO_2 is used for safety, H_2 solubility and H_2O_2 stability. However, the lack of information about the solubility of the reagents makes it difficult to develop a realistic kinetic description of the reactions involved in the DS process. Hence, the first step of the research presented herein dealt with solubility measurements, at temperatures in the range 268-288 K and pressures between 0.37 and 3.5 MPa. Measurements were focused on H_2, i.e. the limiting reagent during the reaction. At all conditions investigated a linear relation between hydrogen partial pressure and concentration was observed. Increasing the temperature resulted in an enhanced H_2 solubility at the same H_2 partial pressure. At constant H_2 fugacity, the presence of CO_2 favored the dissolution of hydrogen in the liquid phase. Correlation and generalization of the measurements were provided through an EoS-based thermodynamic model for the estimation of H_2 solubility at reaction conditions.

A batch apparatus for the direct synthesis of hydrogen peroxide was developed, to carry out activity measurements on new catalysts and develop a quantitative model of the kinetics. Hydrogenation, disproportionation and direct synthesis reactions were studied on a commercial 5 wt.% Pd/C catalysts at temperatures in the range 258-313 K and pressure up to 2 MPa. Separate experiments were performed to highlight the role of each reaction. An enhanced H_2O_2 production was obtained adopting different H_2 feeding policies, although selectivity did not exceeded 30%.

A model of the gas bubbling, batch slurry reactor for H_2O_2 direct synthesis was developed. A sensitivity analysis on the mass transfer coefficients excluded any limitations occurring at experimental conditions. Comparable temperature dependence was observed for H_2O production, hydrogenation and disproportionation (activation energies close to 45 kJ mol^{-1}), while H_2O_2 synthesis had a much lower activation energy (close to 24 kJ mol^{-1}), suggesting that a higher selectivity is achievable at low temperature. Disproportionation reaction had a very limited influence on the overall peroxide production rate, while hydrogenation was the most rapid side reaction. Water formation was significant, prevailing at higher temperatures.

Following these results, Pd and PdAu catalysts supported on SBA15 were prepared and investigated for H_2O_2 direct synthesis. Catalysts were doped with bromine, a promoter in the H_2O_2 direct synthesis. Productivity and selectivity decreased when bromine was incorporated in the catalysts, suggesting a possible poisoning due to the grafting process. A synergetic effect between Pd and Au was observed both in presence and absence of bromopropylsilane grafting on the catalyst. Three modifiers of the SBA15 support (Al, CeO_2 and Ti) were chosen to elucidate the influence of the surface properties on metal dispersion and catalytic performance. Higher productivity and selectivity were achieved incorporating Al into the SBA15 framework, whereas neither Ti nor CeO_2 improved H_2O_2 yields. The enhanced performance observed for the PdAu/Al-SBA15 catalysts was attributed to the increased number of Brønsted acid sites.

Supported catalysts were also synthesized depositing Pd on a highly acidic, macroporous PS-DVB resin (Lewtit K2621). Catalysts with active metal content in the range 0.3-5 wt.% were tested batchwise for the direct synthesis of H_2O_2. Preliminary H_2O_2 measurements and X-ray photoelectron spectroscopy (XPS) analysis revealed that the reduced form of Pd was more selective than PdO towards the peroxide. Transmission electron microscopy (TEM) images

showed that smaller nanoclusters favored the production of H_2O, likely due to their O-O bond breaking aptitude.

Sommario

Il perossido di idrogeno è un potente agente ossidante, molto usato nella pratica industriale. E' uno dei meno tossici, dal momento che l'unico sottoprodotto della sua ossidazione è l'acqua. A livello mondiale, la domanda di H_2O_2 è in costante aumento, non da ultimo grazie a recenti usi in nuovi processi ossidativi, quali l'epossidazione del propilene e la sintesi del caprolattame. Attualmente l'acqua ossigenata viene prodotta quasi esclusivamente attraverso l'auto-ossidazione dell'antrachinone. Sebbene molto sicuro (non vi è mai contatto diretto tra idrogeno ed ossigeno), questo processo presenta alcuni svantaggi, quali ad esempio gli alti costi di esercizio, dovuti in particolare all'alta richiesta energetica per la separazione e la purificazione del perossido prodotto. Si tratta inoltre di un processo potenzialmente inquinante, in quanto fa uso di costosi solventi tossici, e dagli alti costi d'investimento, essendo economicamente vantaggioso solo per grandi produzioni ($>4*10^4$ tonnellate all'anno). Pertanto l'H_2O_2 è attualmente prodotta in pochi grandi impianti e trasferita per grandi distanze all'utente finale. Il trasporto aggiunge costi e rischi, in quanto soluzioni concentrate di H_2O_2 possono decomporre violentemente. Nelle ultime decadi vi è stato un notevole interesse nella ricerca di nuovi processi di produzione del perossido di idrogeno, che fossero contemporaneamente meno costosi ed inquinanti. Tra le varie alternative proposte, la più affascinante è sicuramente la sintesi diretta a partire da H_2 ed O_2. Si tratta di un processo "verde", che si propone di eliminare i sottoprodotti inquinanti e, allo stesso tempo, ridurre i costi di produzione, rendendo economicamente vantaggiosa la produzione in situ presso l'utilizzatore finale. Nonostante il grande interesse sia industriale che accademico suscitato da tale processo negli ultimi trent'anni, a tutt'oggi non vi è nessuna applicazione industriale. Il motivo di ciò è da ricercarsi principalmente nei problemi di sicurezza e selettività che a tutt'ora restano irrisolti.

La mancanza di informazioni sulla solubilità dei reagenti alle condizioni di reazione rende difficoltoso ottenere una descrizione cinetica precisa delle reazioni coinvolte nella sintesi diretta. Pertanto i primi passi della ricerca qui presentata sono stati mossi con l'obiettivo di raccogliere dati di solubilità alle condizioni di reazione (temperatura compresa tra i 268 e i 288 K e pressione tra 0.37 e 3.5 MPa). In particolare, si era interessati all'H_2, in quanto reagente limitante del processo. A tutte le condizioni indagate, è stata riscontrata una

relazione lineare tra la pressione parziale e la concentrazione di H_2. Contrariamente a quanto normalmente avviene, l'incremento di temperatura ha avuto l'effetto di aumentare la solubilità nella fase liquida (a parità di pressione parziale). Inoltre, a parità di fugacità di H_2, la presenza di CO_2 ha favorito la concentrazione dell'H_2 nel liquido. I risultati ottenuti sono stati generalizzati sviluppando un modello per stimare la solubilità dell'H_2 alle condizioni di reazione.

E' stato poi realizzato un apparato batch per la sintesi diretta di acqua ossigenata. Un catalizzatore commerciale a base di Pd (5 wt.%) su carbone è stato utilizzato per studiare le reazioni di idrogenazioni, dismutazione e sintesi a temperature comprese tra 258 e 313 K e pressioni fino a 2.0 MPa. Il ruolo di ciascuna reazione è stato studiato attraverso esperimenti specifici. Appropriate politiche di alimentazione dell'H_2 hanno permesso di realizzare un aumento di produzione rispetto a condizioni tipicamente batch. Tuttavia il catalizzatore testato ha rivelato limiti di selettività, non superando valori del 30% ca.

Per studiare le cinetiche di reazione, è stato sviluppato un modello per il reattore batch. Un'analisi di sensitività sui coefficienti di trasporto di materia (sia dalla fase gassosa alla liquida che dalla liquida al catalizzatore) ha permesso di escludere ogni limitazione tra le fasi coinvolte nelle reazioni. Le reazioni indesiderate (formazione di H_2O, dismutazione ed idrogenazione) hanno rivelato una simile dipendenza dalla temperatura (con un'energia di attivazione di circa 45 kJ mol^{-1}). Una minore energia di attivazione è stata ottenuta per la reazione di sintesi diretta di H_2O_2 (24 kJ mol^{-1}), il che suggerisce che la selettività è favorita alle basse temperature. Un confronto tra le velocità delle reazioni coinvolte ha permesso di identificare la dismutazione come la reazione più lenta di distruzione del perossido. Inoltre, la formazione di acqua era sempre significativa, compromettendo la selettività.

A seguito di questi risultati, si è deciso di focalizzare l'attenzione sul catalizzatore. Catalizzatori mono e bi-metallici sono stati realizzati depositando Pd e PdAu su SBA15, una silice macroporosa e strutturata. Tali catalizzatori sono stati anche dopati con l'aggiunta di bromo, un noto promotore della reazione di sintesi diretta. Sia la selettività che la produttività sono diminuite modificando i catalizzatori con l'alogenio, probabilmente a causa di un avvelenamento durante la procedura di innesto del bromo. Una sinergia tra i metalli Pd e Au è stata osservata sia nei catalizzatori con e che senza bromo. Tre modifiche sono state apportate al miglior catalizzatore sviluppato (PdAu/SBA15) per evidenziare l'influenza delle proprietà superficiali sulla reazione di sintesi diretta. Tre modificatori sono stati incorporati nel

supporto: Al, CeO_2 e Ti. Un aumento sia di selettività che di produttività è stato riscontrato solo con l'aggiunta di Al. Tale risultato è stato attribuito al maggior numero di siti acidi di Brønsted riscontrati su questo catalizzatore.

Un'altra famiglia di catalizzatori, con un contenuto di metallo attivo variabile tra lo 0.3 ed il 5 wt.%, è stata sintetizzata depositando del Pd su una resina acida e macroporosa, miscela di PS e DVB. I risultati preliminari dei test catalitici e delle analisi di spettroscopia fotoelettronica a raggi X (XPS) hanno rivelato che lo stato di ossidazione del palladio più selettivo verso il perossido è quello ridotto, mentre il PdO porta più facilmente alla formazione di H_2O. Le immagini al microscopio elettronico a trasmissione (TEM) hanno mostrato che i nanocluster di Pd più piccoli portato alla formazione preferenziale di H_2O, il che è probabilmente legato alla loro propensione alla rottura del legame O-O.

List of publications

The thesis consists of an extended summary and the following publications for a detailed description of the work. Throughout the text, the publications are referred to by their roman numbers.

I. Gemo, N.; Biasi, P.; Salmi, T. O.; Canu, P. H_2 solubility in methanol in the presence of CO_2 and O_2. *The Journal of Chemical Thermodynamics* **2012***, 0,* 1-9.

II. Biasi, P.; Gemo, N.; Hernández Carucci, J. R.; Eränen, K.; Canu, P.; Salmi, T. O. Kinetics and Mechanism of H_2O_2 Direct Synthesis over a Pd/C Catalyst in a Batch Reactor. *Industrial and Engineering Chemistry Research* **2012***, 26,* 8903-8912.

III. Gemo, N.; Biasi, P.; Canu, P.; Salmi, T. O. Mass transfer and kinetics of H_2O_2 direct synthesis in a batch slurry reactor. *Chemical Engineering Journal* **2012***, 0,* 539-551.

IV. Gemo, N.; Biasi, P.; Canu, P.; Menegazzo, F.; Pinna, F.; Samikannu, A.; Kordás, K.; Salmi, T. O.; Mikkola, J. P. Reactivity aspects of SBA15-based doped supported catalysts: H_2O_2 direct synthesis and disproportionation reactions. *Topics in Catalysis* (accepted manuscript)

List of related contributions

1. CAMURE-8 (Catalysis in Multiphase Reactors) & ISMR-7 (International Symposium on Multifunctional Reactors), Naantali, Finland, May 22nd – 25th 2011, Oral presentation

2. GLS10 (Gas-Liquid and Gas-Liquid-Solid reactor Engineering), Braga, Portugal, June 26th -29th 2011, Poster presentation

3. APCRE'11 (The 6th Asia Pacific Chemical Reaction Engineering Symposium), Beijing, China, 18th -21st September 2011, participant

4. The 15th Nordic Symposium on Catalysis, Mariehamn, Åland (Finland), 10th – 12th June 2012, Oral presentation

5. ISCRE22 (International Symposium on Chemical Reaction Engineering), Maastricht, The Netherlands, September 2th – 5th 2012, Oral presentation

6. Convegno Nazionale GRICU 2012, "Ingegneria Chimica: dalla macroscala alla nanoscala", Pescara, Italy, 16th- 19th September 2012, Poster presentation

7. Gemo, N.; Sterchele, S.; Biasi, P.; Centomo, P.; Canu, P.; Zecca, M.; Mikkola, J. P; Salmi, T. O. Effect of catalyst quantity and Pd loading on the H_2O_2 synthesis from its elements. (in preparation)

Table of contents

1 Introduction 1

1.1 General 1

1.2 Approaches to the direct synthesis 3

1.3 Catalysts 4

1.4 Reaction kinetics 4

1.5 Research strategy 5

2 Experimental & methods 7

2.1 H_2O_2 direct synthesis experiments 7

2.2 Hydrogen solubility measurements 8

2.3 Catalysts preparation 9

2.4 Catalyst characterizations 10

2.4.1 Nitrogen adsorption and CO chemisorption measurements 10

2.4.2 Surface analysis 11

2.4.3 Induced current plasma - mass spectroscopy (ICP-MS) 11

2.4.4 Acidity measurements 11

2.4.5 Thermogravimetric analysis 11

3 Results and discussion 13

3.1 Hydrogen solubility 13

3.1.1 Modeling 16

3.2 H_2O_2 synthesis: hydrogen feeding policies 20

3.3 Kinetics identification 21

3.3.1 H_2O_2 synthesis, hydrogenation and disproportionation: effect of temperature 21

3.3.2 Modeling 23

3.4 SBA15-based doped supported catalysts 35

3.4.1 Non-ordered and ordered mesoporous Si-based catalysts 35

3.4.2 Al, Ti and CeO_2-SBA15 modified catalysts 37

3.5 Pd/K2621 catalysts 39

4 Conclusions 43

5 References 47

6 Publications 57

1 Introduction

1.1 General

Hydrogen peroxide is an attractive, non-polluting oxidizing agent with several industrial applications. It is considered one of the most efficient oxidant by virtue of the high oxygen content and its oxidation potential (1.78 eV), comparable to that of ozone (2.07 eV). It is also one of the greenest since its oxidation by-products comprise water and oxygen only. The current global H_2O_2 production is approximately 2.7 mln tons per year and its demand is increasing by 4% per annum[1]. This growth is mainly due to its recent usage in new large scale oxidation processes (Figure 1.1), such as the epoxidation of propylene to propylene oxide and the synthesis of caprolactam (Sumitomo).

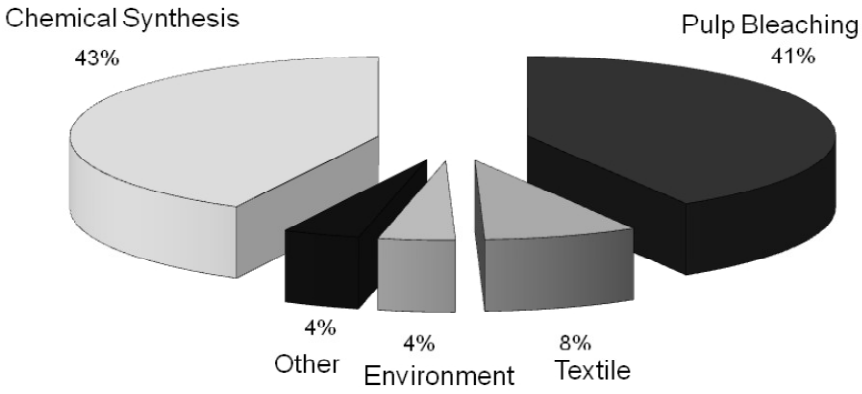

Figure 1.1. Main uses of hydrogen peroxide

H_2O_2 is also widely used in the waste and wastewater treatments, textile, pulp and paper bleaching industries (as an environmentally friendly alternative to chlorine), in mining and processing of metals and in the production of stain free detergents. Large amounts of low concentration H_2O_2 solution are consumed by the cosmetic and pharmaceutical industries for its disinfecting properties, whereas highly pure H_2O_2 is used for etching and purification of electronic materials.

Hydrogen peroxide was first discovered by the French chemist Louis Jacques Thénard in 1818, reacting barium peroxide with nitric acid. Once produced mainly via the electrolysis of

ammonium sulfate, nowadays H_2O_2 is almost exclusively manufactured by the anthraquinone autoxidation process (1936). This process involves a catalytic hydrogenation, followed by an oxidation reaction to yield H_2O_2. Anthraquinone is used as a H_2 carrier to avoid the H_2/O_2 direct contact, so that the process is very safe. However, several drawbacks are involved, such as the use and periodic replacement of toxic and expensive solvents (anthraquinone, ester, hydrocarbons, octanol/methyl-naphthalene) and the high energy cost for the extraction and purification of the H_2O_2 produced. Moreover, it is profitable only for large-scale production. The transportation to the final consumer creates additional costs and safety issues since concentrated H_2O_2 can violently decompose and explode. For all these reasons, in the last decades there have been many efforts to develop cost-effective and greener processes to obtain the peroxide. Different solution were proposed, such as fuel cell technology and H_2/O_2 non-equilibrium plasma reaction. However, the most fascinating alternative to the anthraquinone route is the direct synthesis (DS) from H_2 and O_2. It is an environmentally friendly process (no toxic solvents are required) that would be profitable also for small scale plants, reducing the investments and operating costs for an economically viable in-situ production. During the last thirty years the direct synthesis of hydrogen peroxide has been under intensive study both by industry as well as academia[1-3]. However, despite many efforts, selectivity is still an obstacle to the industrial feasibility. Although the reaction $H_2+O_2 \rightarrow H_2O_2$ is in principle very simple, the complete reaction pathway is more complex (Scheme 1.1).

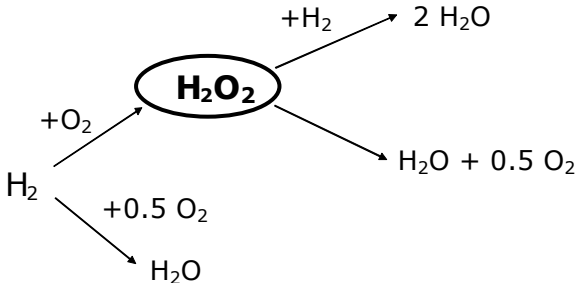

Scheme 1.1. Reactions involved in the direct synthesis of H_2O_2.

All the reactions involved are thermodynamically favored and highly exothermic. Moreover, the contribution of each reaction differs with the conditions (i.e. temperature, pressure, promoters, stabilizers, reactant medium, etc). Two consecutive (hydrogenation and disproportionation) and one parallel reaction (H_2O formation) competing with the selective H_2 oxidation to H_2O_2 are involved. All the undesired reactions are promoted by the same catalyst active for the selective hydrogenation to the peroxide, severely limiting the selectivity. The DS process also imply the direct contact between H_2 and O_2, raising safety concerns[3, 4]. The

flammability limits of H_2 in O_2 are quite narrow (4-94%), so that safe mixtures must be highly diluted. Unfortunately, operations with mixtures outside flammability limits showed a drop of the H_2O_2 production to industrially unacceptable values[2]. For all these reasons, notwithstanding the efforts of several companies (BASF, EniChem S.p.A., Dow Chemical, DuPont, Solvay Interox, Mitsubishi Gas Chemical Co.), the direct synthesis process has yet not been commercialized. The development of this approach for the industrial production of H_2O_2 would be a real breakthrough in the oxidation process technology.

1.2 Approaches to the direct synthesis

H_2O_2 direct synthesis is normally carried out in a three phase system. Basically, hydrogen and oxygen are dissolved in a proper reaction medium (i.e. alcoholic solution or water) and react over a solid catalyst. Since the early 90's, the DS process attracted interests of many research groups, trying to develop new catalyst concepts, reactor design and operation conditions[1, 2, 5-16]. Despite results of different works are difficult to compare, mainly because of the different reaction conditions adopted, a comparison of literature studies can give important insights about the different approaches to the direct synthesis. Batch reactors are usually adopted for catalytic tests[6, 7, 11-13], semi-batch reactors to investigate the operation conditions and enhance the production of H_2O_2[7, 11, 12, 14], membrane reactors and microreactors[5, 10, 17] to operate safely within flammability limits and, therefore, try to enhance both productivity and selectivity.

Methanol is often chosen as the reactant medium[5-8, 11-13], in view of an integration with the propylene oxide synthesis, where the propylene reacts with the hydrogen peroxide in methanol. Water is instead chosen for safety reasons and for its lower cost[9, 10, 14].

Temperatures between -263 and 278 K are suitable to avoid the consecutive reactions (hydrogenation and disproportionation)[6, 13]. Operations at temperatures up to 313 K necessarily require the addition of stabilizers in the reaction medium[9, 14].

An inert gas is usually required to dilute the gas mixture outside flammability limit. At the same time, the inert enhances the total pressure in the system, increasing the rather low solubility of the reagent gases and hence the H_2O_2 production rate. Carbon dioxide is often used for these scopes. Systems involving CO_2-expanded liquids (such as methanol) are a current topic in modern chemical synthesis. Besides advantages due to the mixture physical properties, mainly related to marked modifications of the vapor-liquid equilibrium, CO_2 brings about a reduced impact on environment and minimization of safety issues[4, 18]. Both

homogeneously and heterogeneously[4, 18-20] catalyzed reactions have been tested in CO_2 expanded solvents. Research interest is especially focused on reactions limited by a poor solubility of reactant gas, such as hydrogenations and oxidations, making this gas particularly appealing for the DS process.

1.3 Catalysts

Most of the catalysts for the hydrogen peroxide direct synthesis are based on Pd, supported on a great variety of substrates such as C, SiO_2, ZrO_2 and Al_2O_3[21-24]. Enhanced productivity and selectivity were observed upon addition of a second metal, specifically Au. Although Au-only catalysts are generally less effective then Pd-only catalysts, a synergetic effect was observed combining these two metals[25-33]. An Au-rich core, Pd shell structure was suggested for the Au-Pd nanoclusters, with the Au acting as an electronic promoter for the surface Pd atoms. Other authors[34] proposed that isolated Pd atoms are the most efficient for the H_2O_2 direct synthesis, with Au playing a fundamental role in the isolation of Pd atoms within a gold matrix. Acid are often added to the reaction medium to prevent the hydrogenation/disproportionation reactions. Several papers report the beneficial effect of the H^+ ion in promoting the selectivity towards the peroxide[21, 22, 35-39]. Although different explanation have been proposed[40, 41], including a possible influence on the electronic state of the Pd surface[42], the specific role of the proton remains unclear[2]. Halide are also known to increase the selectivity towards H_2O_2, especially bromide and chlorine[24, 26, 40, 43, 44]. However, highly concentrated acid solutions requires special equipments. Moreover, the presence of proton and halides ions favor the leaching of the active metal, compromising the stability of the catalyst. Solid acid supports are an interesting solution to minimize the presence of inorganic acid in the reaction medium[13, 24, 45, 46].

1.4 Reaction kinetics

Despite numerous studies, a general understanding of the reaction mechanism involved in the DS process has not yet been achieved. The unwanted reactions (Scheme 1.1) could be minimized acting on the operating conditions, in addition to designing a suitable catalyst, but kinetics and mass transfer limitation must be known. Most of the researches concentrate on the catalyst design[7, 32, 47-50], where different metals or combination of metals and supports were studied to minimize the unwanted reactions. However, results are difficult to compare mainly because of the different catalysts and reaction conditions involved. Recently

contributions on the kinetics are growing in the Literature[8, 9, 39, 51, 52]. The main efforts were spent in rationalizing the effect of different reaction conditions on the catalyst and develop models to study the actual mechanism, for further optimization of selectivity and production rate. Still, there is no agreement on the mechanism and conditions favoring the synthesis and the kinetic remains mostly empirical.

1.5 Research strategy

In a context where efforts to develop DS appear to concentrate exclusively on the search for a breakthrough catalyst, we addressed the engineering of the reaction, trying to exploit the potential of the ever improving catalysts.

The determination of H_2 solubility at reaction condition was the starting point of the research. Up to now, the lack of information on vapor-liquid equilibria makes it difficult to obtain a precise kinetic description of this process, where solubility modifications confuse with kinetics. Under H_2 poor conditions, often prevailing in H_2–O_2 mixtures to operate outside the (lower) flammability limit, H_2 solubility is the key information required. In **Publication I**, solubility data for hydrogen in methanol, in CO_2 + CH_3OH and in CO_2 + CH_3OH + O_2 were collected and critically compared with available literature data, in the range $268 < T/K < 288$ and total pressures between 1 and 3.5 MPa (H_2 partial pressure varied between 0 and 1 MPa). A thermodynamic model was also proposed, developing an equation for the estimation of a pseudo Henry constant of H_2.

A proper apparatus was design to study the optimal reaction conditions, as documented in **Publication II**. Methanol was chosen as the reaction medium. CO_2 diluted the H_2/O_2 mixture outside flammability limits. A 5% Pd on carbon catalyst (Evonik) was used both for its commercial availability and for its stable performance. Hydrogenation, disproportionation and direct synthesis experiments were independently carried out to elucidate the role of each reaction. The presence of promoters was deliberately avoided to focus on the catalyst performance solely. Special attention was given to dissolved hydrogen measurements, as they can provide important information on the reaction mechanism. Different H_2 feeding polices were implemented, trying to enhance both the H_2O_2 selectivity and productivity.

A precise kinetic description of the reaction involved in the H_2O_2 direct synthesis is a crucial step for the correct description of the process. **Publication III** deals purely with theoretical speculation on the kinetics and transport limitations. The knowledge gather with the work on

kinetics experiments (**Publication II**) was essential to perform the calculations, together with our previous research on hydrogen solubility (**Publication I**). Extensive modeling was carried out both on direct synthesis, disproportionation and hydrogenation reactions, highlighted in separate experiments. A multiphase reactor model was developed including the influence of transport limitations. The simulations revealed the controlling factors that limits the selective hydrogenation to the peroxide.

The results of the kinetic study encouraged us to investigate the properties of the catalyst to gain more insights on the selectivity performance (**Publication IV**). Monometallic (Pd) and bi-metallic (Pd and Au) catalysts with different surface properties were synthesized and investigated for H_2O_2 direct synthesis. SBA15 mesoporous material was chosen as support because it promotes a high dispersion and stability of metal nanoparticles[11, 48, 53], also acting as a template to control the nanocluster size. Three modifications of the parent SBA15 support material (incorporation of Al, CeO_2 and Ti) were chosen to elucidate the influence of surface properties (such as Brønsted and Lewis acidity) on the metal dispersion and the overall performance of the catalysts. Br-doped catalysts were obtained by grafting bromine on SBA15-based catalysts, so that the presence of the free ions in the solution was avoided.

Catalysts with Pd content in the range 0.3-5 wt.% were synthesis by ion exchange method. A highly acidic, macroporous PS-DVB resin (Lewtit K2621) was adopted as support. Large pore structure and the swelling in polar media facilitate the access of H_2 and O_2 to the active sites, as well as the removal of the peroxide produced. The sulfonic groups in the resin contribute to stabilize the H_2O_2, at the same time avoiding the presence of acid in the reaction environment. Results suggested some interesting features of the catalyst to enhance the selectivity toward the selective hydrogenation to H_2O_2.

2 Experimental & methods

2.1 H_2O_2 direct synthesis experiments

The direct synthesis experiments were carried out in a stainless steel, fixed volume autoclave (Parr Instrument, accessible volume 636 cm^3) equipped with a mechanical stirrer. The apparatus is schematically described in Scheme 2.1.

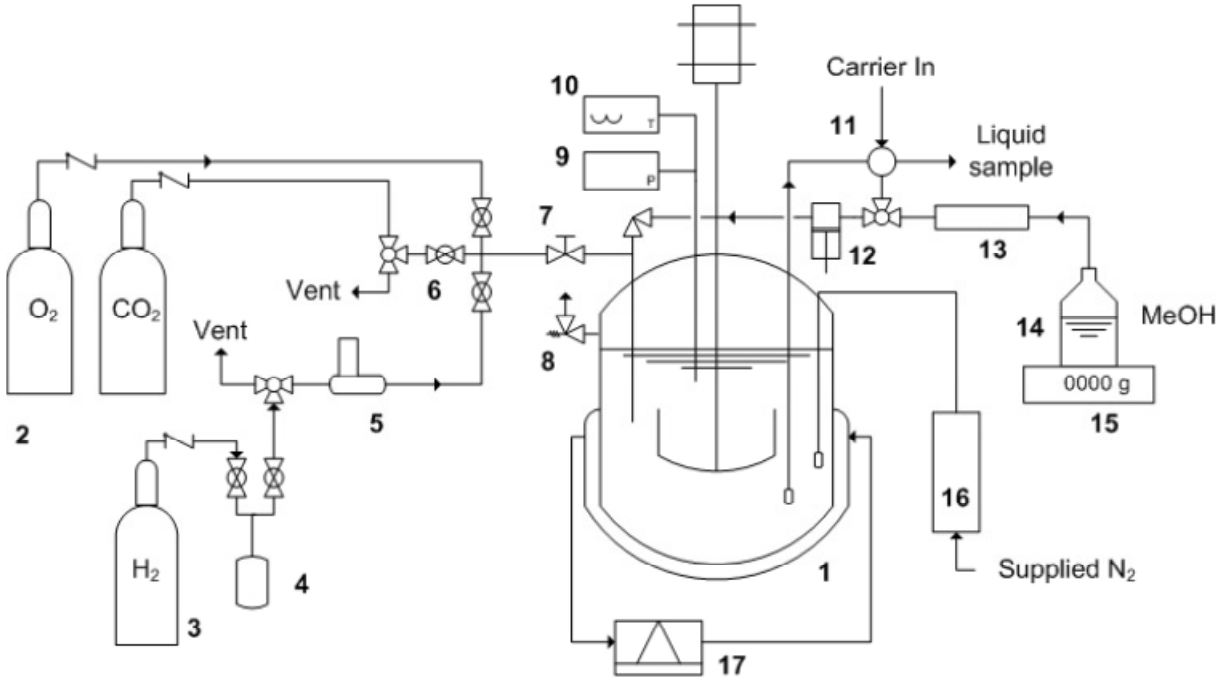

Scheme 2.1. Schematic of the experimental apparatus. 1 – Reactor. 2-3 Gas bottles. 4-5 – Hydrogen vessel and MFC, respectively. 6-7 Valve system for gas loading. 8 – Safety valve. 9-10 Pressure and temperature measurements, respectively. 11 – Liquid sampling valve. 12 - HP pump. 13 – Degasser. 14-15 - Liquid solvent supply and balance, respectively. 16 – Fugatron HYD-100. 17 – Cooling/heating system.

Temperature in the range 258-313 K was controlled with an external flow of heating/cooling fluid and monitored with a thermocouple. Pressure was monitored with a pressure transducer. The reactor was operated batchwise, hydrogen being the limiting reagent. This way it was possible to study the direct synthesis process with a gas mixture always outside flammability limits. In a typical experiment, the catalyst was introduced first. The reactor was then flushed with CO_2 four times to remove air and moisture. Carbon dioxide and oxygen were loaded into the reactor directly from the cylinders, followed by the injection of the methanol via a high

pressure pump. After both pressure and temperature were stable, hydrogen was fed as the limiting reagent. H_2 flow during the introduction was tightly controlled for reproducibility with a mass flow controller. In addition, a constant volume (59 cm^3) vessel was used between the H_2 bottle and the mass flow controller. Loaded with H_2 at a pressure higher than the measuring cell, it double checks the amount of H_2 fed to the reactor, determined from pressure difference inside the H_2 vessel before and after the loading and the quantity fed through the mass flow controller. Methanol was degassed and then introduced in the system via a high pressure pump. Hydrogenation and disproportionation experiments were carried out using N_2 instead of O_2 and H_2, respectively. Liquid samples were withdrawn through an external loop, fitted with a six-way GC valve. The liquid sampling probe was equipped with a 7 μm filter to prevent any block of the sampling valve and pump by small catalyst particles.

Water and H_2O_2 contents were determined by volumetric Karl Fischer and iodometric titration, respectively. Hydrogen dissolved in the liquid phase was measured via an in situ technique, using Fugatron HYD-100. The same instrument was adopted to perform H_2 solubility measurements, as described in the following section.

2.2 Hydrogen solubility measurements

Measurements of hydrogen solubility in binary (H_2 + CH_3OH), ternary (CO_2 + CH_3OH + H_2) and quaternary (CO_2 + CH_3OH + O_2 + H_2) systems were performed in the same apparatus developed for the DS experiments (Scheme 2.1). The external recirculation loop for the liquid phase was removed to perform the measurements. An in situ technique using Fugatron HYD-100 was adopted to measure the hydrogen solubility. The instrument allows continuous, in situ measurements of H_2 solubilized in a liquid phase[54, 55]. It is based on a probe immersed in the liquid phase, with a rigid, dense membrane internally purged with a carrier gas (nitrogen) flowing at 10 Nml min^{-1}. Hydrogen permeates the membrane and is brought to a gas detector by the carrier gas. The instrument has been coupled to gas absorption measurements for calibration, the latter remaining the reference technique used. Comparison between the hydrogen concentration measured via gas absorption technique (C_{H_2}) and reading of the Fugatron instrument provides the calibration constant of the instrument [54], f:

$$f = C_{H_2} / q \qquad 2.1$$

where *q* is the instrument reading, i.e. mole fraction of hydrogen in the carrier gas behind the membrane, reaching the gas detector in the instrument. The calibration constant *f* is indeed quite sensitive to temperature, so that *f(T)* has actually been determined.

Equilibrium configurations at different temperatures, pressures and composition were studied with sequential additions of a given species (H_2, CO_2, and O_2), suitably adjusting the procedure to minimize uncertainties. Whenever compatible with the procedure, methanol was fed last, after each gas, to prevent solubility disturbing the gas quantification by pressure.

2.3 Catalysts preparation

Mesoporous silica SBA15 was synthesized according to a modification of the procedure reported by Zhao et al.[56]. Metal substituted M-SBA15 with Si/M ratio of 25 (where M= Al and Ti) were synthesized by the addition of an appropriate amount of metal precursors. Aluminium isopropoxide and titanium tetraisopropoxide were used as the sources of Al and Ti, respectively. CeO_2 modified SBA15 (20 wt.% theoretical loading) was prepared by means of deposition-precipitation method from the calcined SBA15 material.

PdAu/SBA15 catalyst was synthesized supporting Pd and Au (1:4 mole ratio) on SBA15 by wet impregnation method. $HAuCl_4 \cdot H_2O$ and $PdCl_2$ were used as precursors, added to the solution at the same time. The impregnated catalyst was dried at 378 K overnight and then reduced at 573 K for 8 hours with a 30 ml/min flow of hydrogenwas and then passivated for 24 h under a 2 vol% O_2/N_2 mixture at room temperature. The final metal content observed was 0.3 wt% of Pd and 2.2 wt% of Au, respectively. The synthesis of two Pd/SBA15 (0.3 and 2.5 wt.%) catalysts was carried out following the same procedure, but impregnating the support with Pd only. The active metals were supported on M-SBA15 (M = Al, Ti and CeO_2) also by impregnation method.

Modified mono and bi-metallic catalysts were obtained grafting the reduced form of the original catalysts with 3-bromopropyl-trimethoxy-silane. The active metal contents of the catalysts were 0.19 wt.% and 1 wt.% for Au and Pd, respectively. The catalysts were suspended in dry toluene. Then the 3-bromopropyl-trimethoxy-silane (5 mmol per gram of catalyst) was slowly added to the suspension. The mixture was fluxed at 353 K in inert atmosphere for 24 h. After completion, the catalyst was washed with an excess of dry toluene and dried at 373 K for 24 h in air. A PdAu-Br/SBA15 catalyst was prepared reversing the

order of the described procedures, first grafting the support and then impregnating the active metals.

Pd/Si and PdAu/Si catalysts were prepared using a commercial SiO_2 (Akzo, 329 m^2/g of surface area). The support was impregnated by incipient wetness with H_2PdCl_4 and/or $HAuCl_4$ aqueous solutions (addition of the two precursor solutions was simultaneous for the bimetallic catalyst) to give the desired metal loading (0.5 wt.% Pd for Pd/Si and 1.5 wt% Pd and Au for PdAu/Si). Samples were calcined at 773 K in flowing air for 3 hours.

Pd was also supported on a macroporous resin (Lewatit K2621) by ion exchange method. An aqueous solution of the precursor $Pd(NO_3)_2$ and the support was let react overnight. The amount of $Pd(NO_3)_2$ was adjusted to match 0.3, 0.5, 1, 2.5 and 5 wt.% nominal Pd loadings. Less than 0.1 mol% of the initial amount of Pd was found in the mother liquor (ICP-MS analysis), confirming that the metal loading was essentially equal to the nominal value. The synthesized catalysts were reduced in THF under hydrogen flux at room temperature for 5 hours. After recovery by vacuum filtration, the materials were dried in oven at 383 K overnight.

2.4 Catalyst characterizations

2.4.1 Nitrogen adsorption and CO chemisorption measurements

Surface area and pore size distribution measurements were obtained from N_2 adsorption/desorption isotherms at 77 K (using a Carlo Erba Sorptomatic 1900). Prior to the measurements, the samples were outgassed at 573 K for 2 h under vacuum. The surface area was calculated from the N_2 adsorption isotherm by the Brunauer, Emmett, and Teller (BET) equation, and pore size distribution was determined by the Barrett, Joyner, Halenda and Dollimore/Heal method.

CO chemisorption measurements were performed at 298 K with a Micromeritics pulse flow system. Prior to the measurements, samples were subjected to a pretreatment involving exposure to hydrogen flow for 1 h at 298 K , followed by He purge for 2 h at the same temperature of reduction.

2.4.2 Surface analysis

X-ray photoelectron spectroscopy (XPS) analysis were performed in a Perkin-Elmer 5400 ESCA spectrometer with monochromatized Al Kα radiation (photon energy 1486.6 eV) and a pass energy value of 35 eV. Samples were transferred to the XPS system in an ethanol solvent to protect them from oxidation in ambient air. A low energy electron gun (flood gun) was used to stabilize the charging that arises from loss of photoelectrons during X-ray bombardment. FitXPS software by D. Adams, University of Aarhus, was used in the line fitting procedure. Pd 3d lines were found on a non-linear background and parabolic background was used in the line fitting.

Particle size and distribution, as well as the structure of the support, were assessed by energy filtered transmission electron microscopy (EFTEM, LEO 912 OMEGA, LaB6 filament, 120 kV).

2.4.3 Induced current plasma - mass spectroscopy (ICP-MS)

Active metal content in the reaction medium was accessed by a PerkinElmer Sciex ICP Mass Spectrometer Elan 6100 DRC Plus.

2.4.4 Acidity measurements

For selected catalysts, the nature of the acid sites was determined by Fourier transform infrared (FT-IR) spectroscopy of adsorbed pyridine. The analysis were carried out according to literature procedure[57]. Lewis and Brønsted acid sites were calculated from the IR band area at 1450 and 1545 cm^{-1}, respectively. The integrated molar extinction coefficients were assumed as 1.67 cm/μmol for Brønsted acidity and 2.22 cm/μmol for Lewis acidity.

2.4.5 Thermogravimetric analysis

Thermogravimetric analysis (TGA) measurements were carried out on the grafted SBA15-based catalysts. Samples were heated up to 1173 K with a heating rate of 15 K min^{-1} in air. Prior to the analysis, the samples were pretreated in an oven at 393 K for 2h to eliminate the water eventually present. Weight loss during TGA measurements was due to the loss of the organic part carrying the bromine. Hence, bromine content was estimated from the weight loss upon heating.

3 Results and discussion

3.1 Hydrogen solubility

We investigated hydrogen solubility in three different (binary, ternary and quaternary) species combinations: H_2 + CH_3OH, CO_2 + CH_3OH + H_2 and CO_2 + CH_3OH + O_2 + H_2. The quaternary data are completely original, while the other combinations have been already investigated in literature, as well binary combinations of the four species other than H_2 + CH_3OH, that we did not investigate experimentally. Literature data provide the opportunity to calibrate a thermodynamic model (estimation of binary interaction parameters) to correlate ternary and quaternary data, in addition of validating our experimental methods.

H_2 + CH3OH

Figure 3.1 shows hydrogen liquid phase concentrations measured at 278 K.

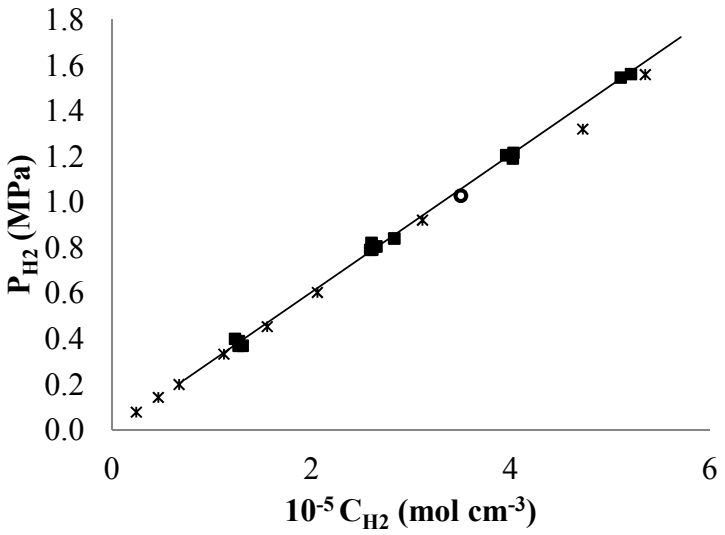

Figure 3.1. CH_3OH + H_2 binary system. Concentration of hydrogen in liquid methanol as a function of its partial pressure above the liquid, at 278 K. ■, this work; *, Descamps et al.[58]; ○, calculated from data of Katayama et al[59].

Plotting experimental C_{H_2} against P_{H_2} allows determining the average Henry's constant as the slope of the resulting linear interpolating function (i.e. Henry's law, $C_{H_2} = H_{H_2} \cdot P_{H_2}$), including

the origin for physical consistency. The determined value of the Henry's constant is 30.14 ± 1.02 (MPa m^3 $kmol^{-1}$), where the error is one standard deviation of the error between calculated H_{H_2} and individual values. This value is quite close to 29.36 (MPa m^3 $kmol^{-1}$) calculated from data reported by Katayama et al.[59] at the same temperature. It also compares well to 28.39 (MPa m^3 $kmol^{-1}$) measured by Descamps et al.[58], who carried out a thorough analysis of literature studies on this system. They already reported that literature estimates differ, even at comparable conditions, concluding that discrepancies are likely due to the analytical techniques and to the small amount of water always present in methanol. At any rate, Figure 3.1 shows that our measurements compare well with those of Descampes[58] and Katayama[59]. Our data for CH_3OH - H_2 provide the opportunity to validate our procedures and the analytical technique.

CO_2 + CH3OH + H_2

Experimental results for CO_2 + CH_3OH + H_2 ternary system at 268, 278 and 288 K are shown in Figure 3.2. At each temperature, a number of combinations of H_2 partial pressure were screened, by sequential additions of hydrogen.

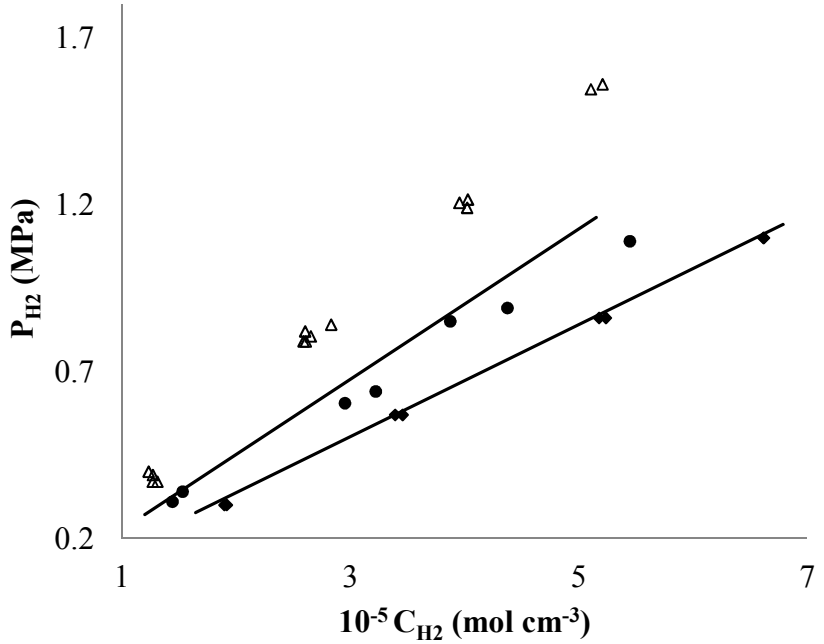

Figure 3.2 CO_2 + CH_3OH + H_2 ternary system. Solubility data of hydrogen: ♦, 288 K; ▲, 278 K; ●, 268 K; solid line, Peng-Robinson EoS after tuning kij; Δ, H_2 + CH_3OH binary at 278 K.

Average Henry's law constants calculated as above with the collected data are 16.7 ± 0.43, 18.9 ± 0.67 and 20.1 ± 0.95 (MPa m^3 $kmol^{-1}$), respectively at 288 K, 278 K and 268 K. A

linear interpolation of the H_{H_2} *(T)* dependency yields H_{H_2} *(MPa m^3 kmol^{-1}) = 65.8 – 0.17•T(K)*. The hydrogen solubility increases with temperature (lower H_{H_2}), as typical of H_2 in CH_3OH. It is also apparent that the hydrogen solubility increases compared to binary system, at the same hydrogen partial pressure. This is attributed to the presence of carbon dioxide: enhancements of H_2 solubility by CO_2 up to 80% has been reported in many organic solvent[59], including methanol. In our conditions, comparing data at 278K we have an increment of 37% due to the use of CO_2. Figure 3.3 compares our data (liquid phase mole fractions calculated with PR-EoS tuned on our measurements, as explained below) with those reported by Bezanehtak et al.[60] at the same temperature and total pressure, showing quite a good agreement.

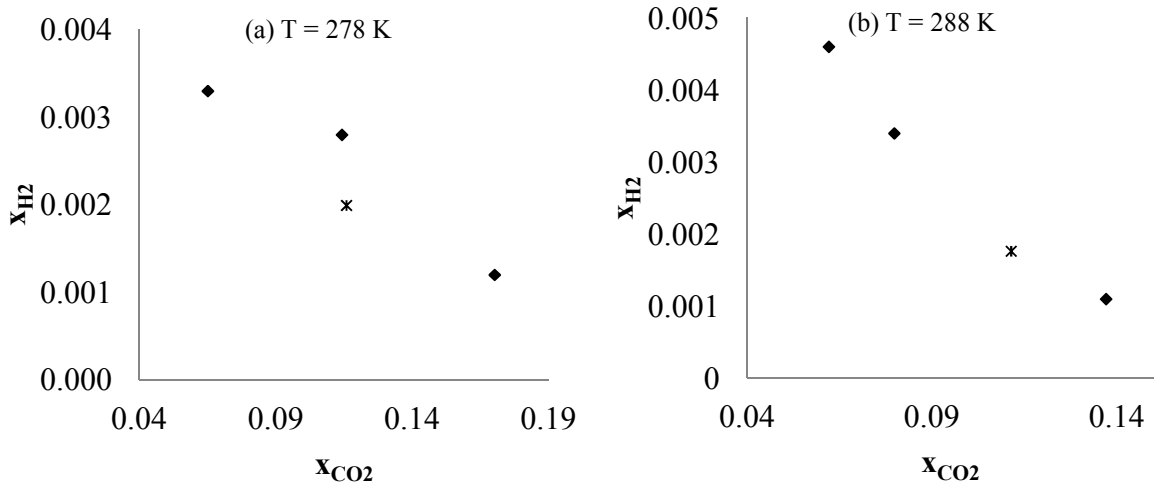

Figure 3.3. CO_2 + CH_3OH + H_2 ternary system. Comparison of H_2 solubility measurements with Literature data at 2 MPa (a, 278 K; b, 288 K): ♦, Bezanehtak et al.[60]; *, this work.

Interestingly, their data show a decreasing H_2 liquid mole fraction whit that of CO_2 increases, against the known evidence that CO_2 increases H_2 solubility. According to the authors, this is an apparent contradiction due to their experimental protocol, where a larger CO_2 amount in the whole V-L cell causes a smaller partial pressure of H_2 in the vapor phase, also lowering its amount in the liquid.

CO_2 + CH_3OH + O_2 + H_2

Figure 3.4 shows the experimental data of hydrogen solubility as a function of hydrogen partial pressure in the quaternary CO_2 + CH3OH + O_2 + H_2 system, measured at 268 and 278 K. Calculated Henry's law constants are 18.24 ± 0.89 and 20.88 ± 1.71 (MPa m^3 kmol^{-1}) at

278 and 268 K, respectively. Being that CO_2 liquid phase molar fraction is always the one used in the ternary case, we conclude that the addition of quite a significant amount of O_2 does not lead to any significant modification of the H_2 solubility. For sake of completeness, the composition of both phases according to PR EoS VLE calculations, result $x_{CO2} = 0.11$ and $0.43 < y_{O2} < 0.53$, depending on temperature and total pressure.

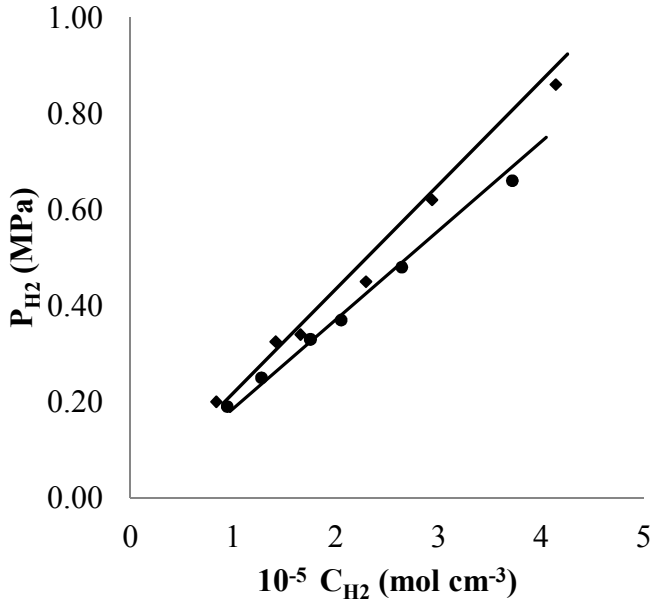

Figure 3.4. $CO_2 + CH_3OH + O_2 + H_2$ quaternary system. Solubility data of hydrogen: ●, 278 K; ♦, 268 K; solid line, Peng-Robinson EoS after tuning k_{ij}.

The linear interpolation of $H_{H_2}(T)$ with quaternary data at the temperature investigated resulted in $H_{H_2}(MPa\ m^3\ kmol^{-1}) = 68.3 - 0.18 \cdot T(K)$. Again, hydrogen solubility increases with increasing temperature, as known.

3.1.1 Modeling

Besides the experimentally measured data and corresponding Henry's constants, any equilibrium state, at predefined combinations of species amount and temperature (including early steps of filling), has been characterized by a flash calculation, using a ϕ-ϕ approach ($K_i = y_i/x_i = \phi_i^L/\phi_i^V$) and the Peng-Robinson Equation of State (PR-EoS). Standard routines has been used, through a well established commercial code (Aspen Plus). Calculations provide the vapor and liquid phase properties, and we focused on molar fractions. Total available amount of species is known from experiments, as well as temperature and total pressure given as input conditions. The calculations become predictive once EoS parameters are tuned on

experimental data. van der Waals mixing rules were adopted, linear for the co-volume *b* and quadratic for the attractive interaction parameter *a*. Due to the presence of supercritical species (H_2 and O_2), a Boston-Mathias alpha function was chosen. Binary interaction parameters k_{ij} have to be tuned. They were assumed to vary with temperature alone; while estimated at any temperature investigated, results (reported in Table 3.1) were fit by the expression:

$$k_{ij} = k_{ij}^{1} + k_{ij}^{2} \cdot T \qquad 3.1$$

We predicted H_2 solubility in ternary and quaternary systems using only binary interaction parameters k_{ij} calibrated on literature binary phase equilibrium, selected to be as close as possible to our experimental conditions (*T*, *P* and liquid phase composition). The objective function to be minimized by manipulating $k_{ij}(T)$ was based on departures between calculated and experimental liquid phase compositions. We assumed that oxygen and hydrogen interaction in the liquid phase are negligible, i.e. $k_{O_2\text{-}H_2} = 0$, according to experimental indications. Comparison of optimization results in term of H_2 solubility prediction accuracy was quantified through the mean absolute percentage error (MAPE):

$$MAPE = \frac{100}{n} \sum_{j=1}^{n} \frac{\left| C_{H_2,j}^{exp} - C_{H_2,j}^{calc} \right|}{C_{H_2,j}^{exp}} \qquad 3.2$$

where *n* is the number of measurements. The model first tuned on literature binary data agrees quite well with all binary literature data. While H_2 liquid phase composition dependence on temperature and pressure in ternary and quaternary systems was reasonable, dissolution of H_2 was systematically underestimated, with a MAPE errors as high as 20%, especially at the higher temperature and pressure. Using also ternary measurements to fit k_{ij} values for H_2 + CH_3OH, the model was significantly improved as compared to ternary experimental data. The prediction of C_{H_2} in quaternary CO_2 + CH_3OH + O_2 + H_2 configurations was also remarkably improved. All the final binary interaction parameters estimated are reported in Table 3.1, along with MAPE errors for all the investigated configurations and temperatures. Their correlation with temperature according to equation (3.1) leads to the coefficients reported in Table 3.2. The actual comparison with our experimental data is reported in Figure 3.2 and Figure 3.4, for ternary and quaternary systems, respectively. MAPE values are quite satisfactory. The calculated hydrogen liquid phase concentration of H_2 for CO_2 + CH_3OH +

H_2 system was always in an excellent agreement with experimental data, the highest MAPE error being 7% at 268 K. Predictions for CO_2 + CH_3OH + O_2 + H_2 quaternary system are also remarkably good, with MAPE errors below 7.6% (Table 3.1).

Table 3.1. Mean Absolute Percentage Error and binary interaction parameters for the Peng-Robinson Equation of State in ternary and quaternary systems.

System	T (K)	MAPE (%)	k_{1-2}	k_{1-3}	k_{2-3}	k_{1-4}	k_{2-4}
$CH_3OH(1) + CO_2(2) + H_2(3)$	268	7.2	0.036	-0.459	0.147	/	/
	278	3.0	0.041	-0.476	0.129	/	/
	288	2.4	0.046	-0.493	0.109	/	/
$CH_3OH(1) + CO_2(2) + H_2(3) + O_2(4)$	268	7.6	0.036	-0.459	0.147	-0.046	0.099
	278	5.4	0.041	-0.476	0.129	-0.028	0.100

Table 3.2. Coefficients for temperature correlation of binary interaction parameters (equation 3.1)

	O_2-MeOH	CO_2-MeOH	CO_2-O_2	CO_2-H_2	MeOH-H_2
k^1_{ij}	-5.338E-01	-9.251E-02	6.968E-02	6.568E-01	0.000E+00
k^2_{ij}	1.820E-03	4.803E-04	1.091E-04	-1.900E-03	-1.711E-03

The developed model allows estimating the CO_2 effect on the hydrogen solubility. Figure 3.5 shows calculated Henry's constants of hydrogen as a function of temperature and total CO_2/CH_3OH molar ratio, $\gamma = n_{CO_2} / n_{CH_3OH}$, according to PR-EoS tuned on literature and our experimental data.

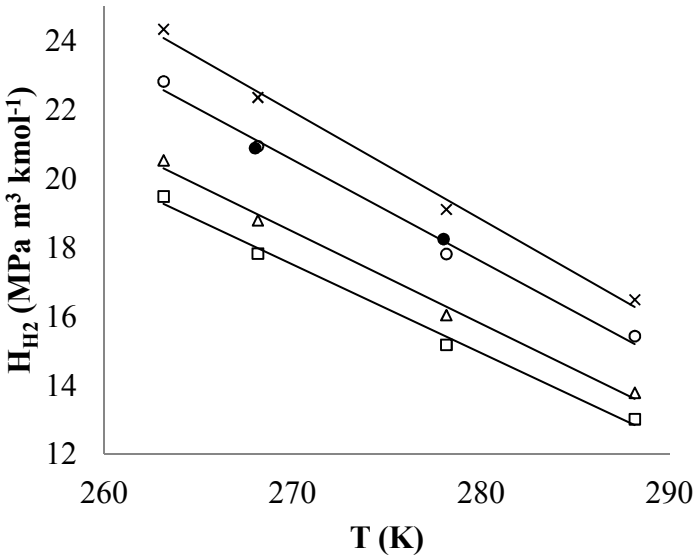

Figure 3.5. Predicted Henry's constants of hydrogen as a function of temperature and $\gamma = n_{CO_2}/n_{CH_3OH}$ calculated from PR-EoS tuned on literature and our experimental data: □, γ = 0.3; Δ, γ = 0.25; ○, γ = 0.15; x, γ = 0.09; ●, experimental data (Results & discussion, *CO_2 + CH_3OH + O_2 + H_2*).

Though predicted $H_{H_2}(T)$ appears slightly curved upwards, linear interpolations are acceptable, leading to the correlation:

$$\begin{aligned} H_{H_2} &= \alpha(\gamma) + \beta(\gamma)\cdot T \\ \alpha(\gamma) &= -91.96\gamma + 114.09 \\ \beta(\gamma) &= 0.26\gamma - 0.33 \end{aligned} \qquad 3.3$$

We already mentioned the significant H_2 solubility enhancement due to CO_2 by comparing binary and ternary data, also shown in Figure 3.2, confirming literature data[60, 61] measured in different conditions. The enhancement factor (EF) was adopted to quantitatively measure the advantage given by CO_2, comparing H_2 solubility without (H_2 + CH_3OH) and with CO_2 (CO_2 + CH_3OH + O_2 + H_2). EF is defined as the ratio of hydrogen composition in methanol ($x_{H_2}^{Binary}$) and CO_2 + CH_3OH + O_2 systems ($x_{H_2}^{Quaternary}$) at the same conditions of temperature and hydrogen fugacity:

$$EF = \frac{x_{H_2}^{Quaternary}}{x_{H_2}^{Binary}} \qquad 3.4$$

Values higher than 1 indicate an increased hydrogen dissolution in the liquid phase caused by carbon dioxide, and thus are desirable. According to the predictions based on this model, EF can approach 2.1 at 278 K and $\gamma = 0.3$.

3.2 H_2O_2 synthesis: hydrogen feeding policies

The reactor was operated batchwise, with H_2 as the limiting reagent, to keep the gas mixture outside (lower) flammability limit. Due to the small amount of H_2 introduced, a low concentration of H_2O_2 is expected. In order to overcome this drawback and in view of a potential industrial application, the same amount of hydrogen was fed into the reactor with different strategies. Experiments were carried out at 283 K and 1.8 MPa, also measuring H_2 in the liquid phase. Two H_2 feeding polices were implemented: four equal hydrogen fillings were introduced 1) after each complete hydrogen conversion and 2) as soon as hydrogen concentration in the liquid phase started to decrease. Results are reported in Figure 3.6.

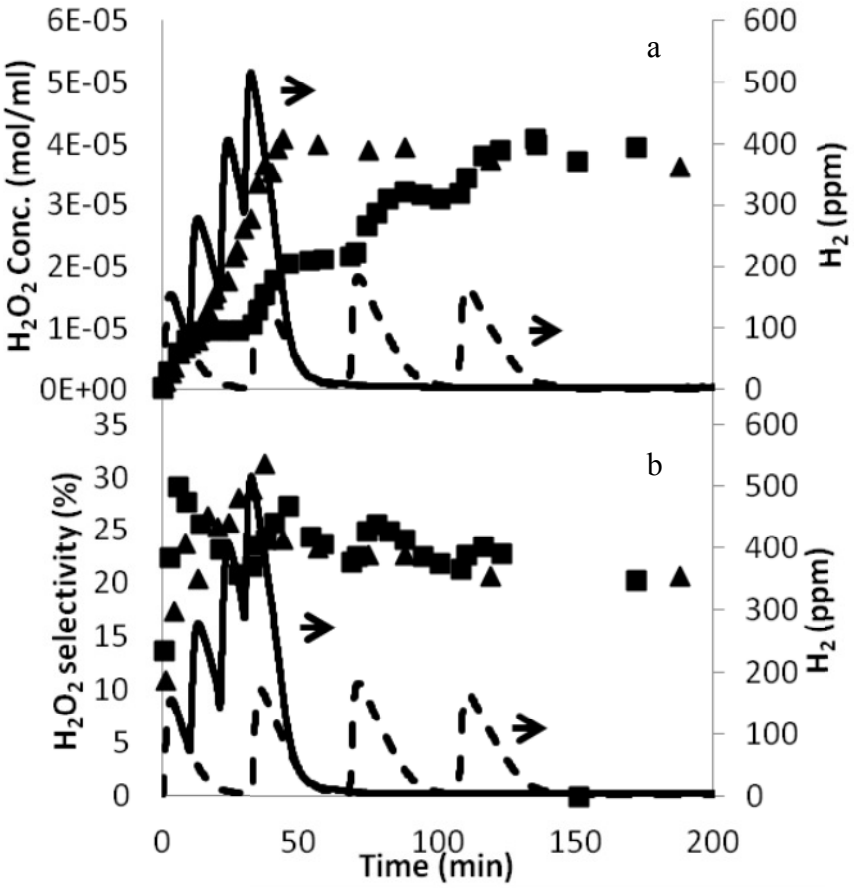

Figure 3.6. H_2O_2 direct synthesis at 283 K and 1.8 MPa with different hydrogen feeding policies: 1) Hydrogen amount fed after its complete conversion (dashed line) and 2) hydrogen subsequently fed as it decreases in the liquid phase (solid line). H_2O_2 concentration (a) and selectivity (b) under feeding policy 1 (■) and 2 (▲).

In experiment type 1) the amount of hydrogen dissolved in the liquid rapidly reached a peak after each introduction, slowly decreasing afterwards. 29% maximum selectivity was observed and H_2O_2 production increased each time H_2 was fed. Interestingly, as soon as hydrogen decreased in the liquid phase, the selectivity towards hydrogen peroxide was also reduced, and the formation of water prevailed. However, every time hydrogen was fed into the reactor, the selectivity increased, although smaller values were achieved. This result is interesting as it suggests a possible relationship between the amount of hydrogen in the liquid phase and the quantity of H_2O_2 produced. It appears that keeping the hydrogen conversion below 100% (i.e. 60%) favors the selectivity. Possibly, the presence/absence of H_2 influenced the oxidation state of the active metal, thus changing the reaction kinetic. In that sense, the presence of H_2 would favor the selectivity towards the peroxide. Hence an experiment was performed avoiding the complete depletion of hydrogen in the liquid phase (feeding policy 2). A higher selectivity could be achieved, reaching a peak around 33%, compared to 29% of the previous experiment. In both cases, after H_2 complete depletion the selectivity reached a similar value, i.e. 20%. Interestingly, the hydrogen peroxide production was similar with the two H_2 feeding policies. These results seem to confirm that the presence of H_2 in the liquid phase favors the production of the peroxide.

3.3 Kinetics identification

3.3.1 H_2O_2 synthesis, hydrogenation and disproportionation: effect of temperature

Kinetic experiments of the hydrogen peroxide direct synthesis were carried out varying the temperature. The H_2:O_2 ratio was set to 1:10, i.e. hydrogen was the limiting reagent. Results of H_2O_2 and H_2O production are reported in Figure 3.7.

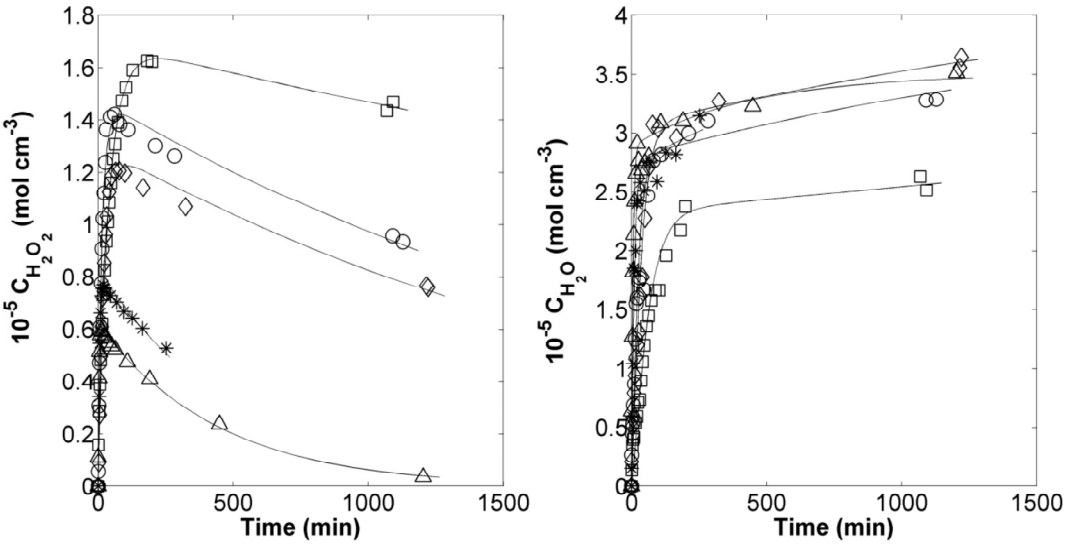

Figure 3.7. H_2O_2 direct synthesis experiments in the batch reactor: □, 258 K; ◇, 268 K; ○, 273; *, 283 K; △, 297 K; solid line, model.

Overall, the water production during the experiments increased constantly and prevailed over the hydrogen peroxide formation, reaching higher concentrations than the peroxide. The H_2O_2 formation increased rapidly in the very beginning, reaching a maximum and gradually decreasing afterwards. The complete consumption of H_2 corresponded to the maximum concentration of H_2O_2: after H_2 was no longer present in the liquid phase, and the direct synthesis as well as the hydrogenation were suppressed. Thus, the only possible reaction was the disproportionation, resulting in a drop of the peroxide formation. Experimental results confirmed that the direct synthesis reaction was very fast at the beginning, but hydrogenation and disproportionation reactions increased as hydrogen concentration in the liquid phase decreases. Interestingly the direct synthesis is favored at lower temperatures.

Palladium based catalysts are well known for being suitable for the direct synthesis of hydrogen peroxide. Unfortunately, they also promote H_2O_2 disproportionation and hydrogenation. To quantify the degree of H_2O_2 loss by disproportionation and hydrogenation, kinetic experiments were carried out with the same catalyst and under the same operation conditions as the direct synthesis. Results are shown in Figure 3.8, as a percentage of the H_2O_2 loss.

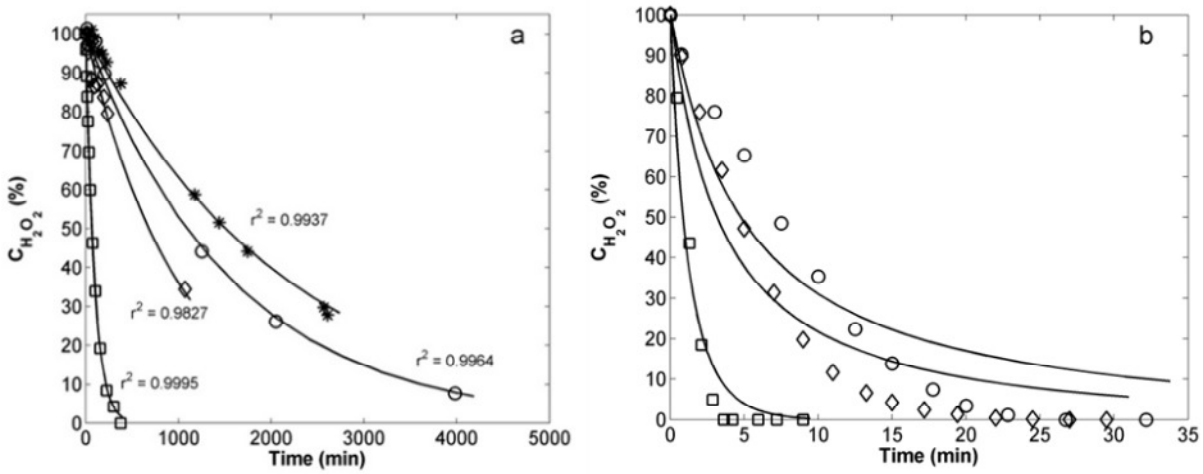

Figure 3.8. H_2O_2 disproportionation (a) and hydrogenation (b) experiments in a batch reactor: □, 313 K; ◇, 283; ○, 273 K; *, 268 K; solid line, model.

Qualitatively, both degradation paths (with/without H_2) were similarly affected by the temperature. However it is apparent that in presence of H_2 the destruction of the peroxide was much faster (min vs hours).

3.3.2 Modeling

Several surface mechanisms on palladium can give the overall process described in Scheme 1.1. In our study, very small surface coverage was assumed, so that pseudo-homogeneous rate equations could be assumed. With the purpose of investigating the multiphase nature of the reaction, the reactions in Scheme 1.1 were assumed elementary and irreversible, occurring on the surface of a non-porous powder catalyst. Accordingly, the following rate expressions for each step are valid:

$$R_{ds} = k_{ds} C^S_{H_2} C^S_{O_2} \qquad 3.5$$

$$R_{wf} = k_{wf} C^S_{H_2} \left(C^S_{O_2} \right)^{1/2} \qquad 3.6$$

$$R_d = k_d C^S_{H_2O_2} \qquad 3.7$$

$$R_h = k_h C^S_{H_2O_2} C^S_{H_2} \qquad 3.8$$

with temperature dependent, Arrhenius-type kinetic constants:

$$k_i = A_i e^{-Ea_i/RT} \qquad 3.9$$

Pre-exponential factor (A_i) and activation energy (Ea_i) of each reaction are determined from our experimental data. According to the stoichiometry, the production rates of each species to be used in individual mass balances are:

$$r_{H_2O_2} = R_{ds} - R_d - R_h \qquad 3.10$$

$$r_{H_2O} = R_{wf} + R_d + 2R_h \qquad 3.11$$

$$r_{H_2} = -R_{ds} - R_{wf} - R_h \qquad 3.12$$

$$r_{O_2} = -R_{ds} - 0.5R_{wf} + 0.5R_d \qquad 3.13$$

Two mass transfer resistances were considered, dissolution of gases into the liquid phase and reactant transport in the liquid to the catalyst surface. Coefficients were calculated according to best available correlation for the reactor used, considering that gas was bubbling in the liquid and catalyst was in the form of fine powder, suspended in the liquid. The species mass balances were written in each phase, i.e. vapor and liquid, the solid being assumed non-porous reduce to a flux balance at its interface. Balances are based on the following assumptions:

a) both liquid and vapor phase are well mixed;
b) carbon dioxide and methanol are not involved in any reaction;
c) any increment of liquid volume due to the accumulation of H_2O_2 and H_2O is neglected, while the change caused by sampling is taken into account.
d) species cannot accumulate on the catalyst surface, nor in the liquid boundary layer surrounding the catalyst particles.

According to these assumptions, the mass balances in the gas and liquid phases can be written as:

$$V^G \frac{dC_i^G}{dt} = a^{LG} K_i^L \left(C_i^L - C_i^{L,*} \right) \qquad i = \mathrm{H_2}, \mathrm{O_2} \qquad 3.14$$

$$V^L \frac{dC_i^L}{dt} = a^{LG} K_i^L \left(C_i^{L,*} - C_i^L \right) - a^{LS} K_i^S \left(C_i^L - C_i^S \right) \qquad i = \mathrm{H_2}, \mathrm{O_2}, \mathrm{H_2O_2}, \mathrm{H_2O} \qquad 3.15$$

At the catalyst surface interface the material balances under assumption d) becomes:

$$0 = a^{LS} K_i^S \left(C_i^S - C_i^L \right) - r_i \cdot mol_{Pd} \qquad i = \mathrm{H_2}, \mathrm{O_2}, \mathrm{H_2O_2}, \mathrm{H_2O} \qquad 3.16$$

where the production rates r_i appears, which are functions of the species concentration facing the catalyst surface, C_i^S . At the gas-liquid interface equilibrium holds. The equilibrium constants were estimated from an equation of state tuned on specific experimental data (**Publication I**).

The proposed model is given by a total of ten equations: 2 ODEs for the gas phase, 4 ODES for the liquid phase and 4 algebraic equations for the catalyst surface, resulting in a low index ADEs system. Its integrations yields the evolution in time of the concentration of reactants (i.e. H_2 and O_2) in the gas and liquid phases and at the catalyst surface (6 unknown functions), and the concentration of H_2O_2 and H_2O in the liquid phase and at the catalytic surface (4 unknowns).

According to the experimental procedure (**Publication II**), the following ten initial conditions are assumed:

$$\begin{aligned}
&a)\, C_{O_2}^G\big|_{t=0} = C_{O_2}^{G,0} && e)\, C_{H_2}^L\big|_{t=0} = C_{H_2O_2}^L\big|_{t=0} = 0 \\
&b)\, C_{H_2}^G\big|_{t=0} = \frac{n_{H_2}}{V^L} && f)\, C_{O_2}^S\big|_{t=0} = C_{O_2}^{L,0} \\
&c)\, C_{O_2}^L\big|_{t=0} = C_{O_2}^{L,0} && g)\, C_{H_2O}^S\big|_{t=0} = C_{H_2O}^{L,0} \\
&d)\, C_{H_2O}^L\big|_{t=0} = C_{H_2O}^{L,0} && h)\, C_{H_2}^S\big|_{t=0} = C_{H_2O_2}^S\big|_{t=0} = 0
\end{aligned} \qquad 3.17$$

Primarily, hydrogen (the limiting reagent) was introduced after all the other species, when stable values of pressure and temperature were reached inside the reactor (filled with O_2, CO_2 and methanol). Since the H_2 feeding was fast compared to the reaction time, hydrogen is assumed not to dissolve in the liquid phase while introduced (conditions 3.17b and 3.17e). The initial concentration of water in the reaction medium (condition 3.17d) was measured prior the introduction of hydrogen.

The material balances equations (3.14-3.16), together with initial conditions (3.17) have been efficiently solved using Matlab's ode15s ADEs solver, also suitable for stiff equations, being based on a multistep, variable order method based on the numerical differentiation formulas. Values of the activation energy and the pre-exponential factor of each reaction were determined by a sequence of isothermal experimental data fitting, providing the four irreversible reaction rate constants k_{ds}, k_{wf}, k_d and k_h at the given temperature. Then an

Arrhenius plot was assembled for each reaction, and the relative activation energy and pre-exponential factors determined by fitting *k(T)*. The following error function was used for each experiment (i.e. a given temperature) to fit the experimental data:

$$err = \frac{\sqrt{\sum_{i=1}^{n_{H_2O_2}^{exp}} \left| C_{H_2O_2,\,i}^{S,\,Exp} - C_{H_2O_2,\,i}^{S,\,Calc} \right|^2}}{\frac{1}{n_{H_2O_2}^{exp}} \sum_{i=1}^{n_{H_2O_2}^{exp}} C_{H_2O_2,\,i}^{S,\,Exp}} + w \frac{\sqrt{\sum_{i=1}^{n_{H_2O}^{exp}} \left| C_{H_2O,\,i}^{S,\,Exp} - C_{H_2O,\,i}^{S,\,Calc} \right|^2}}{\frac{1}{n_{H_2O}^{exp}} \sum_{i=1}^{n_{H_2O}^{exp}} C_{H_2O,\,i}^{S,\,Exp}} \qquad 3.18$$

Note that errors between experimental and calculated concentrations were rescaled. In pure disproportionation and hydrogenation experiments, where water concentration was not measured, we set the parameter w=0; in all other cases, w=1. A Nelder-Mead simplex algorithm with positivity constraints on the parameters (fminsearchbnd function) was used to minimize the error by adjusting the four parameters of the model (k_{ds} k_{wf}, k_d and k_h).

Direct synthesis

Each isothermal run has been simulated and a set of *k*'s estimated, for each step in the mechanism; results are shown in Figure 3.7. The model is always in very good agreement with experimental results. Experimental measurements of H_2O are less precise, due to the different analytical procedure, slightly decreasing the goodness of fit. The kinetic constants calculated at each temperature are collected in Figure 3.9 in the form of Arrhenius plots, and the resulting activation energies and pre-exponential factor are reported in Table 3.3.

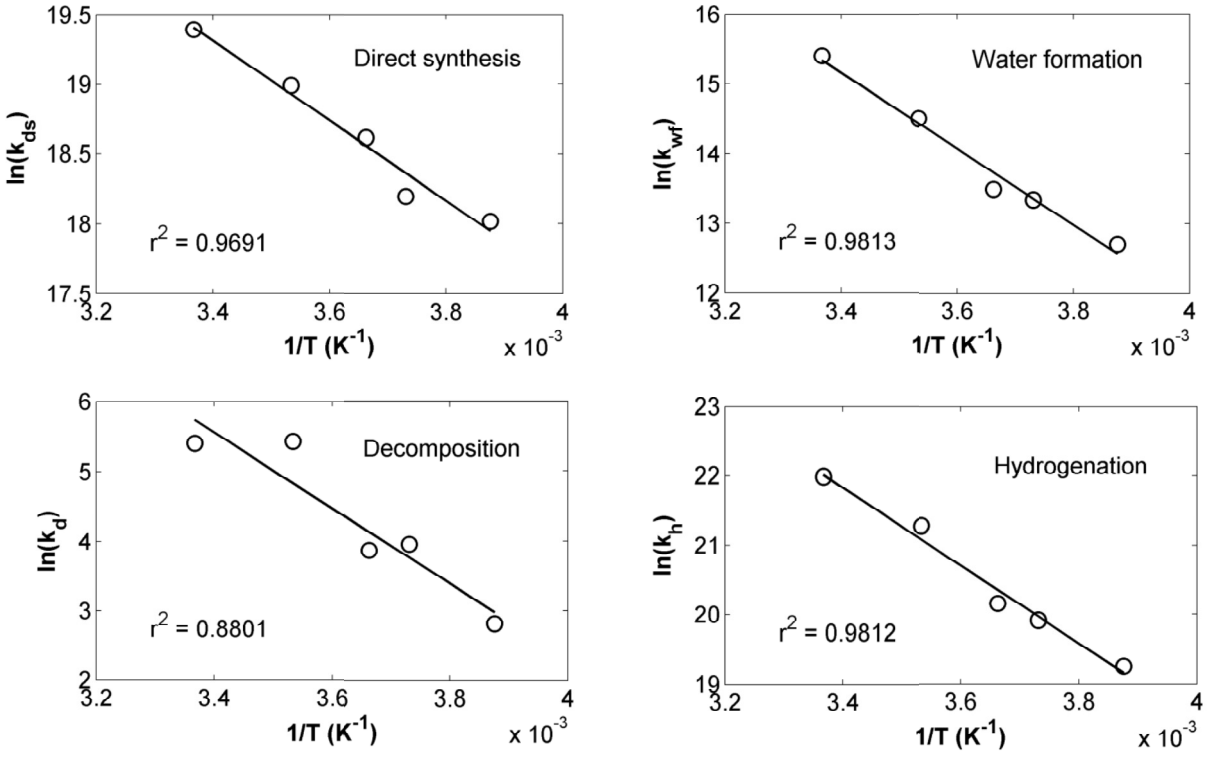

Figure 3.9. Arrhenius plots for the kinetic constants of each individual step in the mechanism.

Table 3.3. Arrhenius constants for the rate equations 3.5-3.8 (direct synthesis experiments).

	Pre-exponential factor	Activation energy (kJ mol^{-1})
Direct synthesis	$4.18 \pm 0.15 \times 10^{12}$	23.84 ± 2.45
Water formation	$4.27 \pm 0.20 \times 10^{14}$	45.31 ± 3.61
Disproportionation	$2.61 \pm 0.45 \times 10^{10}$	45.06 ± 9.60
Hydrogenation	$5.65 \pm 0.22 \times 10^{17}$	46.58 ± 3.72

The temperature dependence of water formation, disproportionation and hydrogenation are all comparable (activation energies close to 45 kJ mol^{-1}). However, the kinetics of these reactions is quite different. *k* values can differ by orders of magnitude, but they are not really comparable, because refer to different overall reaction orders. The most appropriate comparison must inspect the values of the reaction rates during the course of each experiments, as shown in Figure 3.10.

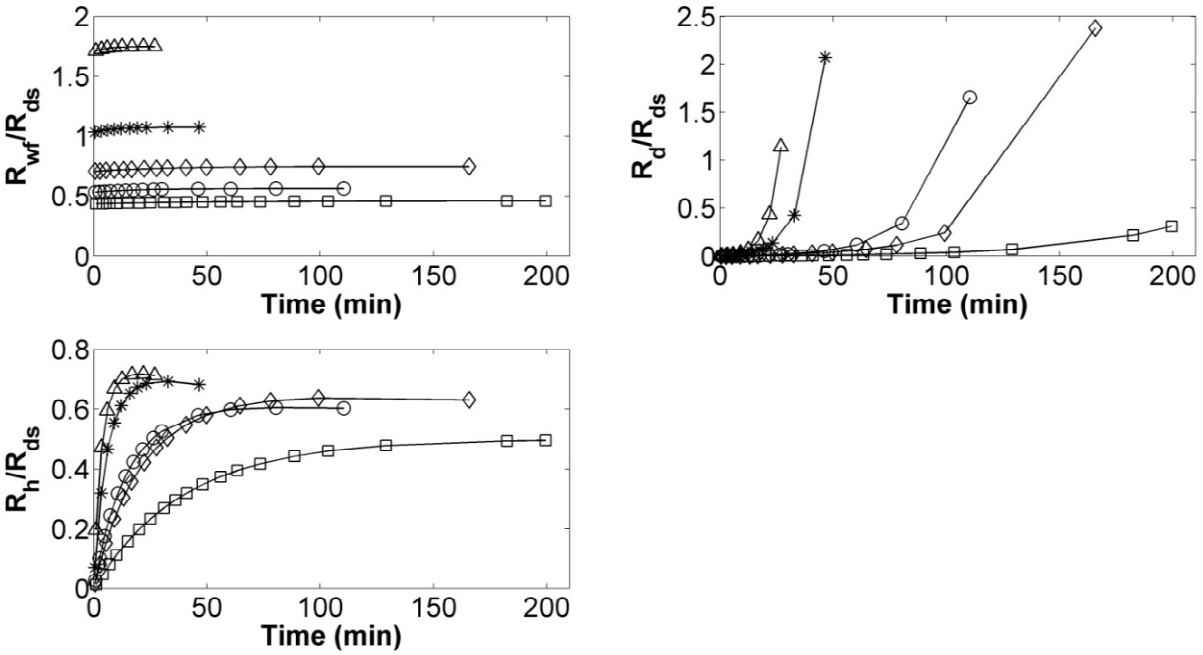

Figure 3.10. Ratio of each reaction rate to the direct synthesis during the reaction course: △, 297 K; *, 283 K; ○, 273 K; ◇, 268; □, 258 K;

Each reaction rate has been related to the one of direct synthesis, R_{wf}/R_{ds}, R_d/R_{ds} and R_h/R_{ds}. Both disproportionation and hydrogenation rates are null at the beginning, requiring the presence of the peroxide (i.e. they are reactions consecutive to the direct synthesis). Their rates increase during the reactions course, at a different pace. Disproportionation reaction is very slow compared to the direct synthesis and becomes important only at a high H_2 conversion, when the direct synthesis reaction slows down. A strong effect of the temperature is also observed on this reaction, where lower temperature is confirmed to stabilize the H_2O_2 produced. The preferred path of H_2O_2 degradation is the hydrogenation reaction: its rate rapidly increases as H_2O_2 becomes available, limiting the H_2O_2 production. However this reaction is always slower than the direct synthesis (R_h/R_{ds} <1) and it can be limited by decreasing the temperature, up to R_h/R_{ds} < 0.5 at 258 K. Unfortunately, the R_{wf}/R_{ds} is always significant because the formation of water really competes with the direct synthesis, prevailing (R_{wf}/R_{ds} >1) at higher temperature, whereas lower temperature favors the direct synthesis (R_{wf}/R_{ds} <1). At a given temperature, the rate of H_2O formation remains very close to that of the direct synthesis (constant R_{wf}/R_{ds}) except for a short initial transient favoring the direct synthesis.

Due to the intrinsic nature of the interconnected reaction mechanism, a correlation between the estimates of reaction rate constants has to be expected. A quantitative evaluation is given

in Figure 3.11 as contour plots for the parameter estimates, at T = 268 K. A small correlation is indicated by contours approaching circles.

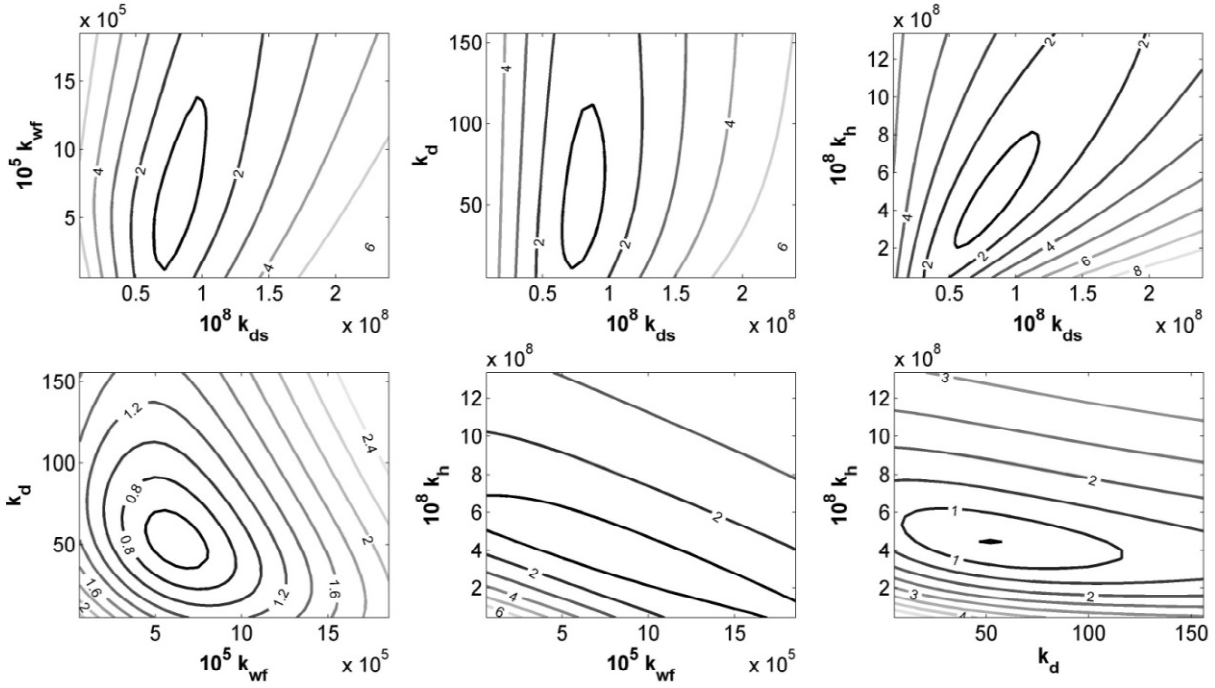

Figure 3.11. Contour plots of regressed kinetic parameters (T = 268 K).

A strong correlation is observed between most reaction constants, and remarkably among direct H_2O_2 synthesis and the other reactions. The lowest correlation occurs between disproportionation and water formation, as expected. The same analysis was carried out for all isothermal data with similar results. In order to improve or double check our estimates and suppress the correlation among the parameters, we studied the disproportionation and hydrogenation rate constants independently, with dedicated experiments.

Disproportionation

Rate expression (3.7) was used to fit the H_2O_2 concentration profiles during disproportionation experiments, to isolate this step. Since in these experiments H_2 was replaced with N_2, calculations were carried out neglecting rate expressions (3.5), (3.6) and (3.8) and hydrogen mass balance (eq. 3.12). Figure 3.8 (a) shows the results as measured and calculated isothermal data of H_2O_2 concentration. Arrhenius plot for disproportionation reaction is reported in Figure 3.12.

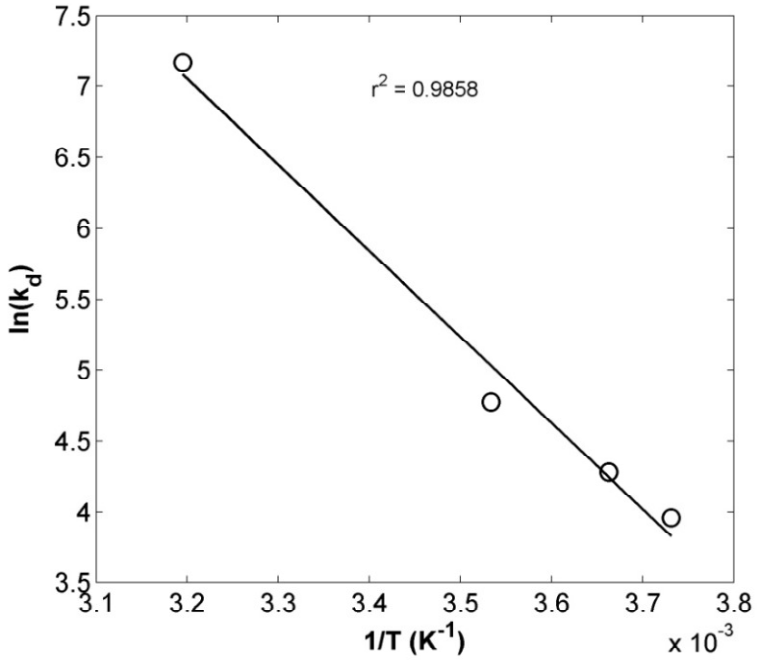

Figure 3.12. Arrhenius plot for disproportionation reaction.

Predictions were in good agreement (r^2 very close to 1) with experimental observations at any temperature considered, confirming that disproportionation is a first order reaction with respect to H_2O_2 concentration. The calculated kinetic parameters are reported in Table 3.4.

Table 3.4. Arrhenius constants for rate equation 3.7 (disproportionation experiments).

Pre-exponential factor ($cm^3\ s^{-1}$)	Activation energy ($kJ\ mol^{-1}$)
$3.11 \pm 0.21 \times 10^{11}$	50.43 ± 4.28

A comparison of the Arrhenius constants obtained by fitting all the rate constant in eqs. (3.5-3.8) together, using the direct synthesis experimental data, shows that the activation energy for k_d obtained here for the disproportionation reaction (50.43 kJ mol^{-1}) compares well with the above value (45.06 kJ mol^{-1}, Table 3.3), being that their confidence intervals overlap substantially. A higher deviation is observed in the pre-exponential factors. However, the deviation on the isothermal kinetic constants k_d is less than 10% (T < 273 K), confirming the results reported in Table 3.3.

Hydrogenation

H_2O_2 hydrogenation experiments were performed substituting O_2 with N_2. Hence, direct synthesis and water formation reactions do not occur. Accordingly, when regressing these data the mass balance of O_2 (eq. 3.13) and rates (3.5) and (3.6) were ignored. Disproportionation rate constants were not regressed and the parameters previously obtained (Table 3.4) were introduced in the model and kept fixed. Only rate expression (3.8) was considered and isothermal hydrogenation reaction constants regressed. The deviation between experimental H_2O_2 concentration measured during pure hydrogenation and the best fit predictions is rather high, as shown in Figure 3.8 (b). Apparently, the kinetic model in this case is not adequate. The decay of H_2O_2 concentration in time is only approximately exponential, as clearly perceivable from Figure 3.8 (b). In the first minutes of reaction, and more clearly at lower temperature, the H_2O_2 concentration decreases more slowly than later on. At higher H_2 conversion, the decay is very rapid, in a way that a second-order rate equation, linearly proportional to each reagent concentration, cannot fit. Consequently, the model switch from under- to overestimation of the measured H_2O_2 concentration, when approx. 70% of the introduced H_2O_2 is consumed. The effect of temperature, within the approximation discussed above, is well described by a linear Arrhenius plot. The calculated activation energy and pre-exponential factor are respectively 17.85 ± 1.00 (kJ mol^{-1}) and 7.47 ± 0.11 x 10^{12} (cm^6 mol^{-1} s^{-1} mol_{Pd}^{-1}). However, the k_h values are much higher compared to the ones reported in Figure 3.9, also reflected in a significantly lower activation energy. We explain both results, a 2-steps H_2O_2 consumption and its higher rate, in terms of differences in the catalyst oxidation state. Synthesis and hydrogenation experiments use a different experimental condition: the former were carried out in large excess of O_2, the latter did not include any O_2, but H_2 was the only reactant present. Accordingly, the active metal on the catalyst can be mostly oxidized in excess of O_2 (synthesis conditions), and reduced in excess of H_2 (hydrogenation conditions). The reduced form of the catalyst can be more effective for the hydrogenation reaction, enhancing its rate, consistently with literature observations[23, 52] that the production of hydrogen peroxide is favored by the oxidized form of Pd. In addition, the H_2O_2 hydrogenation on reduced Pd may occur with a non-elementary mechanism, involving a complex model also accounting for competitive adsorption of H_2 and O_2. According to the discussion above, we rely on the kinetic model and values of Table 3.3 to describe the reaction network at synthesis (i.e. O_2 dominated) conditions. Further, we question the significance of independently estimating the H_2O_2 hydrogenation kinetics in case the catalyst is vulnerable to oxidation/reduction at conditions of the experiments, which is quite

common. Also, in case of non-elementary mechanism, a competitive adsorption on the catalyst sites between H_2 and O_2 is expected in the synthesis experiments, which is not the case for hydrogenation experiments.

Parametric sensitivity on mass transfer coefficients

Values of $K_i^L a^L$ (mass transfer between gas and liquid) for H_2 was calculate in the range 960-1880 h^{-1}, at 258 and 297 K, respectively. The coefficients of mass transfer resistance at the catalyst surface, K_i^S, were in the range $1.4 \cdot 10^{-2}$ - $3.5 \cdot 10^{-2}$ cm s^{-1} at 258 K and 297 K, respectively, for all components. Since we tried to predict the mass transfer rates a priori, using the best available correlations, we expect that the chemical kinetics was properly identified, with the results given in Table 3.3. Would the mass transfer actually control the process, or part of it, we should expect the chemical kinetics to be inaccurately determined. We actually used this reasoning to evaluate the extent of mass transfer control at our experimental conditions. The values of $K_i^L a^L$ and K_i^S were increased or decreased by up to one order of magnitude and the kinetic parameters (activation energy and pre-exponential factors) re-estimated. Different simulations were carried out changing each individual mass transfer coefficients, one at a time. As expected, no influence on the kinetic parameters was observed varying $K_i^L a^L$ and K_i^S values of O_2, H_2O_2 and H_2O, the only critical species being hydrogen, the limiting reagent in all the performed experiments. Further, disproportionation reaction was not affected by hydrogen concentration because of its rate law expression, and it was excluded from this analysis. The sensitivities of the reaction rate constants k to $K_{H_2}^L a^L$ are shown in Figure 3.13.

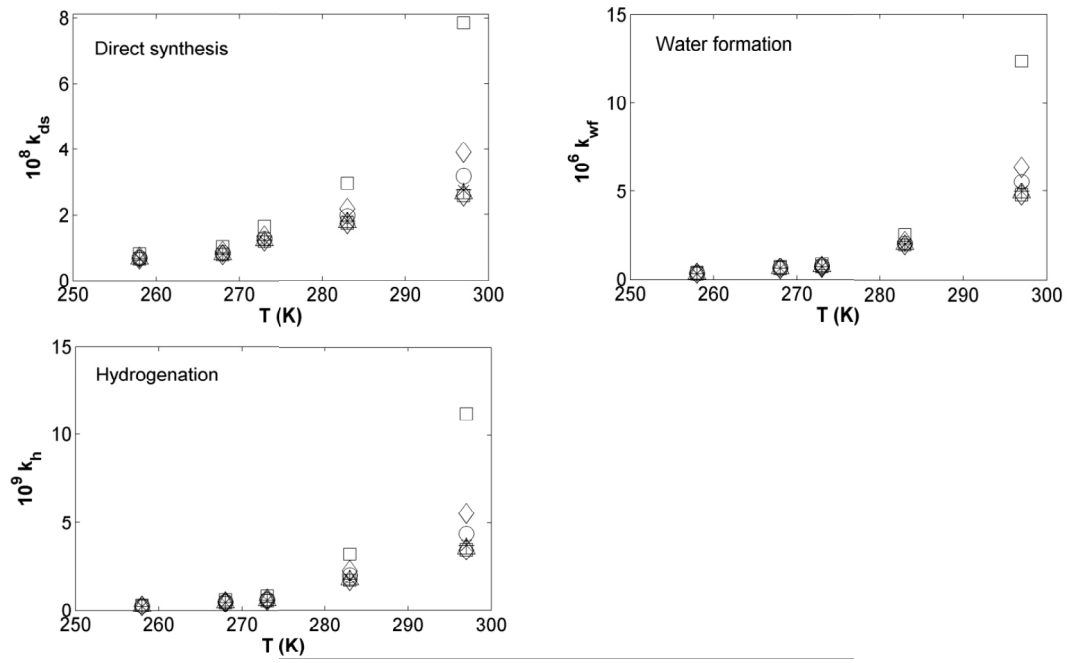

Figure 3.13. Effect of $K_{H_2}^L a^L$ on the reaction rate constants of direct synthesis, water formation and hydrogenation. The value given by correlation 10 has been multiplied by: 0.0035 (□), 0.08 (◇), 0.15 (○), 0.5 (*), 1 (△), 5 (+), 10 (x).

Decreasing H_2 mass transfer coefficients from gas to liquid affects the estimated rate constants of any reaction; the reduced H_2 transfer rate to the liquid phase (and hence to the catalyst) must be balanced by the increased reaction kinetics. Interestingly, limitations in the H_2 mass transfer rate cause an apparent increase in the estimated activation energy, as can be observed in Figure 3.14, recalling the importance of accounting for mass transfer to properly identify the kinetics.

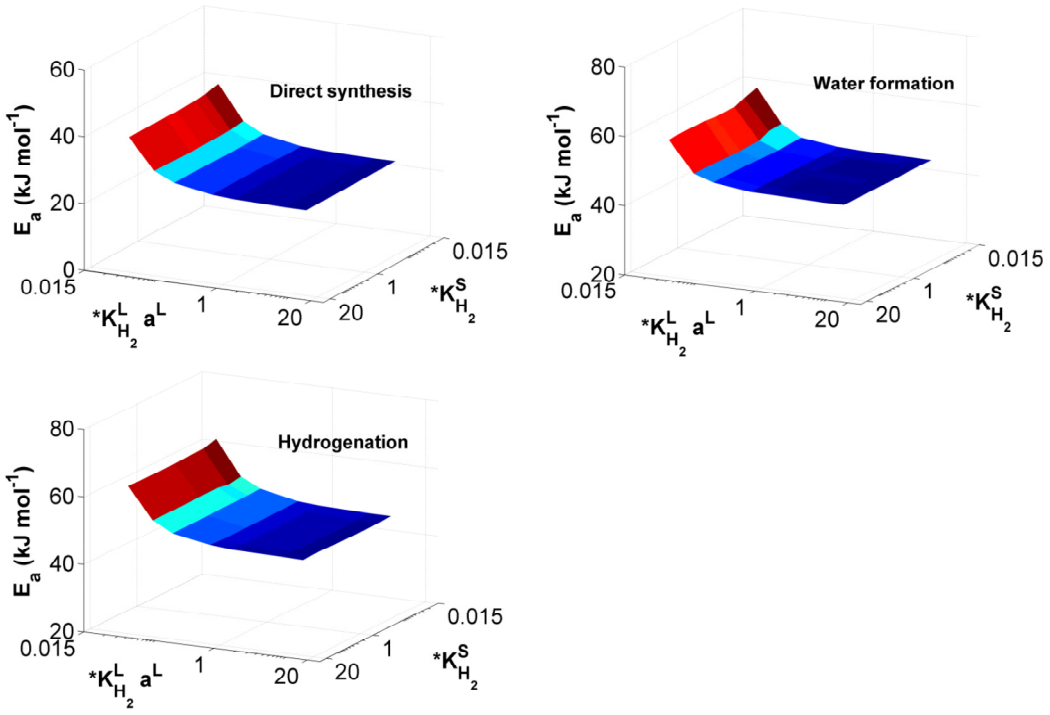

Figure 3.14. Effect of $K^L_{H_2}a^L$ and $K^S_{H_2}$ on the activation energy of direct synthesis, hydrogenation and hydrogenation reactions.

However, some mass transfer effect was only evident at temperatures above 283 K, by artificially lowering $K^L_{H_2}a^L$ at least by one order of magnitude (form 1880 h^{-1} to 140 h^{-1}). Accordingly, we conclude that limitations due to the dissolution rate of hydrogen can be excluded at the experimental conditions, even accounting for uncertainties in the correlations, that could not be as high as 1 order of magnitude.

Figure 3.15 shows the effect of the mass transfer rate from the liquid to the solid surface ($K^S_{H_2}$) on the reaction rate constants of direct synthesis, water formation and hydrogenation.

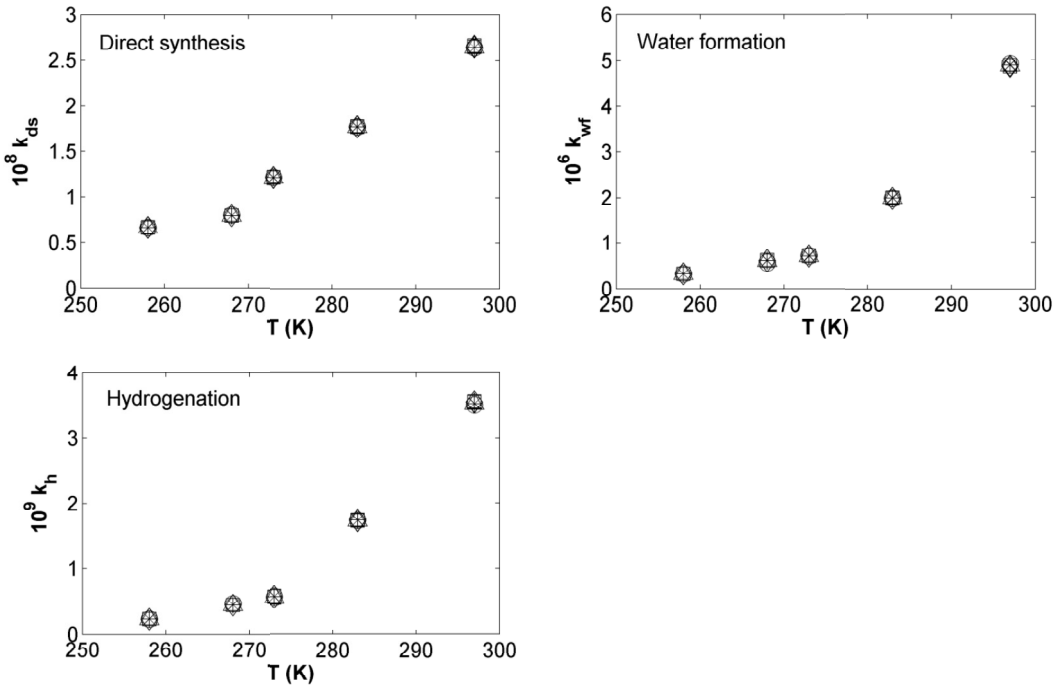

Figure 3.15. Effect of $K_{H_2}^S$ on the reaction rate constants of direct synthesis, water formation and hydrogenation. The value given by correlation 19 has been multiplied by: 0.0035 (□), 0.08 (◇), 0.15 (○), 0.5 (*), 1 (△), 5 (+), 10 (x).

At the highest temperature (i.e. 297 K), where the effect is expected to be more evident, $K_{H_2}^S$ were varied from $3.01 \cdot 10^{-4}$ cm s^{-1} to $8.61 \cdot 10^{-2}$ cm s^{-1}. As can be seen, predicted values of reaction rate constants do not significantly change, even varying the resistance by two orders of magnitude. Accordingly, the activation energy of the three reaction remains constant (Figure 3.14). This proves that any restriction due to the mass transfer limitation to the catalyst surface is negligible at the experimental conditions.

3.4 SBA15-based doped supported catalysts

3.4.1 Non-ordered and ordered mesoporous Si-based catalysts

We investigated the role of Au and incorporated-bromine over five different SBA15-based catalysts. Figure 3.16 illustrates H_2O_2 concentration as a function of time observed with these catalysts.

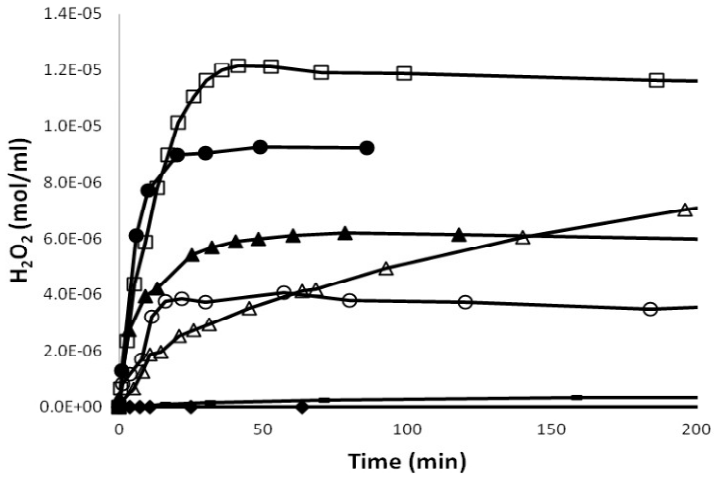

Figure 3.16. H_2O_2 concentration in batch reactor: PdAu/SBA15 (□), Br-PdAu/SBA15 (△), Pd/SBA15 (●), Br-Pd/SBA15 (-), PdAu-Br/SBA15 (♦), Pd/Si (▲), PdAu/Si (○). Conditions: T = 283 K, P = 1.75 MPa

Among the synthesized catalysts, PdAu/SBA15 was the most active one. Figure 3.16 clearly distinguishes the differences in mono- and bimetallic catalysts, where the latter ones always show a much higher H_2O_2 productivity upon short contact time. Monometallic Pd/SBA15 catalyst had a productivity 50% reduced compared to the bimetallic PdAu/SBA15. Its grafted parent (Br-Pd/SBA15) demonstrated a poor H_2O_2 productivity also, i.e. five times lower compared to the bimetallic Br-PdAu/SBA15. Upon testing the monometallic Br-Pd/SBA15 catalyst, H_2O concentration was within the measurement error and, consequently, H_2 conversion and selectivity could not be calculated. The comparison of mono- and bimetallic catalysts (either grafted or not) confirms the synergetic effect between Pd and Au reported in the literature[26, 62].The grafting process had a two-fold effect on the bimetallic catalyst, clearly seen when comparing the performance of the PdAu/SBA15 and Br-PdAu/SBA15. The selectivity was reduced by 15% in the presence of bromine attached on the catalyst. Moreover, the productivity was three times lower over Br-PdAu/SBA15 and also the H_2 conversion was reduced by a factor of 80%. The grafting process could induce poisoning of the catalyst by pore blocking (bromoalkyl species) and/or causing migration and sintering of the metal nanocluster outside the mesoporous of the support. Neither H_2O_2 nor H_2O were observed when the SBA15 was grafted before Pd and Au deposition. The reduction performed at 573 K after the grafting process could induce a partial disproportionation of the bromopropyl groups, leading to coke formation and poisoning of the catalyst. Thermogravimetric Analysis (TGA) measurements confirmed this hypothesis. Weight loss upon heating of the catalyst reduced after Br grafting was 37% lower compared to the

catalysts obtained with the reverse procedure, i.e. grafting the catalysts after active metals deposition, suggesting that partial decomposition of the organic chains occurred during reduction of the PdAu-Br/SBA15 catalyst.

Performances of SBA15-based catalysts were also compared to non-ordered SiO_2-based catalysts, Figure 3.16. The synergetic effect of Pd and Au observed with SBA15 supported catalysts was not observed when using silica as support. Compared to the PdAu/Si, the monometallic Pd/Si catalyst displayed both higher selectivity and productivity, though at lower H_2 conversion. However, the performance of these catalysts was generally lower than that shown by the non-grafted SBA15 supported one, confirming the advantage of using an ordered mesoporous support.

3.4.2 Al, Ti and CeO_2-SBA15 modified catalysts

Starting from the consolidated knowledge that an acid environment favors the H_2O_2 direct synthesis[1, 2, 37, 63], the catalyst displaying the best performance (PdAu/SBA15) was further modified. Three different surface modifiers were chosen: incorporation of Al into the framework is known to give Brønsted acidity[64], CeO_2 adds Lewis acidity[65, 66] while Ti gives mild oxidizing property[67, 68]. H_2O_2 concentrations obtained in batch experiments with PdAu/M-SBA15 (M = Al, Ti and CeO_2) are reported in Figure 3.17.

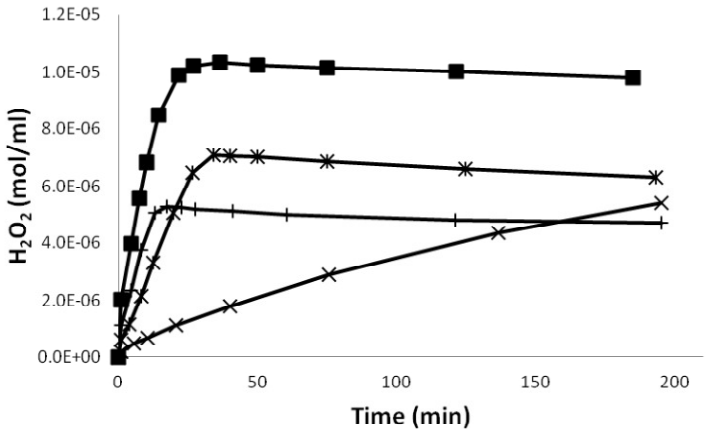

Figure 3.17 H_2O_2 concentration in batch reactor: PdAu/Al-SBA15 (■), PdAu/CeO_2-SBA15 (*), PdAu/Ti-SBA15 (+), Br-PdAu/Al-SBA15 (x). Conditions: T = 283 K, P = 1.75 MPa.

Modifying the support with Al gave the best results, both in terms of productivity and selectivity. Compared with the corresponding unmodified catalyst, the productivity was increased by 37% with comparable selectivity and H_2 conversion. Modification of the support

with CeO_2 or Ti impaired the catalytic performances, decreasing both selectivity and productivity values. A catalytic test was also carried out with the best catalyst (PdAu/Al-SBA15) modified by an addition of bromine (Br-PdAu/Al-SBA15). Bromine was grafted after the deposition of the active metals on the support, whereas the reverse procedure revealed the deactivation of the catalyst. However, doping the catalyst decreased the selectivity and resulted in a drop of productivity by one order of magnitude, confirming the poisoning already observed with the unmodified SBA15-based catalysts. Different surface analysis techniques were carried out on the catalysts to explain these results. All except the Br-PdAu/Al-SBA15 catalysts demonstrated comparable particle size distributions where most of the nanoclusters had a diameter close to that of the support pores (i.e. 6-7 nm) and only occasionally showing diameters up to 25 nm. This confirms that a good control of the nanocluster size was achieved using SBA15 as support. The particle size distributions were almost unchanged in the spent catalysts, confirming the stability of the metal nanoclusters at reaction conditions. A comparison of PdAu/Al-SBA15 with Br-PdAu/Al-SBA15 demonstrated that a broader particle size distribution was obtained after bromine doping (clusters between 6 and 22 nm). The metal nanoparticles possibly migrated on the catalyst surface and agglomerate into larger clusters upon bromine modification. The bromine also caused a noticeable sintering of metal nanoclusters after use. The broader nanocluster size distribution and the poorer stability of the metal nanoclusters are deemed responsible for the lower activity of the bromine containing catalyst. Compared to the other catalysts, the PdAu/CeO_2-SBA15 revealed a more homogeneous surface, where the support channels were less clearly distinguishable. This difference in the surface structure is possibly due the presence of CeO_2. All SBA15-based catalysts were prepared via a direct synthesis method[56], except CeO_2 modification, carried out by a post-synthesis method. The high CeO_2 loading (20 wt%) may have caused partial pore blocking. To verify this hypothesis, nitrogen physisorption (BET method) measurements were carried out on the catalysts. The specific surface area of the PdAu/M-SBA15 (M = Al and Ti) catalysts resulted in 600 m^2/g. Only the CeO_2-modified catalyst had a lower area of 430 m^2/g, confirming partial pore blocking caused by the CeO_2 doping. The decreased available surface area can also be responsible for the lower activity of this particular catalyst.

FT-IR spectroscopy by means of pyridine adsorption was performed on these catalysts to characterize the Lewis and Brønsted acidity present. The presence of Brønsted and/or Lewis acid sites was confirmed in the modified supports. The enhanced performance of the

PdAu/Al-SBA15 catalyst can be explained by the presence of Brønsted acid sites: hydrogenation of H_2O_2 is suppressed when the peroxide is surrounded by protons[2, 63], and hence the increased Brønsted acidity as a result of increased Al (modifier) enhanced the peroxide productivity.

3.5 Pd/K2621 catalysts

Another series of catalysts was synthesized supporting Pd on an acidic, macroporous resin (Lewatit K2621). Two series of experiments were carried out batchwise at 283 K, using catalyst amounts in the range 0.075-0.5 g (Pd content 1 wt.%) and catalysts with Pd content in the range 0.3-5 wt.% (catalysts quantity 0.15 g). A careful analysis excluded any mass transfer limitation. Results of the former series of experiments are shown in Figure 3.18, whereas Figure 3.19 reports the results of the latter series.

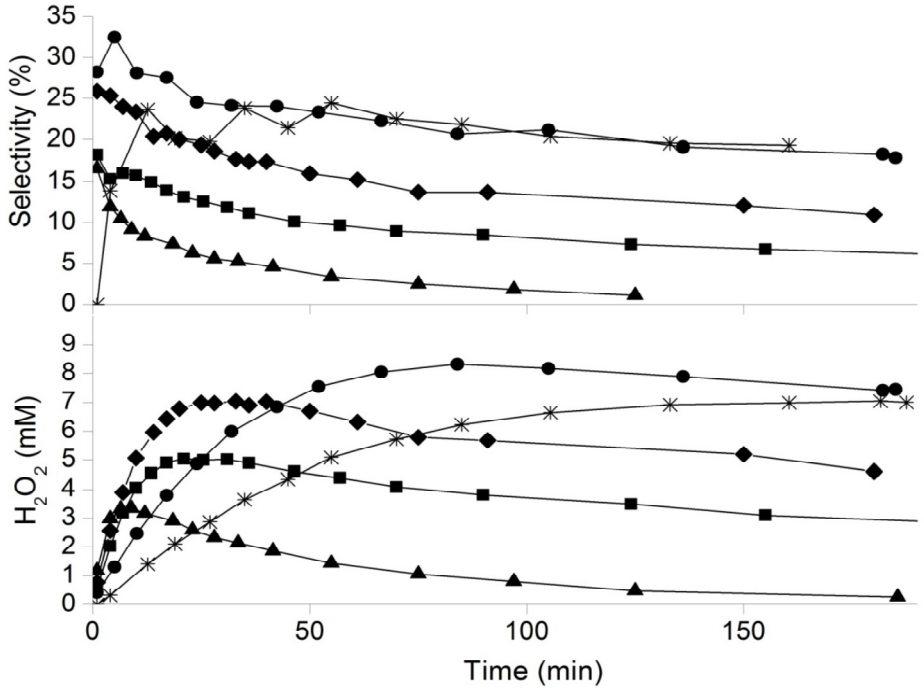

Figure 3.18. H_2O_2 concentration and selectivity in batch experiments with different amount of 1 wt.% Pd/K2621 catalyst: * 0.075 g; ● 0.11 g; ♦ 0.15 g; ■ 0.3 g; ▲ 0.5 g.

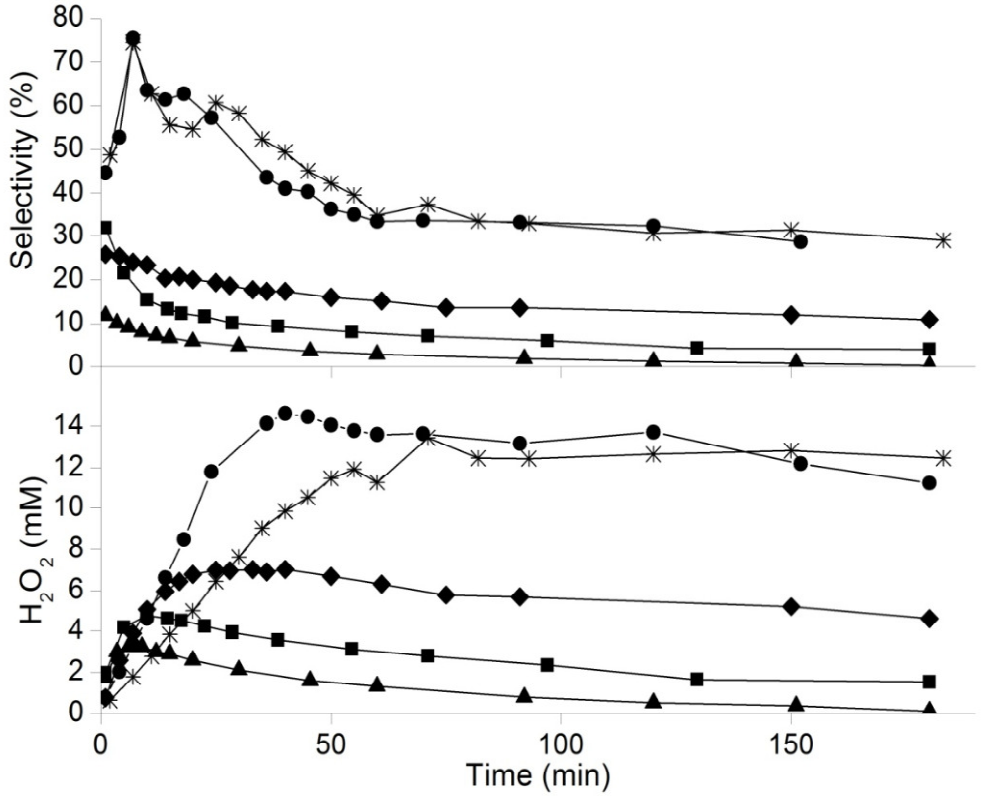

Figure 3.19. H_2O_2 concentration and selectivity in batch experiments with different Pd loading on K2621 support: * 0.3 wt.%; ● 0.5 wt.%; ♦ 1 wt.%; ■ 2.5 wt.%; ▲ 5 wt.%. Catalyst amount: 0.15 g.

Enhancing the catalyst quantity had a two-fold effect (Figure 3.18). H_2O_2 production rate increased with the catalyst amount, i.e. the H_2O_2 peak was reached more rapidly. More surprisingly, the maximum peroxide concentration decreased enhancing the catalyst quantity in the reactor. The selectivity was also impaired enhancing the catalyst quantity. This is unexpected, since the amount of catalyst should similarly affect all the reactions involved in the direct synthesis process, with unchanged selectivity. Enhancing the Pd wt.% had a similar effect (Figure 3.19), resulting in an increased H_2O_2 production rate and in a decreased maximum peroxide concentration. Accordingly, the lower the Pd content, the higher the selectivity. Interestingly, value as high as 60% were obtained with 0.3-0.5 wt.% Pd at short contact time. Average particle size and surface oxidation state of the used catalysts were accessed by TEM and XPS analysis, respectively. Both H_2O_2 selectivity and productivity increased increasing the nanocluster diameter, as shown in Figure 3.20 (a).

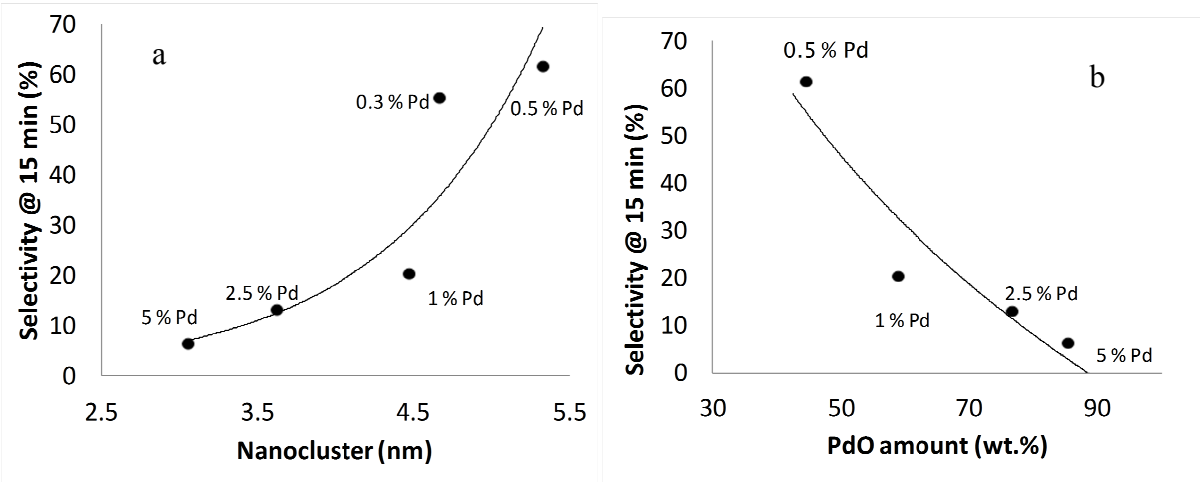

Figure 3.20. Performance of Pd/K2621 catalysts with different Pd loadings: H_2O_2 selectivity at 15 min of reaction as a function of Pd nanocluster size (a) and PdO amount (b).

Small Pd particles, containing highly energetic defects, edges and corners, likely favored the cleavage of the O-O bonding, hence favoring the undesired formation of H_2O[41, 51]. XPS analysis of the catalysts after reaction reveled that catalysts with lower Pd loading were pourer in surface Pd oxide and favored the H_2O_2 formation (Figure 3.20 (b)). Difference of surface Pd oxide are likely due to the different H_2/Pd ratio in the catalytic test. This could also explain the results shown in Figure 3.18: decreasing the amount of catalyst also lowers the H_2/Pd ratio. However, at the time of writing, analysis on these results were still in progress.

4 Conclusions

Hydrogen solubility was investigated in three different systems: pure methanol, CO_2 + CH_3OH and CO_2 + CH_3OH + O_2 at temperatures between 268 K and 288 K and for pressure up to 3.49 MPa. For all studied conditions, the solubility of hydrogen in the liquid phase increased with H_2 partial pressure, as expected. A linearity of hydrogen concentration with hydrogen partial pressure was confirmed, likely due to the low solubility of H_2. In both ternary CO_2 + CH_3OH + H_2 and quaternary CO_2 + CH_3OH + O_2 + H_2 systems, increasing the temperature resulted in an enhanced hydrogen solubility at the same H_2 partial pressure. In the presence of CO_2, concentration of hydrogen in the liquid phase was significantly larger than in pure methanol at the same H_2 fugacity, with an enhancement factor as high as 2.1 (at CO_2/CH_3OH molar ratio = 0.3). A model based on Pr-EoS was proposed for the estimation of H_2 Henry's constant as a function of temperature and CO_2/CH_3OH molar ratio, useful to predict H_2 solubility in H_2O_2 direct synthesis kinetic studies, where hydrogen is introduced as the limiting reagent, due to safety reasons.

A batch apparatus for the direct synthesis of hydrogen peroxide was developed to safely operate outside flammability limits. A 5% Pd on carbon commercial catalyst was used for direct synthesis experiments. An enhanced H_2O_2 production was obtained adopting different H_2 feeding policies, although selectivity did not exceeded 30%. A relation between selectivity and the hydrogen dissolved in the liquid phase was suggested.

A kinetic analysis was performed to identify the role of each reaction involved in the complex reaction mechanism. Batchwise direct synthesis, hydrogenation and disproportionation data were collected at temperatures in the range 258 – 297 K and pressure between 1.4 and 2.0 MPa (depending on the temperature) using a commercial 5% Pd on carbon catalyst in a methanolic solution and in the absence of halides and acids. A model of a gas bubbling, batch slurry reactor for H_2O_2 direct synthesis was formulated, including mass transfer resistances between gas and liquid and bulk of the liquid-catalyst surface. A sensitivity analysis on the mass transfer coefficients to allow for uncertainties in the correlations proved that no resistances in the liquid occur, while gas-liquid H_2 transfer rate may be limiting, although unlikely, requiring that literature coefficients overestimate the real transfer rate by an order of

magnitude. Comparable activation energies close to 45 kJ mol^{-1} were observed for H_2O production, hydrogenation and disproportionation, while H_2O_2 synthesis had a different temperature dependence (23 kJ mol^{-1}), suggesting that a higher selectivity is achievable at low temperature. Disproportionation had a very limited influence on the overall peroxide production rate, with $R_d/R_{ds} > 0.5$ only at high H_2 conversion, when the direct synthesis reaction slows down. Hydrogenation was the preferred path of H_2O_2 degradation as its reaction rate rapidly increased with H_2 conversion. Water formation was always significant, prevailing ($R_{wf}/R_{ds} > 1$) at higher temperature, whereas lower temperature favors the direct synthesis ($R_{wf}/R_{ds} < 1$). Independent investigations on disproportionation in the absence of H_2 confirmed the results, whereas H_2O_2 hydrogenation experiments (carried out in the absence of O_2) highlighted significant difference in the kinetics. This observation seems to confirm the influence of dissolved H_2 in the direct synthesis process, apparently due to different oxidation states of the catalyst.

Further investigations on the catalyst properties were carried out. Pd and PdAu catalysts supported on mesoporous ordered SBA15 and doped M-SBA15 (M = Al, Ti and CeO_2) were synthesized. A good control of both the catalysts dispersion and nanoparticle stability was achieved using SBA15. A synergetic effect between Pd and Au was observed when comparing mono- and bimetallic SBA15-based catalysts, both bromine-grafted and unmodified. However, the selectivity decreased when bromine was incorporated in the catalysts. Possibly the introduction of relatively bulky bromoalkyl–species caused the blocking/poisoning of the catalyst. The performance of the unordered SiO_2 based catalysts was inferior compared to the ordered mesoporous ones, confirming the advantage of using the latter support. The catalyst showing the best performance (PdAu/SBA15) was modified to gain more surface acidity. Higher productivity and slightly higher selectivity were achieved incorporating Al into the framework, likely due to the increased number of Brønsted acid sites including Al into the support framework.

Catalysts supported on a strongly acidic, macroporous resin (Lewatit K2621) were prepared by ion-exchange method. Different active metal (Pd) contents, as well as different amounts of catalyst, were tested batchwise. Results revealed that smaller nanoclusters favor the production of H_2O, likely due to their O-O bond breaking aptitude. Further, preliminary analysis suggest that the reduced form of Pd is more active than the oxidized form in promoting the selective hydrogenation to H_2O_2.

Many paths have been opened as logical continuation of this work. More investigations are suggested to identify the most suitable surface mechanism describing the overall process. A semi-batch apparatus, with a continuous gas phase bubbling through a static liquid, is being considered to study the dependence of the reaction rates on H_2 and O_2 partial pressures, and hence access the partial reaction orders. Literature density functional theory calculations could help to developed a reaction mechanism also accounting for adsorption of reagents (ether associative or dissociative), desorption of products and reaction intermediates.

A relation between selectivity and the oxidation state of the active metal has been proposed. Different reaction conditions could help to better understand the role of the Pd oxide, for instance using O_2 as the limiting reagent. The reduced state of the catalyst would be this way maintained during the reaction, possibly favouring a higher selectivity.

An experimental study on Pd single crystals with different surface structures could help to identify the best catalyst structure and optimize the selectivity. Moreover, Pd is well known to form hydride in the presence of H_2, whose catalytic properties are still little known. An investigation on model catalysts (where the surface/volume ratio is very small) is encouraged to understand the role that the bulk of the active metal has in the DS process. These tasks will provide useful insights to developed a better catalyst.

This work has shown that the direct synthesis of hydrogen peroxide is a feasible process and the results achieved are very promising. The ultimate goal should be the implementation and optimization of a continuous process, for a cost-effective in situ production. In that sense, a microreactor is being considered to operate safely even within flammability limits at high H_2 concentrations.

5 References

1. Campos-Martin, J. M.; Blanco-Brieva, G.; Fierro, J. L. G. Hydrogen Peroxide Synthesis: An Outlook beyond the Anthraquinone Process. *Angewandte Chemie International Edition* **2006**, *42,* 6962-6984.

2. Samanta, C. Direct synthesis of hydrogen peroxide from hydrogen and oxygen: An overview of recent developments in the process. *Applied Catalysis A: General* **2008**, *2,* 133-149.

3. Centi, G.; Perathoner, S.; Abate, S. Direct Synthesis of Hydrogen Peroxide: Recent Advances. In *Modern Heterogeneous Oxidation Catalysis;* Wiley-VCH Verlag GmbH & Co. KGaA: 2009; Vol. 33, pp 253-287.

4. Piqueras, C. M.; García-Serna, J.; Cocero, M. J. Estimation of lower flammability limits in high-pressure systems. Application to the direct synthesis of hydrogen peroxide using supercritical and near-critical CO_2 and air as diluents. *Journal of Supercritical Fluids* **2011**, *1,* 33-40.

5. Pashkova, A.; Dittmeyer, R.; Kaltenborn, N.; Richter, H. Experimental study of porous tubular catalytic membranes for direct synthesis of hydrogen peroxide. *Chem. Eng. J.* **2010**, *3,* 924-933.

6. Edwards, J. K.; Solsona, B.; Ntainjua N, E.; Carley, A. F.; Herzing, A. A.; Kiely, C. J.; Hutchings, G. J. Switching off hydrogen peroxide hydrogenation in the direct synthesis process. *Science* **2009**, *5917,* 1037-1041.

7. Menegazzo, F.; Signoretto, M.; Manzoli, M.; Boccuzzi, F.; Cruciani, G.; Pinna, F.; Strukul, G. Influence of the preparation method on the morphological and composition properties of Pd-Au/ZrO_2 catalysts and their effect on the direct synthesis of hydrogen peroxide from hydrogen and oxygen. *Journal of Catalysis* **2009***, 1,* 122-130.

8. Menegazzo, F.; Burti, P.; Signoretto, M.; Manzoli, M.; Vankova, S.; Boccuzzi, F.; Pinna, F.; Strukul, G. Effect of the addition of Au in zirconia and ceria supported Pd catalysts for the direct synthesis of hydrogen peroxide. *Journal of Catalysis* **2008***, 2,* 369-381.

9. Voloshin, Y.; Halder, R.; Lawal, A. Kinetics of hydrogen peroxide synthesis by direct combination of H_2 and O_2 in a microreactor. *Catalysis Today* **2007***, 1–2,* 40-47.

10. Inoue, T.; Kikutani, Y.; Hamakawa, S.; Mawatari, K.; Mizukami, F.; Kitamori, T. Reactor design optimization for direct synthesis of hydrogen peroxide. *Chem. Eng. J.* **2010***, 3,* 909-914.

11. Abate, S.; Lanzafame, P.; Perathoner, S.; Centi, G. SBA-15 as a support for palladium in the direct synthesis of H_2O_2 from H_2 and O_2. *Catalysis Today* **2011***, 1,* 167-174.

12. Abate, S.; Arrigo, R.; Schuster, M. E.; Perathoner, S.; Centi, G.; Villa, A.; Su, D.; Schlögl, R. Pd nanoparticles supported on N-doped nanocarbon for the direct synthesis of H_2O_2 from H_2 and O_2. *Catalysis Today* **2010***, 1–4,* 280-285.

13. Burato, C.; Campestrini, S.; Han, Y.; Canton, P.; Centomo, P.; Canu, P.; Corain, B. Chemoselective and re-usable heterogeneous catalysts for the direct synthesis of hydrogen peroxide in the liquid phase under non-explosive conditions and in the absence of chemoselectivity enhancers. *Applied Catalysis A: General* **2009***, 2,* 224-231.

14. Rueda, T. M.; Serna, J. G.; Alonso, M. J. C. Direct production of H_2O_2 from H_2 and O_2 in a biphasic $H_2O/scCO_2$ system over a Pd/C catalyst: Optimization of reaction conditions. *The Journal of Supercritical Fluids* **2012**, *0,* 119-125.

15. Biasi, P.; Menegazzo, F.; Pinna, F.; Eränen, K.; Salmi, T. O.; Canu, P. Continuous H_2O_2 direct synthesis over PdAu catalysts. *Chem. Eng. J.* **2011**, 172-177.

16. Moreno, T.; García-Serna, J.; Plucinski, P.; Sánchez-Montero, M. J.; Cocero, M. J. Direct synthesis of H_2O_2 in methanol at low pressures over Pd/C catalyst: Semi-continuous process. *Applied Catalysis A: General* **2010**, *1-2,* 28-33.

17. Voloshin, Y.; Lawal, A. Kinetics of hydrogen peroxide reduction by hydrogen in a microreactor. *Applied Catalysis A: General* **2009**, *1,* 9-16.

18. Jessop, P. G.; Subramaniam, B. Gas-Expanded Liquids. *Chem. Rev.* **2007**, *6,* 2666-2694.

19. Savage, P. E.; Gopalan, S.; Mizan, T. I.; Martino, C. J.; Brock, E. E. Reactions at supercritical conditions: Applications and fundamentals. *AIChE J.* **1995**, *7,* 1723-1778.

20. Subramaniam, B. Gas-expanded liquids for sustainable catalysis and novel materials: Recent advances. *Coord. Chem. Rev.* **2010**, *15–16,* 1843-1853.

21. Choudhary, V. R.; Sansare, S. D.; Gaikwad, A. G. Direct Oxidation of H_2 to H_2O_2 and Decomposition of H_2O_2 Over Oxidized and Reduced Pd-Containing Zeolite Catalysts in Acidic Medium. *Catalysis Letters* **2002**, *1-2,* 81-87.

22. Chinta, S.; Lunsford, J. H. A mechanistic study of H_2O_2 and H_2O formation from H_2 and O_2 catalyzed by palladium in an aqueous medium. *Journal of Catalysis* **2004**, *1,* 249-255.

23. Lunsford, J. H. The direct formation of H_2O_2 from H_2 and O_2 over palladium catalysts. *Journal of Catalysis* **2003***, 1–2,* 455-460.

24. Melada, S.; Rioda, R.; Menegazzo, F.; Pinna, F.; Strukul, G. Direct synthesis of hydrogen peroxide on zirconia-supported catalysts under mild conditions. *Journal of Catalysis* **2006***, 2,* 422-430.

25. Landon, P.; Collier, P. J.; Papworth, A. J.; Kiely, C. J.; Hutchings, G. J. Direct formation of hydrogen peroxide from H_2/O_2 using a gold catalyst. *Chem. Commun.* **2002***, 18,* 2058.

26. Landon, P.; Collier, P. J.; Carley, A. F.; Chadwick, D.; Papworth, A. J.; Burrows, A.; Kiely, C. J.; Hutchings, G. J. Direct synthesis of hydrogen peroxide from H_2 and O_2 using Pd and Au catalysts. *Physical Chemistry Chemical Physics* **2003***, 9,* 1917-1923.

27. Edwards, J. K.; Solsona, B. E.; Landon, P.; Carley, A. F.; Herzing, A.; Kiely, C. J.; Hutchings, G. J. Direct synthesis of hydrogen peroxide from H_2 and O_2 using TiO_2-supported Au-Pd catalysts. *Journal of Catalysis* **2005***, 1,* 69-79.

28. Edwards, J. K.; Solsona, B.; Landon, P.; Carley, A. F.; Herzing, A.; Watanabe, M.; Kiely, C. J.; Hutchings, G. J. Direct synthesis of hydrogen peroxide from H_2 and O_2 using Au-Pd/Fe_2O_3 catalysts. *Journal of Materials Chemistry* **2005***, 43,* 4595-4600.

29. Li, G.; Edwards, J.; Carley, A. F.; Hutchings, G. J. Direct synthesis of hydrogen peroxide from H_2 and O_2 using zeolite-supported Au-Pd catalysts. *Catalysis Today* **2007***, 3-4,* 361-364.

30. Edwards, J. K.; Thomas, A.; Solsona, B. E.; Landon, P.; Carley, A. F.; Hutchings, G. J. Comparison of supports for the direct synthesis of hydrogen peroxide from H_2 and O_2 using Au-Pd catalysts. *Catalysis Today* **2007***, 3-4,* 397-402.

31. Li, G.; Edwards, J.; Carley, A. F.; Hutchings, G. J. Direct synthesis of hydrogen peroxide from H_2 and O_2 using zeolite-supported Au catalysts. *Catalysis Today* **2006**, *4 SPEC. ISS.,* 369-371.

32. Li, G.; Edwards, J.; Carley, A. F.; Hutchings, G. J. Direct synthesis of hydrogen peroxide from H_2 and O_2 and in situ oxidation using zeolite-supported catalysts. *Catalysis Communications* **2007**, *3,* 247-250.

33. Solsona, B. E.; Edwards, J. K.; Landon, P.; Carley, A. F.; Herzing, A.; Kiely, C. J.; Hutchings, G. J. Direct Synthesis of Hydrogen Peroxide from H_2 and O_2 Using Al_2O_3 Supported Au−Pd Catalysts. *Chem. Mater.* **2006**, *11,* 2689-2695.

34. Chen, M.; Kumar, D.; Yi, C.; Goodman, D. W. The Promotional Effect of Gold in Catalysis by Palladium-Gold. *Science* **2005**, *5746,* 291-293.

35. Dissanayake, D. P.; Lunsford, J. H. The direct formation of H_2O_2 from H_2 and O_2 over colloidal palladium. *Journal of Catalysis* **2003**, *1,* 113-120.

36. Dissanayake, D. P.; Lunsford, J. H. Evidence for the Role of Colloidal Palladium in the Catalytic Formation of H_2O_2 from H_2 and O2. *Journal of Catalysis* **2002**, *2,* 173-176.

37. Han, Y.; Lunsford, J. H. Direct formation of H_2O_2 from H_2 and O_2 over a Pd/SiO_2 catalyst: the roles of the acid and the liquid phase. *Journal of Catalysis* **2005**, *2,* 313-316.

38. Liu, Q.; Lunsford, J. H. The roles of chloride ions in the direct formation of H_2O_2 from H_2 and O_2 over a Pd/SiO_2 catalyst in a H_2SO_4/ethanol system. *Journal of Catalysis* **2006**, *1,* 237-243.

39. Moreno, T.; García-Serna, J.; Cocero, M. J. Decomposition reaction of H_2O_2 over Pd/C catalyst in an aqueous medium at high pressure: Detailed kinetic study and modelling. *Journal of Supercritical Fluids* **2011***, 3,* 227-235.

40. Choudhary, V. R.; Samanta, C. Role of chloride or bromide anions and protons for promoting the selective oxidation of H_2 by O_2 to H_2O_2 over supported Pd catalysts in an aqueous medium. *Journal of Catalysis* **2006***, 1,* 28-38.

41. Abate, S.; Centi, G.; Melada, S.; Perathoner, S.; Pinna, F.; Strukul, G. Preparation, performances and reaction mechanism for the synthesis of H_2O_2 from H_2 and O_2 based on palladium membranes. *Catalysis Today* **2005***, 2–4,* 323-328.

42. Liu, Q.; Lunsford, J. H. Controlling factors in the direct formation of H_2O_2 from H_2 and O_2 over a Pd/SiO_2 catalyst in ethanol. *Applied Catalysis A: General* **2006***, 1,* 94-100.

43. Samanta, C.; Choudhary, V. R. Direct synthesis of H_2O_2 from H_2 and O_2 over Pd/H-beta catalyst in an aqueous acidic medium: Influence of halide ions present in the catalyst or reaction medium on H_2O_2 formation. *Catalysis Communications* **2007***, 1,* 73-79.

44. Choudhary, V. R.; Samanta, C.; Gaikwad, A. G. Drastic increase of selectivity for H_2O_2 formation in direct oxidation of H_2 to H_2O_2 over supported Pd catalysts due to their bromination. *Chemical Communications* **2004***, 18,* 2054-2055.

45. Blanco-Brieva, G.; Cano-Serrano, E.; Campos-Martin, J. M.; Fierro, J. L. G. Direct synthesis of hydrogen peroxide solution with palladium-loaded sulfonic acid polystyrene resins. *Chem. Commun.* **2004***, 10,* 1184.

46. Burato, C.; Centomo, P.; Rizzoli, M.; Biffis, A.; Campestrini, S.; Corain, B. Functional Resins as Hydrophilic Supports for Nanoclustered Pd(0) and Pd(0)-Au(0) Catalysts Designed

for the Direct Synthesis of Hydrogen Peroxide. *Advanced Synthesis & Catalysis* **2006**, *1-2,* 255-259.

47. Ntainjua N., E.; Edwards, J. K.; Carley, A. F.; Lopez-Sanchez, J. A.; Moulijn, J. A.; Herzing, A. A.; Kiely, C. J.; Hutchings, G. J. The role of the support in achieving high selectivity in the direct formation of hydrogen peroxide. *Green Chemistry* **2008**, *11,* 1162-1169.

48. Ghedini, E.; Menegazzo, F.; Signoretto, M.; Manzoli, M.; Pinna, F.; Strukul, G. Mesoporous silica as supports for Pd-catalyzed H_2O_2 direct synthesis: Effect of the textural properties of the support on the activity and selectivity. *Journal of Catalysis* **2010**, *2,* 266-273.

49. Melada, S.; Pinna, F.; Strukul, G.; Perathoner, S.; Centi, G. Direct synthesis of H_2O_2 on monometallic and bimetallic catalytic membranes using methanol as reaction medium. *Journal of Catalysis* **2006**, *2,* 213-219.

50. Melada, S.; Pinna, F.; Strukul, G.; Perathoner, S.; Centi, G. Palladium-modified catalytic membranes for the direct synthesis of H_2O_2: preparation and performance in aqueous solution. *Journal of Catalysis* **2005**, *1,* 241-248.

51. Deguchi, T.; Iwamoto, M. Reaction mechanism of direct H_2O_2 synthesis from H_2 and O_2 over Pd/C catalyst in water with H+ and Br− ions. *Journal of Catalysis* **2011**, *2,* 239-246.

52. Inoue, T.; Schmidt, M. A.; Jensen, K. F. Microfabricated multiphase reactors for the direct synthesis of hydrogen peroxide from hydrogen and oxygen. *Industrial and Engineering Chemistry Research* **2007**, *4,* 1153-1160.

53. Abate, S.; Perathoner, S.; Centi, G. Deactivation mechanism of Pd supported on ordered and non-ordered mesoporous silica in the direct H_2O_2 synthesis using CO_2-expanded methanol. *Catalysis Today* **2012***, 1,* 170-177.

54. Meyberg, M.; Roessler, F. In Situ Measurement of Steady-State Hydrogen Concentrations during a Hydrogenation Reaction in a Gas-Inducing Stirred Slurry Reactor. *Ind Eng Chem Res* **2005***, 25,* 9705-9711.

55. Schärringer, P.; Müller, T. E.; Kaltner, W.; Lercher, J. A. In Situ Measurement of Dissolved Hydrogen during the Liquid-Phase Hydrogenation of DinitrilesMethod and Case Study. *Ind Eng Chem Res* **2005***, 25,* 9770-9775.

56. Zhao, D.; Huo, Q.; Feng, J.; Chmelka, B. F.; Stucky, G. D. Nonionic Triblock and Star Diblock Copolymer and Oligomeric Surfactant Syntheses of Highly Ordered, Hydrothermally Stable, Mesoporous Silica Structures. *Journal of the American Chemical Society* **1998***, 24,* 6024-6036.

57. Emeis, C. A. Determination of Integrated Molar Extinction Coefficients for Infrared Absorption Bands of Pyridine Adsorbed on Solid Acid Catalysts. *Journal of Catalysis* **1993***, 2,* 347-354.

58. Descamps, C.; Coquelet, C.; Bouallou, C.; Richon, D. Solubility of hydrogen in methanol at temperatures from 248.41 to 308.20 K. *Thermochimica Acta* **2005***, 1–2,* 1-7.

59. Katayama, T.; Nitta, T. Solubilities of hydrogen and nitrogen in alcohols and n-hexane. *J. Chem. Eng. Data* **1976***, 2,* 194-196.

60. Bezanehtak, K.; Dehghani, F.; Foster, N. R. Vapor−Liquid Equilibrium for the Carbon Dioxide + Hydrogen + Methanol Ternary System. *J. Chem. Eng. Data* **2004***, 3,* 430-434.

61. Lopez-Castillo, Z.; Aki, S. N. V. K.; Stadtherr, M. A.; Brennecke, J. F. Enhanced Solubility of Hydrogen in CO_2-Expanded Liquids. *Industrial and Engineering Chemistry Research* **2008***, 3,* 570-576.

62. Edwards, J. K.; Carley, A. F.; Herzing, A. A.; Kiely, C. J.; Hutchings, G. J. Direct synthesis of hydrogen peroxide from H_2 and O_2 using supported Au-Pd catalysts. *Faraday Discussions* **2008**, 225-239.

63. Park, S.; Lee, J.; Song, J. H.; Kim, T. J.; Chung, Y.; Oh, S.; Song, I. K. Direct synthesis of hydrogen peroxide from hydrogen and oxygen over Pd/HZSM-5 catalysts: Effect of Brönsted acidity. *Journal of Molecular Catalysis A: Chemical* **2012***, 0,* 230-236.

64. Koekkoek, A. J. J.; van Veen, J. A. R.; Gerrtisen, P. B.; Giltay, P.; Magusin, P. C. M. M.; Hensen, E. J. M. Brønsted acidity of Al/SBA-15. *Microporous and Mesoporous Materials* **2012***, 0,* 34-43.

65. Akondi, A. M.; Trivedi, R.; Sreedhar, B.; Kantam, M. L.; Bhargava, S. Cerium-containing MCM-41 catalyst for selective oxidative arene cross-dehydrogenative coupling reactions. *Catalysis Today* **2012***, 1,* 35-44.

66. Timofeeva, M. N.; Jhung, S. H.; Hwang, Y. K.; Kim, D. K.; Panchenko, V. N.; Melgunov, M. S.; Chesalov, Y. A.; Chang, J. -. Ce-silica mesoporous SBA-15-type materials for oxidative catalysis: Synthesis, characterization, and catalytic application. *Applied Catalysis A: General* **2007***, 1,* 1-10.

67. Chen, S.; Tang, C.; Lee, J.; Jang, L.; Tatsumi, T.; Cheng, S. Effect of calcination on the structure and catalytic activities of titanium incorporated SBA-15. *Journal of Materials Chemistry* **2011***, 7,* 2255-2265.

68. Trukhan, N. N.; Romannikov, V. N.; Shmakov, A. N.; Vanina, M. P.; Paukshtis, E. A.; Bukhtiyarov, V. I.; Kriventsov, V. V.; Danilov, I. Y.; Kholdeeva, O. A. H_2O_2-based selective oxidations over titaniumsilicates of SBA-15 type. *Microporous and Mesoporous Materials* **2003***, 2–3,* 73-84.

6 Publications

I

J. Chem. Thermodynamics 54 (2012) 1–9

Contents lists available at SciVerse ScienceDirect

J. Chem. Thermodynamics

journal homepage: www.elsevier.com/locate/jct

Review

H_2 solubility in methanol in the presence of CO_2 and O_2

Nicola Gemo [a,b], Pierdomenico Biasi [b], Tapio O. Salmi [b], Paolo Canu [a,*]

[a] Dipartimento di Principi e Impianti di Ingegneria Chimica "I. Sorgato" (DIPIC), University of Padova, via Marzolo 9, 35131 Padova, Italy
[b] Process Chemistry Centre (PCC), Laboratory of Industrial Chemistry and Reaction Engineering, Åbo Akademi, Biskopsgatan 8, 20500 Turku, Finland

ARTICLE INFO

Article history:
Received 19 January 2012
Received in revised form 15 March 2012
Accepted 17 March 2012
Available online 27 March 2012

Keywords:
Hydrogen solubility
CO_2-expanded liquid
$CO_2 + CH_3OH + O_2 + H_2$

ABSTRACT

Hydrogen solubility in methanol, (methanol + carbon dioxide) and (methanol + carbon dioxide + oxygen) was measured and correlated at different temperatures ($268 < T/K < 288$) and pressures ($0.37 < P/MPa < 3.5$). Hydrogen content in the liquid phase was measured using a gas absorption method and Fugatron HYD-100 instrument. Experiments were performed in a fixed volume cell at constant temperature and hydrogen content was varied with subsequent loadings in the cell environment. At all conditions investigated a linear relation between hydrogen partial pressure and concentration was observed. Results were correlated and generalized as Henry's constants for H_2, as a function of temperature and CO_2/methanol overall ratio. Correlation and generalization of the measurements was provided through a thermodynamic model, based on Peng–Robinson equation of state with van der Waals mixing rules and Boston–Mathias α-function. H_2 solubility in methanol was confirmed to grow with temperature and amount of CO_2; at constant H_2 partial pressure, O_2 does not affect H_2 solubility.

Contents

1. Introduction . . . 01
2. Experimental . . . 02
 2.1. Materials . . . 02
 2.2. Apparatus . . . 02
 2.3. H_2 solubility measurements . . . 02
 2.4. Procedures . . . 03
  2.4.1. Binary system . . . 03
  2.4.2. Ternary systems . . . 04
  2.4.3. Quaternary systems . . . 04
3. Results and discussion . . . 04
 3.1. $H_2 + CH_3OH$ . . . 05
 3.2. $CO_2 + CH_3OH + H_2$ . . . 05
 3.3. $CO_2 + CH_3OH + O_2 + H_2$ . . . 06
4. Modelling . . . 07
5. Conclusions . . . 08
 Acknowledgments . . . 09
 References . . . 09

1. Introduction

Systems involving CO_2-expanded liquids are a current topic in modern chemical synthesis. Besides advantages due to the mixture physical properties, mainly related to marked modifications of the vapour–liquid equilibrium (VLE), CO_2 brings about a reduced impact on environment and minimization of safety issues [1,2]. Both homogeneously and heterogeneously [1–4] catalyzed reactions have been tested in CO_2 expanded solvents. Research interest is especially focused on reactions limited by a poor solubility of reactant gas, such as hydrogenations [5–7] and oxidations [8–10]. Reaction rates may also take advantage of CO_2 enhanced transport properties [1] (*i.e.*, diffusivities and viscosity) in addition to the

* Corresponding author. Fax: +39 049 8275461.
E-mail address: paolo.canu@unipd.it (P. Canu).

0021-9614/$ - see front matter © 2012 Elsevier Ltd. All rights reserved.
http://dx.doi.org/10.1016/j.jct.2012.03.021

increased solubility of reactant gases. Chen *et al.* [6], while studying the hydrogenation of *p*-chloronitrobenzene in CO_2-expanded methanol, found a conversion enhancement when operating with CO_2 that they referred to an increase in hydrogen solubilization. Musie *et al.* [9,10] carried out homogeneous oxidations in CO_2-expanded solvents; they measured reaction rates 1 to 2 orders or magnitude larger than with a pure organic solvent as reaction medium, suggesting that a larger O_2 solubility due to CO_2 was the cause. Other authors [11–13] explained the enhancement of H_2 and O_2 solubility by the increased free volume in the solution caused by dissolved CO_2. Our motivation is specifically based on the interest in H_2O_2 direct synthesis reaction, where proper estimation of the phase equilibria of H_2, O_2, CO_2 and methanol, is crucial in optimizing the reaction conditions and determining the intrinsic reaction kinetics.

A significant number of vapour–liquid equilibrium data is available for *binary* systems involving the four species (H_2, O_2, CO_2, and CH_3OH) of our interest [14–24]. Only few data were published for *ternary* systems including both CO_2 and CH_3OH, *i.e.*, (CO_2 + CH_3OH + H_2) and (CO_2 + CH_3OH + O_2). Measurements of the (CO_2 + CH_3OH + H_2) system at T = 313 K were reported by Xie *et al.* [25] and Lopez-Castillo *et al.* [11] The same combination was also investigated by Bezanehtak *et al.* [26] at T = 278, 288 and 298 K. Vapour–liquid equilibrium data for the (CO_2 + CH_3OH + O_2) ternary system are available only at T = 313 K [12]. No data were found for the *quaternary* mixture (CO_2 + CH_3OH + O_2 + H_2). The latter system has crucial importance on hydrogen peroxide direct synthesis [27–31], whereas the above mentioned gases are dissolved in a liquid phase (*i.e.*, methanol) with H_2 acting as the limiting reagent. Up to now, the lack of information on vapour-liquid equilibria makes it difficult to obtain a precise kinetic description of the reactions involved in this process, where solubility modifications confuse with kinetics. Under H_2 poor conditions, often prevailing in H_2–O_2 mixtures to operate outside the (lower) flammability limit, H_2 solubility is the key information required. In this work, solubility data for hydrogen in methanol, in (CO_2 + CH_3OH) and in (CO_2 + CH_3OH + O_2) are collected and critically compared with available literature data, within the range 268 < T / K < 288 and total pressures between 1 and 3.5 MPa (H_2 partial pressure, P_H, varied between 0 and 1 MPa). Measurements of hydrogen solubility were carried out in a fixed volume cell. In addition to the standard gas absorption method, we also used the Fugatron HYD-100 instrument, which allows measuring hydrogen concentration in the liquid phase in the reactor environment [32,33].

2. Experimental

2.1. Materials

The chemicals used in the present work (see table 1) were carbon dioxide and oxygen with a certified purity of 0.9999 in mole fraction (Oy AGA Ab, Espoo, Finland), hydrogen with a mole fraction certified purity of 0.99999 (Oy AGA Ab, Espoo, Finland) and methanol (0.998 mol fraction purity, J.T. Baker). All materials were used as received.

TABLE 1
Specification of the chemicals used in this study.

Chemical name	Source	Certified purity/mole fraction[a]
Carbon dioxide	AGA	0.9999
Oxygen	AGA	0.9999
Hydrogen	AGA	0.99999
Methanol	J.T. Baker	0.998

[a] No further purification was done before use.

2.2. Apparatus

Measurements of hydrogen solubility in binary (H_2 + CH_3OH), ternary (CO_2 + CH_3OH + H_2) and quaternary (CO_2 + CH_3OH + O_2 + H_2) systems were performed using the experimental setup schematically described in scheme 1.

The equilibrium cell is a stainless steel, fixed volume autoclave (Parr Instrument) equipped with a mechanical stirrer (Heidolph RZR 2021). The accessible gas volume was 636 cm^3, including piping, precisely measured according to the procedure described below. Temperature inside the equilibrium cell was controlled with an external flow of heating/cooling fluid (B. Braun, Thermomix UB/Frigomix) and monitored with a K-type thermocouple (accuracy ±1 K) connected to a digital temperature indicator. Pressure was monitored with a Keller PA-21R pressure transducer (accuracy ±0.01 MPa). CO_2 and O_2 were transferred to the system directly from the cylinders via a throttle valve. H_2 flow during each sequential injection was tightly controlled for reproducibility with mass flow meters (Brooks Instruments 5850 E Series). In addition, a constant volume (59 cm^3) vessel was used between the H_2 bottle and the mass flow controller (scheme 1). Loaded with H_2 at a pressure higher than the measuring cell, it double checks the amount of H_2 fed to the reactor, determined from pressure difference inside the H_2 vessel before and after the loading and the quantity fed through the mass flow controller.

Methanol was degassed using an Agilent 1100 series degasser and then introduced in the system via a high pressure piston metering pump (Eldex Laboratories, Inc).

2.3. H_2 solubility measurements

An *in situ* technique using Fugatron HYD-100 was adopted to measure the hydrogen solubility, in view of its use to monitor and control hydrogenation reactions at comparable conditions. The instrument has been coupled to gas absorption measurements for calibration, the latter remaining the reference technique used. Fugatron HYD-100 allows continuous, in situ measurements of H_2 solubilized in a liquid phase [32,33]. It is based on a probe immersed in the liquid phase, with a rigid, dense membrane internally purged with a carrier gas (nitrogen) flowing at 10 $Ncm^3 \cdot min^{-1}$. Hydrogen permeates the membrane and is brought to a gas detector by the carrier gas. Hence, a small amount of hydrogen continuously flows through the probe to the detector. Hydrogen loss for the analysis was evaluated by integrating the instrument measurement and the amount loss was less than 0.2% of the total H_2 introduced during each experiment. Accordingly, pressure in the equilibrium vessel within the experimental time does not show any detectable loss due to the instrument uptake. The instrument reading also reached a very stable value after any hydrogen addition to the equilibrium cell. Both evidences confirm that the H_2 loss for the analysis was not detectable and had no significant influence on measurements.

Prior to the experimental campaign, the cross-sensitivity with methanol, oxygen and carbon dioxide was explored. No signal was observed when the probe was immersed in the mixture without H_2 being present, proving the selectivity of the membrane and excluding any interference with others species.

The instrument provides a measurement linearly proportional to the H_2 concentration in the liquid. While this could be enough to monitor H_2 consumption in hydrogenation reactions [32], relating actual H_2 concentration to the initial value, here we need an absolute measure. Accordingly, we calibrated the instrument with the gas absorption method.

The method is based on the estimation of the amount of H_2 in a given liquid mixture volume (*i.e.*, its liquid phase concentration), from experimental measurements. These are the total amount of H_2 in the cell and that in the vapour phase above the liquid. Besides

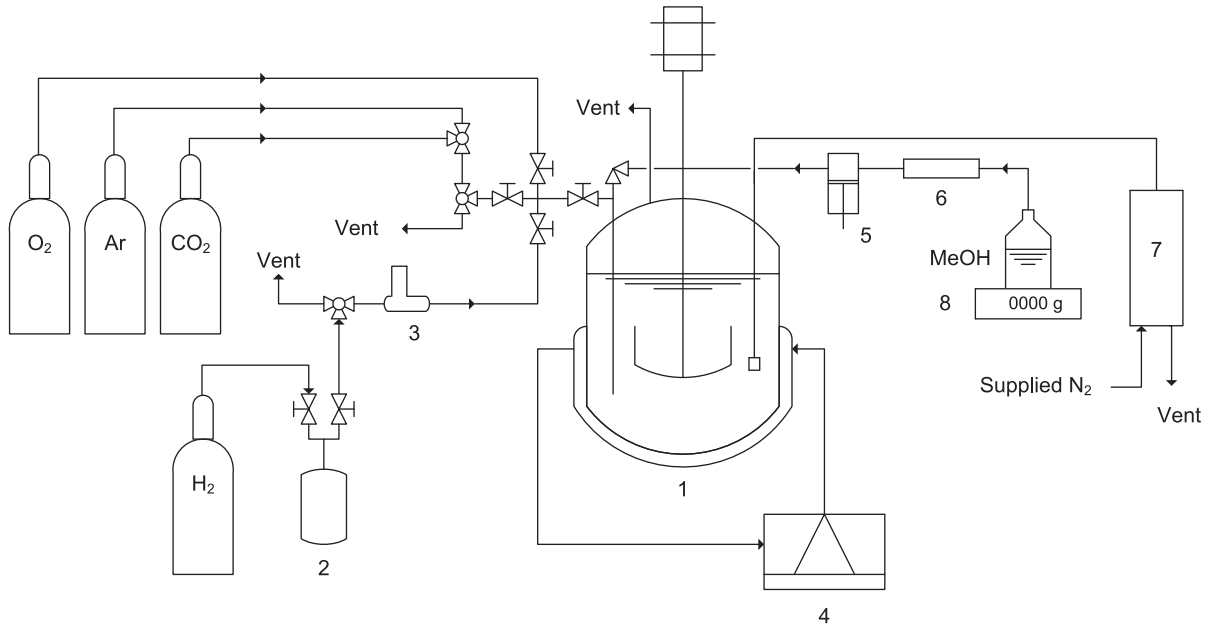

SCHEME 1. Experimental apparatus: 1, Equilibrium vessel; 2, hydrogen reservoir; 3, hydrogen mass flow controller; 4, temperature control; 5, methanol pump; 6, Degasser; 7, Fugatron HYD-100 H_2 analyzer; 8, precision balance.

the simple case of binary H_2/CH_3OH mixtures, the estimation is not obvious, due to the non-ideal behaviour of the gas phase that includes CO_2, at the temperature and pressure domain investigated. Accordingly, the estimation strategies vary for binary, ternary and quaternary systems, as explained in the Procedures section.

Comparison between the hydrogen concentration (c_{H_2}) measured and reading of the Fugatron instrument provides the calibration constant [32], *f*:

$$f = c_{H_2}/q, \tag{1}$$

where *q* is the instrument reading, *i.e.*, mole fraction of hydrogen in the carrier gas behind the membrane, reaching the gas detector in the instrument. The calibration constant *f* is indeed quite sensitive to temperature, so that *f*(*T*) has actually been determined. On the other hand, it is not affected by total pressure and liquid phase composition, as mentioned above.

2.4. Procedures

Precise knowledge of net available volumes (equilibrium cell and H_2 vessel) is mandatory for an accurate estimation of gas amounts. Connection pipes and internals, such as stirring system and Fugatron probe, make the accessible volume different from the nominal. Accurate volume measurements before the experimental campaign were carried out using an auxiliary vessel with a precisely determined volume (1000 cm^3), connected to the equilibrium cell through an on/off valve, thus assembling an overall volume only partially known. Air inside both vessels was evacuated pressuring and depressurizing with N_2 up to 0.3 MPa, repeated three times. Then, the equilibrium cell alone was filled with N_2 up to 2 MPa and equilibrated at $T = 293$ K. The valve connecting the two vessels was then opened to slowly transfer N_2 inside the secondary vessel, of known volume. Once stabilized, pressure and temperature were measured again. Using the ideal gas law, volume of the equilibrium cell was calculated from the initial and final pressures and temperature measurements, given that the amount of N_2 remains constant. The same procedure was adopted to measure the volume of the H_2 reservoir. The procedure was repeated four times with a standard deviation < 1.5%.

Then, equilibrium configurations at different temperatures, pressures and composition were studied with sequential additions of a given species (H_2, CO_2, and O_2), suitably adjusting the procedure to minimize uncertainties, as specified below. Whenever compatible with the procedure, methanol was fed last, after each gas, to prevent solubility disturbing the gas quantification by pressure.

2.4.1. Binary system

The liquid phase concentration of hydrogen in ($CH_3OH + H_2$) system was evaluated at $T = 278$ K and variable pressure, up to 1.56 MPa with the purpose of validating our procedures and methods against literature data. Equilibrium vessel and piping were swept first by cycling (three times) pressurization (0.3 MPa) and evacuation (0.1 MPa) with argon. The procedure was repeated 3 times with H_2 to evacuate argon and set the initial amount of H_2 in the equilibrium cell, precisely determined by pressure, temperature, available cell volume and ideal gas law. An accurately weighed amount of methanol (typically 330 g) was introduced later, with a metering pump. Stirring (1000 rpm) was turned on; after approx. one hour the pressure and Fugatron reading were definitely stable, proving that VLE and instrument steady-state were fully set.

Hydrogen was further introduced with several additions of approx. 0.4 MPa from the dedicated vessel, to investigate the composition space. After each H_2 addition, its amount in the vapour phase of the equilibrium vessel was recalculated by the ideal gas equation, using the equilibrium temperature and pressure, and the net gas phase volume (total accessible vessel volume subtracted the volume of the methanol initially loaded). We assumed that the partial pressure of methanol in the gas phase was negligible, at the relatively low temperature investigated. Based on available correlations for pure methanol vapour pressure, in the worst case (T /K = 278 and P /MPa = 0.37) the mole fraction of methanol in the vapour phase is less than 1.5%, decreasing below 0.35% at the highest pressure. The imbalance between moles of H_2 added ($n_{H_2}^{added}$) and moles in the gas phase ($n_{H_2}^{G}$) gives the amount of H_2 in the liquid phase, $n_{H_2}^{L}$:

$$n^{L}_{H_2} = n^{added}_{H_2} - n^{G}_{H_2}. \quad (2)$$

Hydrogen concentration in the liquid phase, C_{H_2}, and Henry's law constant, H_{H_2}, are then calculated from definitions:

$$C_{H_2} = n_{H_2}/V^{L}, \quad (3)$$

$$H_{H_2} = P_{H_2}/C_{H_2}. \quad (4)$$

We further assumed that the small amount of solubilized hydrogen does not modify significantly the liquid mixture volume [14]. Hence, the volume of the liquid phase (V^L) was calculated by the molar density of pure methanol at the temperature of interest [34]. Measured C_{H_2} also provide valuable data to calibrate the Fugatron instruments, *i.e.*, $f(T)$ identification, to reliably use it in other conditions.

2.4.2. Ternary systems

The liquid phase concentration of hydrogen in (CO_2 + CH_3OH + H_2) ternary system was measured at T = 268, 278 and 288 K varying hydrogen partial pressure, while keeping the same CO_2/CH_3OH overall ratio. Before each experiment, the empty vessel and piping were purged three times by cycling pressure (up to 0.3 MPa) with CO_2. The vessel was thermally equilibrated at T = 293 K and pressure continuously logged. Eventually, the measuring vessel was filled with CO_2 up to a pressure of 3.9 MPa. The total amount of CO_2 in the cell was evaluated with its gas density, calculated with the Peng–Robinson equation of state [35] (PR-EoS) and the available vessel volume. Though the initial amount of CO_2 is estimated by way of a calculated property, thus not exactly a measurement, the accuracy of the PR-EoS for a single phase/single component calculation of gas density sufficiently far from supercritical conditions is quite good. Methanol was then introduced in the equilibrium cell as explained for binary systems. It should be noticed that loading CO_2 as a gas, before any liquid is present in the cell, allows to accurately dose its amount as well as that of methanol; the reverse (feeding the liquid before the gas) does not allow to calculate the CO_2 fed by pressure measurements in the cell, because of its rapid and extensive solubilization.

The vessel was then brought to the desire temperature ($268 < T/K < 288$) and stirring (1000 rpm). After less than 30 min temperature and pressure were stable, confirming the faster dissolution rate of CO_2.

Methanol is known as a CO_2 expanding solvent [1,3,4,11] especially approaching supercritical conditions [1]. The volume expansion depends only on CO_2 dissolved in the liquid phase [13–17], and it can be significant. At given pressure, temperature and total amount of each species (CO_2 and CH_3OH) inside the cell, both phases thermodynamic state (including composition and densities) has been determined with a binary flash calculation, using a $\phi-\phi$ approach and PR-EoS. Further details on the thermodynamic model are given below. The volume increment due to CO_2 swelling was calculated as +10% by PR-EoS. Estimates from available experimental data [14] at our CO_2 liquid phase mole fraction suggest a larger volume increment of +18% compared to pure methanol. We trusted the measurements, using the 18% increment for further calculation, assuming the EoS estimation of liquid volume to be less reliable. Keeping the CO_2 and CH_3OH constant, CO_2 liquid phase composition varied less that 3.3%, within the investigated temperature range, because of H_2 (and then pressure) increments, resulting in a negligible variation in methanol volume enhancement, according to literature [13–17].

After equilibrating methanol and CO_2, known amounts of H_2 were introduced from its storage vessel, with consecutive additions, up to a maximum H_2 partial pressure of 1.27 MPa (gas phase mole fraction up to 57%). The amount of H_2 in the gas phase of the cell after each addition was estimated by the increment of pressure in the cell after equilibration and consequently the amount of H_2 in the liquid phase by difference with the amount fed. As above, we assumed that H_2 does not affect the liquid phase volume [14].

Due to the broader temperature range investigated in the (CO_2 + CH_3OH + H_2) combination, solubility measurements supply the single temperature binary data to calibrate the Fugatron instrument, using H_2 liquid phase concentration obtained with gas absorption method, as previously described.

2.4.3. Quaternary systems

The liquid phase concentration of hydrogen in (CO_2 + CH_3OH + O_2 + H_2) was measured at T = 268 and 278 K. Before each experiment, the system was purged with 0.3 MPa of O_2 three times, as already explained. Once purging was completed, 0.8 MPa of O_2 was added in the measuring vessel full of O_2. Moles of O_2 added were calculated using the ideal gas law (PR EoS confirms). The CO_2 was then loaded into the vessel filled with O_2, adding the same 3.9 MPa used in ternary experiments, up to a total pressure of 4.8 MPa. The density of (O_2 + CO_2) gas mixture at specified conditions was computed with PR EoS and used to estimate the total amount of CO_2 introduced. Again, a known amount of methanol was injected through the metering pump. The mixture was cooled at the desired experimental temperature. Stirring the mixture at 1000 rpm stabilized temperature and pressure readings in less than 1 h. As for binary and ternary systems, hydrogen was introduced last, with successive injections, up to a maximum partial pressure of 0.86 MPa, and maximum gas phase mole fraction of 57%. The concentration of H_2 in the liquid phase of the cell after each addition was estimated as in the ternary case, using the liquid CO_2/CH_3OH mixture volume estimated from literature, assuming that the small amounts of H_2 and O_2 dissolved did not affect the liquid volume.

3. Results and discussion

We investigated hydrogen solubility in three different (binary, ternary and quaternary) species combinations: (H_2 + CH_3OH), (CO_2 + CH_3OH + H_2) and (CO_2 + CH_3OH + O_2 + H_2). The quaternary data are completely original, while the other combinations investigated are reported in the literature, as well binary as combinations of the four species other than (H_2 + CH_3OH) that we did not investigate experimentally. Literature data provide the opportunity to

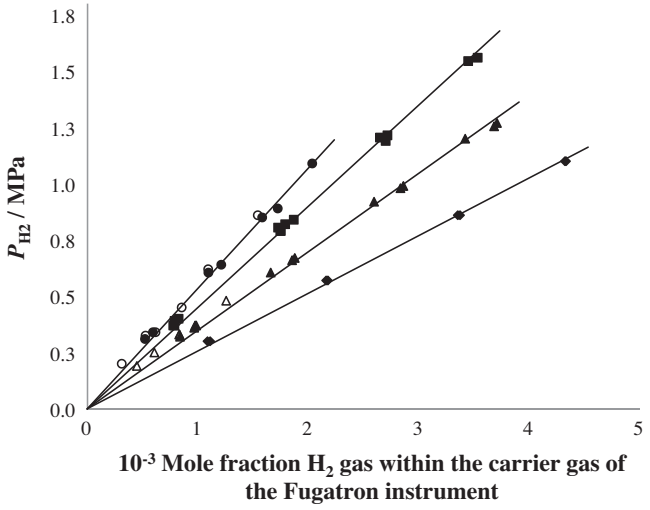

FIGURE 1. Plot of Fugatron readings vs. H_2 partial pressure. H_2 + CH_3OH at T = 278 K (■); CO2 + CH_3OH + H_2 at 288 K (♦), 278 K (▲), and 268 K (●); CO_2 + CH_3OH + O_2 + H_2 at 278 K (Δ) and 268 K (○).

TABLE 2
$CH_3OH + H_2$ binary system. Liquid phase H_2 concentration measured at different hydrogen partial pressures, at $T = 278$ K.

P_{H_2}/MPa	$10^{-5}\ C_{H_2}$/(mol·cm^{-3})
0.37	1.31
0.37	1.27
0.39	1.27
0.40	1.23
0.79	2.61
0.79	2.59
0.81	2.65
0.82	2.60
0.84	2.83
1.19	4.02
1.21	3.95
1.22	4.03
1.55	5.10
1.56	5.21

Error in C_{H_2} is $0.01 \cdot 10^{-5}$ mol·cm^{-3}.

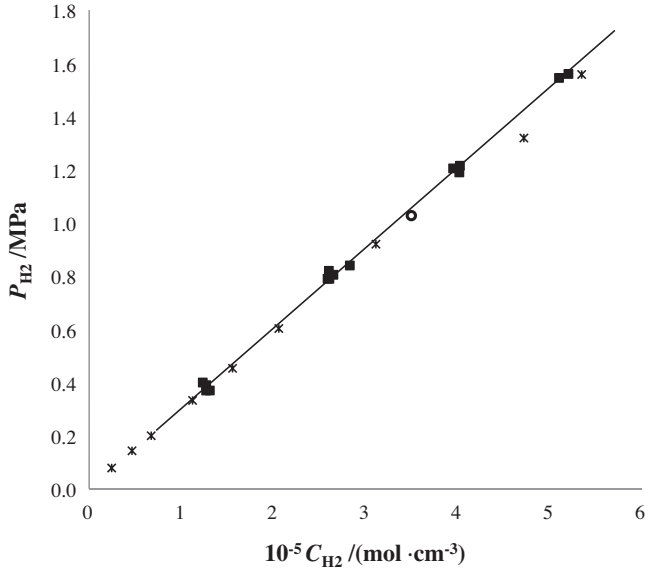

FIGURE 2. $CH_3OH + H_2$ binary system. Plot of concentration of hydrogen in liquid methanol as a function of its partial pressure above the liquid, at $T = 278$ K. ■, This work; ∗, Descamps *et al.* [23]; ○, calculated from data of Katayama *et al.* [24].

calibrate a thermodynamic model (estimation of binary interaction parameters) to correlate ternary and quaternary data, in addition of validating our experimental methods.

Before presenting and discussing each single set of data, we show in figure 1 all the original data of H_2 partial pressure in the gas phase vs. H_2 mole fractions in the carrier gas behind the membrane (Fugatron HYD-100 readings). Linearity is evident for all systems, at the conditions investigated, notwithstanding the wide range of H_2 concentration in the gas phase investigated (up to 57%). In addition, the data confirm the insensitivity of the permeation instrument to the total pressure, whose effect should cause a significant curvature, which is clearly not the case. Since Fugatron readings are themselves proportional to C_{H_2} [32], the observed linearity also confirms the validity of Henry's law at all examined conditions, caused by a rather small solubility of H_2 in the liquid.

We can also anticipate from figure 1 that the H_2 solubility at given partial pressure of hydrogen in the gas and temperature is extremely close, whether O_2 is present or not, suggesting that no H_2–O_2 interactions occurs in the liquid phase.

In the following, raw instrument measurements, q, will be converted to C_{H_2} given the calibration function $f(T)$ determined above, by absorption measurements, for the purpose of calculating the Henry's constant and its dependencies.

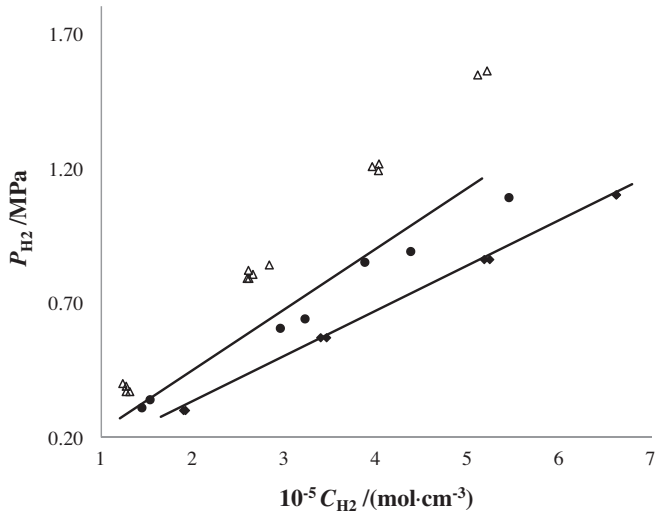

FIGURE 3. $CO_2 + CH_3OH + H_2$ ternary system. Solubility data of hydrogen: ♦, $T = 288$ K; ▲, 278 K; ●, 268 K; solid line, Peng–Robinson EoS after tuning k_{ij}; Δ, $H_2 + CH_3OH$ binary at 278 K.

3.1. $H_2 + CH_3OH$

Table 2 reports values of hydrogen liquid phase concentrations measured at $T = 278$ K according to the procedure described above, *i.e.*, progressively increasing the amount of hydrogen in the atmosphere above methanol.

Plotting experimental C_{H_2} against P_{H_2} (figure 2) allows determining the average Henry's constant as the slope of the resulting linear interpolating function (*i.e.*, Henry's law, $C_{H_2} = H_{H_2} \cdot P_{H_2}$), including the origin for physical consistency. The determined value of the Henry's constant is (30.14 ± 1.02) (MPa·m^3·kmol^{-1}), where the error is one standard deviation of the error between calculated H_{H_2} and individual values. This value is quite close to 29.36 (MPa·m^3·kmol^{-1}) calculated from data reported by Katayama *et al.* [24] at the same temperature. It also compares well to 28.39 (MPa·m^3·kmol^{-1}) measured by Descamps *et al.* [23], who carried out a thorough analysis of literature studies on this system. They already reported that literature estimates differ [14–16], even at comparable conditions, concluding that discrepancies are likely due to the analytical techniques and to the small amount of water always present in methanol. At any rate, figure 2 shows that our measurements compare well with those of Descampes [23] and Katayama [24]. Our data for CH_3OH–H_2 provide the opportunity to validate our procedures and the analytical technique.

3.2. $CO_2 + CH_3OH + H_2$

Experimental results for the $(CO_2 + CH_3OH + H_2)$ ternary system at $T = 268$, 278 and 288 K are listed in table 3. At each temperature, a number of combinations of H_2 partial pressure were screened, by sequential additions of hydrogen.

Hydrogen concentration in the liquid phase as a function of its partial pressure is shown in figure 3. Average Henry's law constants calculated as above with the collected data are (16.7 ± 0.43), (18.9 ± 0.67) and (20.1 ± 0.95) (MPa·m^3·kmol^{-1}), respectively at $T = 288$ K, 278 K and 268 K. A linear interpolation of the $H_{H_2}(T)$ dependency yields H_{H_2} /(MPa·m^3·kmol^{-1}) = 65.8–0.17 T /K. The hydrogen solubility increases with temperature (lower H_{H_2}), as typical of H_2 in CH_3OH. It is also apparent that the hydrogen solu-

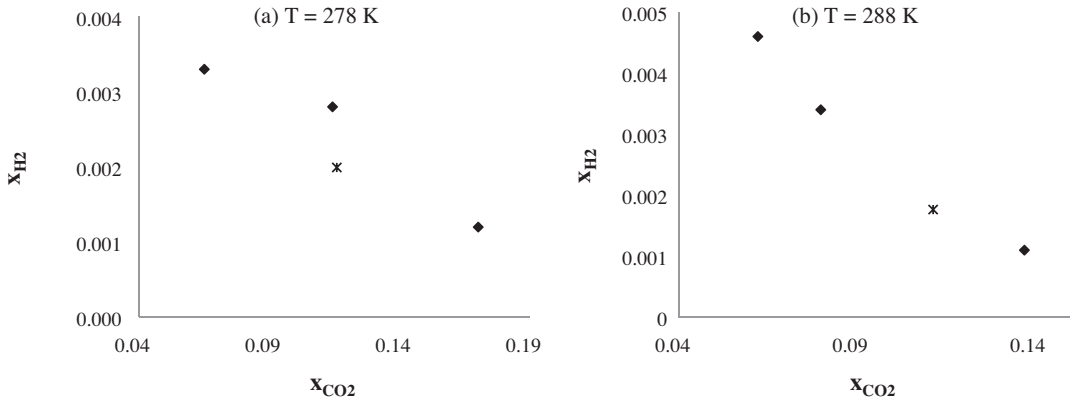

FIGURE 4. $CO_2 + CH_3OH + H_2$ ternary system. Comparison of H_2 solubility measurements with literature data at 2 MPa (a, T = 278 K; b, 288 K): ♦, Bezanehtak *et al.* [26]; ∗, this work.

TABLE 3
$CO_2 + CH_3OH + H_2$ ternary system. Values of the measured and calculated (PR-EoS) liquid phase concentration of H_2 at different hydrogen overall concentration, temperature, and total pressure.

T /K	P /MPa	P_{H_2} /MPa	$10^{-5}\ C^{Exp}_{H_2}$ /(mol·cm^{-3})	$10^{-5}\ C^{Calc}_{H_2}$ /(mol·cm^{-3})	ΔC_{H_2} /%
288	1.60	0.30	1.90	1.79	5.8
	1.60	0.30	1.92	1.79	6.8
	1.87	0.57	3.39	3.40	0.1
	1.87	0.57	3.46	3.40	1.8
	2.16	0.86	5.18	5.12	1.0
	2.16	0.86	5.24	5.20	2.2
	2.40	1.10	6.62	6.55	1.0
	2.40	1.10	6.6	6.55	0.9
278	1.42	0.32	1.77	1.64	7.1
	1.44	0.37	1.80	1.90	5.4
	1.44	0.36	1.81	1.85	2.2
	1.71	0.61	3.24	3.11	4.0
	1.74	0.67	3.37	3.44	2.0
	1.74	0.66	3.33	3.39	1.7
	2.02	0.92	4.93	4.73	4.1
	2.06	0.99	5.12	5.08	0.7
	2.06	0.98	5.09	5.03	1.1
	2.30	1.20	6.36	6.16	3.1
	2.34	1.27	6.61	6.52	1.3
	2.34	1.26	6.65	6.45	3.1
268	1.13	0.31	1.44	1.38	4.6
	1.17	0.34	1.53	1.51	1.4
	1.43	0.61	2.95	2.69	9.0
	1.47	0.64	3.22	2.84	11.8
	1.67	0.85	3.87	3.77	2.6
	1.72	0.89	4.37	3.95	9.7
	1.91	1.09	5.44	4.84	11.2

Error in $C^{Exp}_{H_2}$ is $0.01 \cdot 10^{-5}$ mol·cm^{-3}.

bility increases compared to binary system, at the same hydrogen partial pressure. This is attributed to the presence of carbon dioxide: enhancements of H_2 solubility by CO_2 up to 80% has been reported in many organic solvent [24], including methanol. In our conditions, comparing data at T = 278 K we have an increment of 37% due to the use of CO_2.

Figure 4 compares our data (liquid phase mole fractions calculated with PR-EoS tuned on our measurements, as explained below) with those reported by Bezanehtak *et al.* [26] at the same temperature and total pressure, showing quite a good agreement. Interestingly, their data show a decreasing H_2 liquid mole fraction whit that of CO_2 increases, against the known evidence that CO_2 increases H_2 solubility. According to the authors, this is an apparent contradiction due to their experimental protocol, where a larger CO_2 amount in the whole V–L cell causes a smaller partial pressure of H_2 in the vapour phase, also lowering its amount in the liquid.

We point out that the data reported by Bezanehtak *et al.* [26] were measured at 2 MPa. Since our data were measured at slightly different pressure, H_2 concentrations shown in figure 4b were linearly interpolated from data at 1.87 and 2.16 MPa (see table 3).

3.3. $CO_2 + CH_3OH + O_2 + H_2$

Table 4 reports the experimental data of hydrogen solubility for the quaternary ($CO_2 + CH_3OH + O_2 + H_2$) system, measured at T = 268 and 278 K. Figure 5 shows the experimental values as a function of hydrogen partial pressure. Calculated Henry's law constants are (18.24 ± 0.89) and (20.88 ± 1.71) (MPa·m^3·kmol^{-1}) at T = 278 and 268 K, respectively. Being that CO_2 liquid phase molar fraction is always the one used in the ternary case, we conclude that the addition of quite a significant amount of O_2 does not lead to any significant modification of the H_2 solubility. For sake of

TABLE 4
$CO_2 + CH_3OH + O_2 + H_2$ quaternary system. Measured and calculated liquid phase concentration of hydrogen at different hydrogen partial pressure and temperatures.

T /K	P /MPa	P_{H_2} /MPa	$10^{-5}\ C^{Exp}_{H_2}$ /(mol·cm^{-3})	$10^{-5}\ C^{Calc}_{H_2}$ /(mol·cm^{-3})	ΔC_{H_2} /%
278	3.02	0.19	0.941	1.03	9.1
	3.09	0.25	1.27	1.35	6.0
	3.16	0.33	1.75	1.78	1.9
	3.19	0.33	1.75	1.78	1.7
	3.16	0.37	2.05	2.00	2.5
	3.31	0.48	2.64	2.59	1.8
	3.49	0.66	3.72	3.56	4.1
268	2.83	0.20	0.834	0.923	10.7
	2.89	0.33	1.41	1.50	6.2
	2.97	0.34	1.65	1.57	5.2
	3.08	0.45	2.29	2.08	9.4
	3.18	0.62	2.94	2.86	2.5
	3.42	0.86	4.14	3.97	4.2

Error in $C^{Exp}_{H_2}$ is $0.01\cdot10^{-5}$ mol·cm^{-3}.

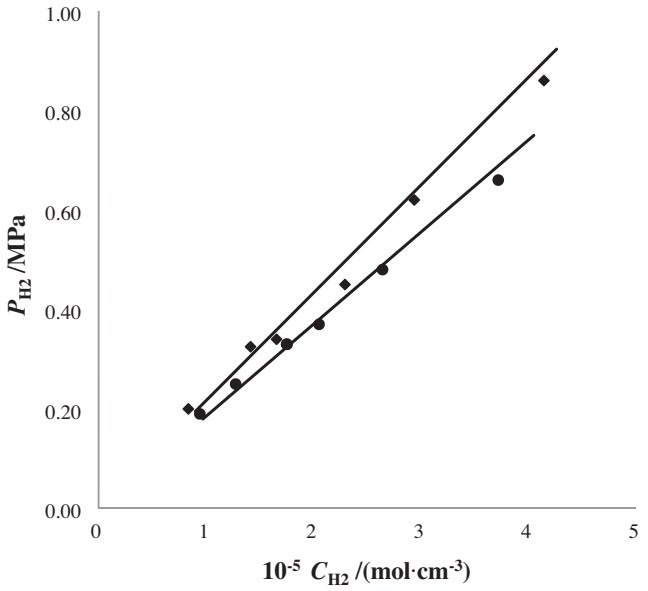

FIGURE 5. $CO_2 + CH_3OH + O_2 + H_2$ quaternary system. Solubility data of hydrogen: ●, T = 278 K; ♦, 268 K; solid line, Peng–Robinson EoS after tuning k_{ij}.

completeness, the composition of both phases according to PR EoS VLE calculations, result $x_{CO2} = 0.11$ and $0.43 < y_{O2} < 0.53$, depending on temperature and total pressure.

The negligible effect of O_2 on H_2 solubility was already anticipated, see figure 1. Accordingly, we can improve the linear interpolation of H_{H_2} (T) including quaternary data at the temperature investigated, resulting in H_{H_2} /(MPa·m^3·kmol^{-1}) = 68.3–0.18·T /K. Again, hydrogen solubility increases with increasing temperature, as known. We could not find any literature data to compare with.

4. Modelling

Besides the experimentally measured data and corresponding Henry's constants, any equilibrium state, at predefined combinations of species amount and temperature (including early steps of filling), has been characterized by a flash calculation, using a $\phi-\phi$ approach $(K_i = y_i/x_i = \phi_i^L/\phi_i^V)$ and the Peng–Robinson equation of state (PR-EoS):

$$P = \frac{RT}{V_m - b} - \frac{a}{V_m(V_m + b) + b(V_m - b)}. \tag{5}$$

Here V_m refers to the molar volume. Standard routines have been used, through a well established commercial code [36]. Calculations provide the vapour and liquid phase properties, and we focused on mole fractions. The total available amount of species is known from experiments, as well as temperature and total pressure and are given as input conditions. The calculations become predictive once EoS parameters are tuned on experimental data. Typical mixing rules of pure species parameters have been used; linear for the co-volume b and quadratic for the attractive interaction parameter a:

$$\begin{aligned} b &= \sum_{i=1}^{NC} x_i b_i, \\ a &= \sum_{i=1}^{NC}\sum_{j=1}^{NC} x_i x_j \sqrt{a_i a_j}(1 - k_{ij}),\ \ k_{ii} = 0,\ \ k_{ij} = k_{ji}, \\ b_i &= 0.07780\frac{RT_{C,i}}{P_{C,i}}, \\ a_i &= \alpha_i \cdot 0.45724\frac{R^2 T^2_{C,i}}{P_{C,i}}. \end{aligned} \tag{6}$$

Here x represent the mole fraction, while subscript i and c indicate species and critical property, respectively. Due to the presence of supercritical species (H_2 and O_2), a Boston–Mathias alpha function [37] was chosen for $\alpha_i(T)$:

$$\begin{aligned} &T_{r,i} \leqslant 1, \quad \alpha_i(T) = [1 + m_i(1 - \sqrt{T_{r,i}})]^2, \\ &T_{r,i} > 1, \quad \alpha_i(T) = \exp[c(1 - T^d_{r,i})],\ \ c = 1 + m_i/2,\ \ d = m_i/2, \\ &m_i = 0.37464 + 1.54226\omega_i - 0.26992\omega_i^2, \end{aligned} \tag{7}$$

where subscript r indicates a reduced property and ω the acentric factor. Binary interaction parameters k_{ij} have to be tuned. They are assumed to vary with temperature alone; while estimated at any temperature investigated, results (reported in table 6) were fit by the expression:

$$k_{ij} = k^1_{ij} + k^2_{ij} \cdot T. \tag{8}$$

TABLE 5
Vapour–liquid equilibrium binary data from the literature, used to estimate binary interaction parameters.

Components	T /K	References
CO_2–H_2	278–290.15–298.15	[14]
CH_3OH–H_2	298.15–323.15–373.15	[17]
CH_3OH–CO_2	273.15–290	[18]
	258	[19]
	313–320.15	[20]
O_2–CO_2	223.15/273.15	[21]
CH_3OH–O_2	298.34–323.32–348.29	[22]

TABLE 6
Mean absolute percentage error and binary interaction parameters for the Peng–Robinson equation of state in ternary and quaternary systems.

System	T /K	MAPE /%	k_{1-2}	k_{1-3}	k_{2-3}	k_{1-4}	k_{2-4}
$CH_3OH(1) + CO_2(2) + H_2(3)$	268	7.2	0.036	−0.459	0.147	/	/
	278	3.0	0.041	−0.476	0.129	/	/
	288	2.4	0.046	−0.493	0.109	/	/
$CH_3OH(1) + CO_2(2) + H_2(3) + O_2(4)$	268	7.6	0.036	−0.459	0.147	−0.046	0.099
	278	5.4	0.041	−0.476	0.129	−0.028	0.100

TABLE 7
Coefficients for temperature correlation of binary interaction parameters (equation (8)).

	O_2–MeOH	CO_2–MeOH	CO_2–O_2	CO_2–H_2	MeOH–H_2
k^1_{ij}	−5.338E−01	−9.251E−02	6.968E−02	6.568E−01	0.000E+00
k^2_{ij}	1.820E−03	4.803E−04	1.091E−04	−1.900E−03	−1.711E−03

We predicted H_2 solubility in ternary and quaternary systems using only binary interaction parameters k_{ij} calibrated on literature binary phase equilibrium data (table 5), selected to be as close as possible to our experimental conditions (T, P and liquid phase composition).

The objective function to be minimized by manipulating $k_{ij}(T)$ was based on departures between calculated and experimental liquid phase compositions. We assumed that oxygen and hydrogen interaction in the liquid phase are negligible, *i.e.*, $k_{O_2-H_2} = 0$, according to experimental indications. Comparing the optimization results in term of H_2 solubility prediction, the accuracy was quantified through the mean absolute percentage error (MAPE):

$$\mathrm{MAPE} = \frac{100}{n}\sum_{j=1}^{n}\frac{\left|C^{\mathrm{exp}}_{H_2,j} - C^{\mathrm{calc}}_{H_2,j}\right|}{C^{\mathrm{exp}}_{H_2,j}}, \tag{9}$$

where n is the number of measurements.

The model first tuned on literature binary data agrees quite well with all binary literature data. While H_2 liquid phase composition dependence on temperature and pressure in ternary and quaternary systems was reasonable, dissolution of H_2 was systematically underestimated, with a MAPE errors as high as 20%, especially at the higher temperature and pressure. Using also ternary measurements to fit k_{ij} values for (H_2 + CH_3OH), the model was significantly improved as compared to ternary experimental data. The prediction of C_{H_2} in quaternary (CO_2 + CH_3OH + O_2 + H_2) configurations was also remarkably improved. All the final binary interaction parameters estimated are reported in table 6, along with MAPE errors for all the investigated configurations and temperatures. Their correlation with temperature according to equation (8) leads to the coefficients reported in table 7. The actual comparison with our experimental data is given in tables 3 and 4 and also reported in figures 3 and 5, for ternary and binary systems, respectively. MAPE values are quite satisfactory. The calculated hydrogen liquid phase concentration of (H_2 for CO_2 + CH_3OH + H_2) system was always in an excellent agreement with experimental data, the highest MAPE error being 7% at T = 268 K. Predictions for (CO_2 + CH_3OH + O_2 + H_2) quaternary system are also remarkably good, with MAPE errors below 7.6% (table 6).

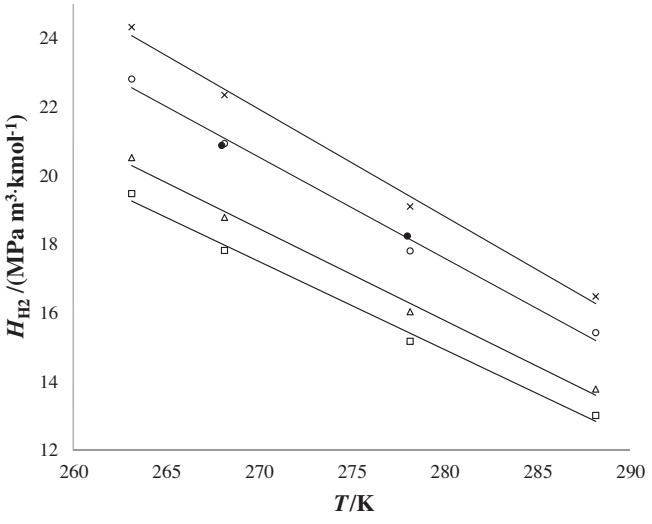

FIGURE 6. Predicted Henry's constants of hydrogen as a function of temperature and $\gamma = n_{CO_2}/n_{CH_3OH}$ calculated from PR-EoS tuned on literature and our experimental data: □, γ = 0.3; Δ, γ = 0.25; ○, γ = 0.15; ×, γ = 0.09; ●, experimental data (see Section 3, CO_2 + CH_3OH + O_2 + H_2).

The developed model allows estimating the CO_2 effect on the hydrogen solubility. Figure 6 shows calculated Henry's constants of hydrogen as a function of temperature and total CO_2/CH_3OH mole ratio, $\gamma = n_{CO_2}/n_{CH_3OH}$, according to PR-EoS tuned on literature and our experimental data.

Though predicted $H_{H_2}(T)$ appears slightly curved upwards, linear interpolations are acceptable, leading to the correlation:

$$\begin{aligned} &H_H/(\mathrm{MPa}\cdot\mathrm{m}^3\cdot\mathrm{kmol}^{-1}) = \alpha(\gamma) + \beta(\gamma)T/\mathrm{K},\\ &\alpha(\gamma) = -91.96\gamma + 114.09,\\ &\beta(\gamma) = 0.26\gamma - 0.33. \end{aligned} \tag{10}$$

We already mentioned the significant H_2 solubility enhancement due to CO_2 by comparing binary and ternary data, also shown in figure 3, confirming literature data [11,26] measured under different conditions. To measure quantitatively the advantage given by CO_2, we used the enhancement factor (EF) [12], comparing H_2 solubility without (H_2 + CH_3OH) and with CO_2 (CO_2 + CH_3OH + O_2 + H_2). EF is defined as the ratio of hydrogen composition in methanol ($x^{\mathrm{Binary}}_{H_2}$) and ($CH_3OH$ + CO_2) systems ($x^{\mathrm{Quaternary}}_{H_2}$) at the same conditions of temperature and hydrogen fugacity:

$$\mathrm{EF} = \frac{x^{\mathrm{Quaternary}}_{H_2}}{x^{\mathrm{Binary}}_{H_2}}. \tag{11}$$

Values higher than 1 indicate increased hydrogen dissolution in the liquid phase caused by carbon dioxide, and thus are desirable. According to the predictions based on this model, EF can approach 2.1 at T = 278 K and γ = 0.3.

5. Conclusions

We investigated hydrogen solubility in three different systems: pure methanol, (CO_2 + CH_3OH) and (CO_2 + CH_3OH + O_2) at temperatures between 268 and 288 K and for pressure up to 3.49 MPa. A gas absorption method was adopted along with an in situ technique using Fugatron HYD-100 instrument. Whenever possible, results were compared with available literature data, showing good agreement. For all conditions studied, the solubility of hydrogen in the liquid phase increased with H_2 partial pressure, as expected.

The linearity of hydrogen concentration with hydrogen partial pressure was confirmed by the solubility measurements (Fugatron HYD-100) and is likely due to the low solubility of H_2, in any case. In both ternary ($CO_2 + CH_3OH + H_2$) and quaternary ($CO_2 + CH_3OH + O_2 + H_2$) systems, increasing the temperature resulted in an enhanced hydrogen solubility at the same H_2 partial pressure. In the presence of CO_2, the concentration of hydrogen in the liquid phase was significantly larger than in pure methanol at the same H_2 fugacity, with an enhancement factor as high as 2.1 (at CO_2/CH_3OH molar ratio = 0.3). The experimental data were modelled with the Peng–Robinson equation of state with van der Waals mixing rules and Boston–Mathias correction; binary interaction parameters were tuned with binary data from the literature, together with our ternary measurements. The EoS-based correlation allowed development maps and the equation for H_2 Henry's constant as a function of temperature and CO_2/CH_3OH mole ratio, useful to predict the H_2 solubility in H_2O_2 direct synthesis kinetic studies, where hydrogen is introduced as the limiting reagent, due to safety reasons. This work identifies the lack of information on vapour–liquid equilibria hindering a correct description of the reaction mechanism and kinetics of the direct synthesis of hydrogen peroxide.

Acknowledgments

This work is a part of the activities at the Åbo Akademi Process Chemistry Centre (PCC) within the Finnish Centre of Excellence Programmes (2000–2005 and 2006–2011) by the Academy of Finland. Nicola Gemo gratefully acknowledges the Cariparo Foundation, the PCC (Process Chemistry Centre), Åbo Akademi, Finland, and the Johan Gadolin Scholarship for financial support.

References

[1] P.G. Jessop, B. Subramaniam, Chem. Rev. 107 (2007) 2666–2694.
[2] C.M. Piqueras, J. García-Serna, M.J. Cocero, J. Supercrit. Fluids 56 (2010) 33–40.
[3] B. Subramaniam, Coordination Chemistry Review 254 (2010) 1843–1853.
[4] P.E. Savage, S. Gopalan, T.I. Mizan, C.J. Martino, E.E. Brock, AIChE J 41 (1995) 1723–1778.
[5] G. Combes, E. Coen, F. Dehghani, N. Foster, J. Supercrit. Fluids 36 (2005) 127–136.
[6] Y.C. Chen, C.S. Tan, J. Supercrit. Fluids (2007) 272–278.
[7] E. Bogel-Łukasik, J. Wind, R. Bogel-Łukasik, M. Nunes da Ponte, J. Supercrit. Fluids (2010) 46–52.
[8] G. Musie, M. Wei, B. Subramaniam, D.H. Busch, Coord. Chem. Rev. 219 (2001) 789–820.
[9] M. Wei, G.T. Musie, D.H. Busch, B. Subramaniam, J. Am. Chem. Soc. 124 (2002) 2513–2517.
[10] M. Wei, G.T. Musie, D.H. Busch, B. Subramaniam, Green Chem. 6 (2004) 387–393.
[11] Z.K. Lopez-Castillo, N.V.K. Aki, M.A. Stadtherr, J.F. Brennecke, Ind. Eng. Chem. Res. 47 (2008) 570–576.
[12] Z.K. Lopez-Castillo, S.N.V.K. Aki, M.A. Stadtherr, J.F. Brennecke, Ind. Eng. Chem. Res. 45 (2006) 5351–5360.
[13] J.C. Chang, C. Day, C. Ko, K. Chiu, Fluid Phase Equilibria (1997) 243–258.
[14] K. Bezanehtak, G.B. Combes, F. Dehghani, N.R. Foster, D.L. Tomasko, J. Chem. Eng. Data. 47 (2002) 161–168.
[15] M. Wainwright, T. Ahn, D. Trimm, J. Chem. Eng. Data. 32 (1987) 22–24.
[16] Q. Liu, F. Takemura, A. Yabe, Chem. Eng. Data 41 (1996) 1141–1143.
[17] E. Brunner, W. Hultenschmidt, G. Schlichtharle, J. Chem. Thermodyn 19 (1987) 273–291.
[18] J.H. Hong, R. Kobayashi, Fluid Phase Equilibria 41 (1988) 269–276.
[19] Bass, J.K. Ferrell, R.W. Rousseau, Final technical report North Carolina State Univ. at Raleigh. Dept. of, Chemical Engineering, 1979, p. 1–40.
[20] Seung Nam Joung, Chang Woo Yoo, Hun Yong Shin, Sun Young Kim, Ki-Pung Yoo, Chul Soo Lee, Wan Soo Huh, Fluid Phase Equilibria 185 (2001) 219–230.
[21] A. Fredenslund, G.A. Sather, J. Chem. Eng. Data (1970) 15–17.
[22] K. Fischer, M. Wilken, J. Chem. Thermodyn. 33 (2001) 1285–1308.
[23] C. Descamps, C. Coquelet, C. Bouallou, D. Richon, Thermochim. Acta 430 (2005) 1–7.
[24] T. Katayama, T. Nitta, J. Chem. Eng. Data 21 (1976) 194–196.
[25] X. Xie, J.S. Brown, D. Bush, C.A. Eckert, J. Chem. Eng. Data 50 (2005) 780–783.
[26] K. Bezanehtak, F. Dehghani, N.R. Foster, J. Chem. Eng. Data 49 (2004) 430–434.
[27] P. Biasi, F. Menegazzo, F. Pinna, K. Eranen, P. Canu, T.O. Salmi, Ind. Eng. Chem. Res. 49 (2010) 10627–10632.
[28] F. Menegazzo, M. Signoretto, M. Manzoli, F. Boccuzzi, G. Cruciani, F. Pinna, G. Strukul, J. Catal. 268 (2009) 122–130.
[29] C. Burato, S. Campestrini, Y.F. Han, P. Canton, P. Centomo, P. Canu, B. Corain, Appl. Cat. A: Gen. 358 (2009) 224–231.
[30] C.M. Piqueras, J. García-Serna, M.J. Cocero, J. Sup. Fluids 56 (2011) 33–40.
[31] J.K. Edwards, A. Thomas, B.E. Solsona, P. Landon, A.F. Carley, G.J. Hutchings, Catal. Today 122 (2007) 397–402.
[32] M. Meyberg, F. Roessler, Ind. Eng. Chem. Res. 44 (2005) 9705–9711.
[33] P. Scharringer, T.E. Müller, W. Kaltner, J.A. Lercher, Ind. Eng. Chem. Res. 44 (2005) 9770–9775.
[34] NIST Chemistry WebBook, NIST Standard Reference Database Number 69, <http://webbook.nist.gov> (retrieved 11 January 2011).
[35] D.Y. Peng, D.B. Robinson, Ind. Eng. Chem. Fund. 15 (1976) 59–64.
[36] Aspen Properties V7.1, Aspen Technology, Inc., 200 Wheeler Road, Burlington, Massachusetts 01803.
[37] P.M. Boston, P.M. Mathias, in: Proceedings of the 2nd International Conference on Phase Equilibria and Fluid Properties in the Chemical Process Industries, West Berlin, March, 1980, pp. 823–849.

JCT 12-39

II

I&EC research
Industrial & Engineering Chemistry Research

Article

pubs.acs.org/IECR

Kinetics and Mechanism of H_2O_2 Direct Synthesis over a Pd/C Catalyst in a Batch Reactor

Pierdomenico Biasi,*[,†,‡] Nicola Gemo,[‡,†] José Rafael Hernández Carucci,[†,§] Kari Eränen,[†] Paolo Canu,[‡] and Tapio O. Salmi[†]

[†]Process Chemistry Centre (PCC), Laboratory of Industrial Chemistry and Reaction Engineering Åbo Akademi, Biskopsgatan 8, 20500, Turku, Finland

[‡]Dipartimento di Ingegneria Industriale, University of Padova, via Marzolo 9, 35131 Padova, Italy

[§]BiCHEM Technology BV, High Tech Campus 48-2, 5656 AE, Eindhoven, The Netherlands

Supporting Information

ABSTRACT: Kinetic experiments of the decomposition, hydrogenation, and direct synthesis of hydrogen peroxide were performed on a commercial Pd/C catalyst. Temperature effects and subsequent hydrogen addition were investigated without using promoters. The hydrogen amount in the liquid phase was measured online by using a Fugatron Instrument to investigate the effect of the gas on the direct synthesis. Decomposition and hydrogenation reactions were affected differently by the temperatures used during the experiments. The formation of hydrogen peroxide showed different behaviors with different hydrogen feeding policies. The hydrogen dissolved in the liquid phase measured experimentally was correlated with the hydrogen peroxide production. As the amount of dissolved hydrogen increases in the liquid phase the direct synthesis rate increases, while the reaction slows down as the hydrogen pressure is decreased. The selectivity is also affected by the H_2 recharges. Every time that hydrogen is recharged in the reactor (during the direct synthesis) the selectivity toward H_2O_2 increases. Two different methods to recharge H_2 during the reaction were analyzed. The first method consists in feeding the hydrogen when it is totally consumed, the second one in refilling hydrogen in the reactor before its total consumption. The hydrogen solubility was found as an important parameter for the direct synthesis. An explanation on hydrogen peroxide formation was given taking into account the H_2/Pd ratio.

1. INTRODUCTION

Hydrogen peroxide is an attractive oxidizing agent and its direct synthesis has been studied for many decades. Despite the efforts to find an innovative process to manufacture hydrogen peroxide from the elements, such technology has not been accomplished yet, due to problems related to flammability limits[1−4] between hydrogen and oxygen and consecutive/parallel reactions.[3,5,6] The direct synthesis consists principally in one reaction: hydrogen and oxygen are dissolved in a liquid phase and react on a solid catalyst. Although this process seems to be so simple, two consecutive reactions (i.e., decomposition and hydrogenation of hydrogen peroxide) take place over the same catalyst used for the direct synthesis.[7,8] Moreover, a parallel reaction forming water from hydrogen and oxygen can take place over the catalyst surface.

Despite numerous studies on the direct synthesis of H_2O_2, a general understanding of the mechanism, solubility problems, and how to avoid consecutive and parallels reactions without promoters has not been achieved.[9,10] The studies on the direct synthesis have mainly been focused on the catalyst design and screening; however, such tests are almost impossible to compare due to different conditions used (i.e., solvent, halides, acids, inert gases, pressure, temperature, and many others).[2,4,5,11−15] Numerous catalysts based on Pd and PdAu have been investigated[12,15−18] and different ideas have been published on the reaction mechanism and the role of each promoter, including halides and acids.[8,13,19−23] Still there is no agreement on the mechanism and conditions favoring the synthesis due to the complicated character of the system. This is the reason why a precise kinetic analysis is needed to understand the real mechanism of the direct synthesis. Kinetic studies are important to improve the operation conditions in continuous reactors, for which a complete understanding of the regimes and mechanism is needed to enhance the catalyst performance.[21,24,25] Kinetic analyses have lately started to appear in the field of direct synthesis of hydrogen peroxide.[21,24−26] However, these studies remain scarce, and more effort has to be focused on this area if the correct mechanism of the direct synthesis is to be understood.

To understand better the difficult to analyze results of different groups on hydrogen peroxide direct synthesis we report a table (Table 1) where a comparison of different works[2,12,15,23,27−32] is done. In this table, catalysts, reactors, operative conditions, additives, and results are compared. Batch reactors are adopted for catalytic tests,[12,15,29−31] semibatch reactors to investigate the operation conditions and enhance the quantity of H_2O_2 obtained,[15,29,30,32] membrane reactors and microreactors[2,27,28] to operate safely within flammability and,

Special Issue: CAMURE 8 and ISMR 7

Received: September 21, 2011
Revised: April 9, 2012
Accepted: April 9, 2012
Published: April 24, 2012

Table 1. Comparison between This Work and Different Reactor Systems[a]

ref	catalyst	reactor	liquid phase	gas composition	temperature (°C)	pressure bar	additives	productivity	selectivity (%)	H_2 conversion (%)
this work	5% Pd/C	batch	CH_3OH	H_2:O_2:CO_2 = 9.6:22.2:68.2	5−40	20	//	146 a	35%	100
27	2% Pd/SiO_2	microreactor	H_2O	9.1% H_2 in air	50	21	1% (w/w) H_2SO_4 10 ppm NaBr	120 b	50	25
28	5% Pd/C	microreactor	H_2O	D_2/O_2 2/3	20	21	0.025 M H_2SO_4	0.17 c	59.4	5.7
	5% Pd/Al_2O_2	microreactor	H_2O	D_2/O_2 2/3	20	10.5	0.005 M H_3PO_4 5.1×10^{-4} MNaBr	0.034 c	85.4	1.9
15	2.5% PdAu/ZrO_2	G-CSTR	CH_3OH	H_2:O_2 = 4:96	20	amb	0.03 M H_2SO_4	1429 d	54	100
	2.5% PdAu/ZrO_2	batch	CH_3OH	H_2:O_2:CO_2 = 3.6:7.2:89.2	20	10	0.01 M H_2SO_4	18000 d	59	100
23	2.5% Pd-ZS	G-CSTR	CH_3OH	H_2:O_2 = 4:96	20	amb	0.03 M H_2SO_4	400 d	22	100
	2.5% Pd-ZS	G-CSTR	CH_3OH	H_2:O_2 = 4:96	20	amb	0.03 M H_2SO_4	670 d	45	100
	2.5% PdAu-ZS	G-CSTR	CH_3OH	H_2:O_2 = 4:96	20	amb	0.03 M H_2SO_4	1270 d	60	100
2	Pd/TiO_2 (membrane)	continuous membrane	CH_3OH	n.d.	//	50	16 mg/L NaBr 0.03 M H_2SO_4	1.7 c	83	//
29	Pd/SBA	batch	CH_3OH	H_2:O_2:CO_2:N_2 = 7.7:15.4:61.5:15.4	20	6.5	0.02 M H_2SO_4	28 e	55	//
	Pd/SBA	semibatch	CH_3OH	H_2:O_2:CO_2: N_2 = 7.7:15.4:61.5:15.4	20	5		130 e	42	//
30	0.9 Pd/NCNT-like	batch	CH_3OH	H_2:O_2:CO_2 = 10:20:70	20	10	0.01 M H_2SO_4	128 f	45	100
		semibatch	CH_3OH	H_2:O_2:CO_2 = 10:20:70	20	10				100
31	1%Pd/K2621	batch	CH_3OH	H_2:O_2:CO_2 = 1.25:18.6:80.25	−10	20	//	//	70	60
12	5% PdAu/C modified	batch	CH_3OH	H_2:O_2:CO_2 = 3.63:6.87:89.5	2	30	//	160 f	98	40
32	5%Pd/C	semibatch	H_2O	H_2:O_2:CO_2 = 4:16:80 H_2:O_2:N_2 = 4:16:30	40	80	0.004 M H_3PO_4 0.03 M NaBr	188 d	63	32

[a]For the productivity: a) mol H_2O_2/(h*mol_{Pd}), b) gH_2O_2/ (g_{Pd}*h), c) $molH_2O_2$/(g_{cat}*h), d) $mmolH_2O_2$/(g_{cat}*h), e) mgH_2O_2/(mg_{Pd}*h) (at 1 h reaction), f) $molH_2O_2$/(kg_{cat}*h).

dx.doi.org/10.1021/ie2021398 | Ind. Eng. Chem. Res. 2012, 51, 8903−8912

therefore, try to enhance both productivity and selectivity. The temperature adopted varies from −10 to 40 °C. Temperatures between −10 and 5 °C[12,31] are suitable to avoid the consecutive reactions (hydrogenation and decomposition), although in an industrial perspective they would probably imply production costs that are too high. Most of the works are actually carried out around 20 °C,[15,23,28−30] a suitable temperature from an industrial point of view. Higher temperatures, reaching values of 40−50 °C,[27−32] are used with the addition of additives to make the direct synthesis faster and to avoid consecutive reactions as well. Pressure is an important parameter to control the direct synthesis. A higher dissolution of the gases (i.e., reagents), obtained with pressure higher than ambient, enhance the production rate of the hydrogen peroxide formed due to the higher concentration of the reagents in the liquid phase.[2,12,23,27−32] Pressure varies from 1 bar to 80 bar, more specific, 1 bar,[15,23] 5−10 bar,[15,28−30] 20−30 bar,[12,27,28,31] 50 bar,[2] and up to 80 bar.[32] Another way to obtain a higher selectivity is to operate in acidic conditions: it is widely recognized that low pH stabilizes hydrogen peroxide, limiting the hydrogenation and decomposition reactions. H_2SO_4 and H_3PO_4 are normally used to keep stable the pH between 3 and 5.[2,15,23,27−30,32] A possible substitute of the acidic compounds is the carbon dioxide: it dissolves in the liquid phase and in the presence of water forms carbonic acid, reducing the pH of the liquid phase where the H_2O_2 is formed.[12,15,29−32] Moreover carbon dioxide in methanol enhances hydrogen solubility,[12,31] which is desired, as specified above. Carbon dioxide is also used in the direct synthesis to expand the solvent (i.e., methanol), but to make more feasible the process in an industrial scale nitrogen[27,29,32] is preferred. Indeed, for cost reasons the use of air (i.e., a mixture of oxygen and nitrogen) would be much better than carbon dioxide. Halogens are also known to enhance the selectivity to the peroxide, but their presence in the solution is undesired and thus their use is limited.[2,27,28,32] Methanol was chosen as the reactant medium in many cases,[2,12,15,23,29−31] in view of an integration with the propylene oxide synthesis, where the propylene reacts with the hydrogen peroxide in methanol. Water was chosen instead for safety reasons and for its low cost.[27,28,32] It is interesting that with a catalyst containing acidic functions on the support the direct synthesis can achieve 98% of selectivity.[12]

The analysis of the reaction conditions reported above show the difficult to compare results obtained by different research groups. For example it is hard to compare studies carried out at different temperatures, because a general understanding of the reaction mechanism has not yet been reached, and therefore the temperature dependence of the consecutive/parallel reactions (see Scheme 1) remains uncertain. The presence/absence and the different concentrations of additives could also be responsible for the differences within the reported literature data, although an enhancement of selectivity could be observed in the presence of acids and bromine together.[2,27,28,32]

Scheme 1. Reactions Involved in the Direct Synthesis of H_2O_2

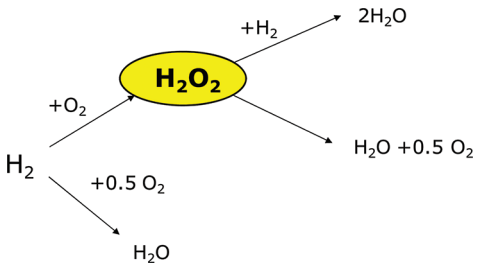

A comparison of the literature results can give important information on the studies and the trends on direct synthesis research, but works carried out by different research groups are in so different operative condition that is very difficult to analyze them together. For instance, reaction rate depends not only on temperature, pressure, and additive type/concentration but also on liquid composition, which in turn is influenced by solvent type, total composition of the gases, temperature, and pressure. Although almost all the reported works were carried out outside flammability limits (using CO_2 to dilute the gas mixture), the ranges of gas composition were rather broad.[2,12,15,23,27−32]

In the present study, experimental kinetics for the hydrogenation, decomposition and direct synthesis in the absence of halides and acids were determined over a 5% Pd on carbon catalyst. The catalyst used for the experiments was chosen both for its commercial availability and for its stable performance. Special attention has been paid on the hydrogen measurements in the liquid phase. A Fugatron instrument was used to constantly monitor, during the reaction, the amount of hydrogen dissolved and consumed in the liquid phase. Online measurements of dissolved hydrogen can provide important information on the reaction mechanism and thanks to this, hypothesis can be proposed for further kinetic and reactor modeling. The work shows that by measuring the hydrogen amount in the liquid phase and relating it with the selectivity and the production rate of hydrogen peroxide, critical information about the direct synthesis reaction can be obtained. Moreover, by monitoring and controlling the hydrogen solubility (mass transfer) the selectivity and the hydrogen peroxide formation can be enhanced.

2. EXPERIMENTAL SECTION

Materials. 5% Pd/C catalyst (Degussa) was used as received. Methanol for HPLC was used as reaction medium (J.T. Baker 99.99%), H_2 and O_2 as reagents and CO_2 as inert were used for the direct synthesis (AGA high purity), H_2O_2 30% w/w (Merck) for the decomposition and hydrogenation experiments, potassium iodide (Sigma-Aldrich), hydranal-composite 2 (Fluka), dry methanol for KFT (Fluka), acetic acid (Sigma-Aldrich), sodium thiosulfate penta-hydrate 99.5% (Sigma-Aldrich), starch (Sigma-Aldrich), potassium dichromate (Riedel de Haën), and ammonium molybdate tetrahydrate (Fluka) were used in the chemical analyses.

Reactor Setup for the Experiments. The apparatus used to perform the direct synthesis experiments is schematically described in Figure 1. The experiments were performed in a tailored batch reactor (1), i.e., a stainless steel autoclave reactor (Parr) with a volume of 600 mL and a maximum working pressure of 200 bar. The mixing was done by a Heidolph RZR 2021 rotor operating at 1000 rpm. The reactor was fitted with a K-type thermocouple (10) connected to a computer that allowed registering the temperature during the experiments. CO_2 and O_2 (2) were loaded into the reactor directly from gas cylinders. Hydrogen (3) was fed by a Brooks mass flow controller (5) to avoid overpressure in the reactor and to ensure a constant and reproducible flow. A 35 mL vessel (4) coupled with a pressure transducer and a heating jacket was placed before the mass flow controller (MFC) for hydrogen

dx.doi.org/10.1021/ie2021398 | Ind. Eng. Chem. Res. 2012, 51, 8903−8912

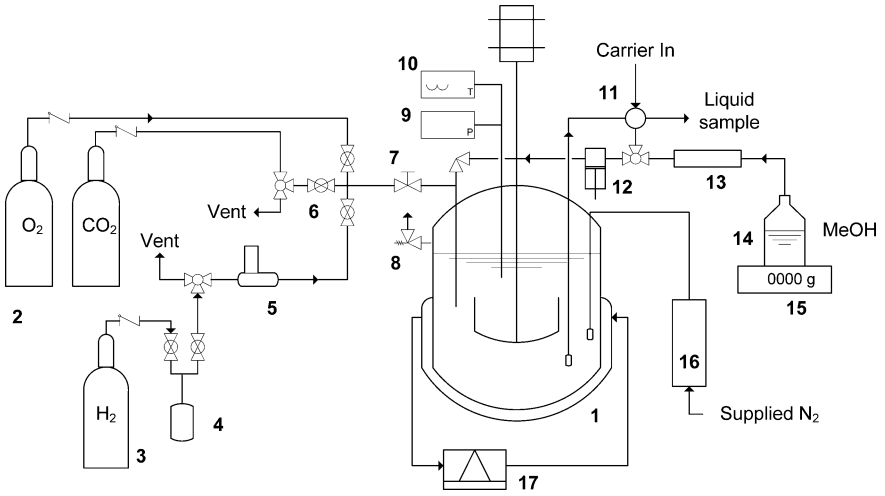

Figure 1. Schematic of the experimental apparatus. 1 − Reactor. 2−3 Gas bottles. 4−5 − Hydrogen vessel and MFC, respectively. 6−7 Valve system for gas loading. 8 − Safety valve. 9−10 Pressure and temperature measurements, respectively. 11 − Liquid sampling valve. 12 − HP pump. 13 − Degasser. 14−15 − Liquid solvent supply and balance, respectively. 16 − Fugatron HYD-100. 17 − Cooling/heating system.

feeding. This was used to precisely calculate the amount of hydrogen fed into the reactor. A system of on/off valves (6) was arranged after the gas cylinders to ensure a separation between the cylinders and the reactor. A regulation valve was used to dose the gas from the cylinders (7). Each cylinder was also equipped with a one-way valve to avoid backmixing from the reactor environment to the pipelines. A safety valve (8) ensured to avoid overpressure inside the reactor. The pressure was constantly monitored through a pressure transducer (9) and registered by a computer. A mechanical pressure gauge was also used to monitor the pressure in the vessel.

Liquid samples were withdrawn through a six-way GC valve (11). An HP (high pressure) pump (12) ensured the liquid recirculation and dosed the solvent inside the reactor before and during the experiments. Methanol was degassed using an Agilent 1100 series degasser (13) and introduced into the system directly from a glass bottle (14). A precision balance (15) allowed the exact quantification of the methanol fed into the reactor. The liquid sampling probe was equipped with a 7 μm filter to prevent any block of the sampling valve and pump by small catalyst particles. A cooling/heating system was included (17) in order to control the temperature and to maintain it constant during the experiments.

Hydrogen dissolved in the liquid phase was measured with Fugatron HYD-100 (16). Its signal is proportional to the partial pressure of the dissolved gas. The instrument is provided with a probe to be immersed in the liquid, with a rigid membrane internally purged with a carrier gas and connected to an electrochemical detector: hydrogen permeates the membrane and reaches the detector with the carrier gas. Experiments were performed batchwise, and the hydrogen flowing to the instrument was evaluated by time integral of the instrument response: during the experiments less than 0.2% was subtracted from the reaction environment for analysis.

H_2O_2 Experiments and Analyses. Before the experimental campaign started, a four hour passivation treatment was performed on the reactor, using 30 wt.% nitric acid at 40 °C. The reactor was then tested for both decomposition and hydrogenation of hydrogen peroxide. A solution of 0.5 wt.% H_2O_2 in methanol was loaded inside the batch vessel. A CO_2−O_2 mixture (75−25 vol.% respectively) was introduced until reaching a pressure of 10 bar. The percentage of O_2 was substituted with a mixture consisting of N_2 (85 vol%) and H_2 (15%) in the hydrogenation tests. The experiments were carried out at 10 °C varying the stirring rate (0, 500, and 1000 rpm). After four hours of operation, no H_2O_2 decomposition or hydrogenation was detected.

The protocol developed for the experiments was as follows: 0.15 g of a 5% Pd/C catalyst was loaded in the reactor. The reactor was then flushed with CO_2 four times to remove air and moisture present in the reactor. Carbon dioxide (18.4 bar) and oxygen (6 bar) were loaded into the reactor directly from the cylinders at 25 °C, followed by the injection of 400 mL of methanol by an HPLC pump. After the desired methanol amount was fed, the pump was then set to recirculate the liquid phase. The stirrer was turned on, and the desired temperature was fixed (−5 °C, 0 °C, 10 °C, and 40 °C). After both pressure and temperature were stable, the stirrer and pump were turned off. The vessel (4) before MFC (5) was loaded with pure hydrogen at a higher pressure than the reactor. Hydrogen was always the limiting reagent, fed from the vessel into the reactor through the mass flow controller. The moles of hydrogen introduced were calculated with the ideal gas law by the pressure difference in the loading vessel, knowing its temperature and volume. Immediately after the hydrogen loading had been completed, stirring was turned on again at 1000 rpm, along with the recirculation pump. A fast hydrogen introduction compared to the reaction rates was implemented (seconds vs minutes). Hence, the reaction was assumed to start when both stirrer and pump were turned on.

Hydrogenation and decomposition experiments were carried out following the same procedure, but using N_2 instead of O_2 and H_2, respectively.

The decomposition, hydrogenation, and direct synthesis experiments were performed at −5 °C, 0 °C, 10 °C, and 40 °C at 18 bar using methanol as a reaction medium. Temperatures between −5 and 40 °C were chosen because 1) the decomposition and hydrogenation of H_2O_2 are slower, while the synthesis is less affected by the temperature, 2) the solubility of CO_2 in methanol rises, thus increasing the hydrogen solubility in the mixture, 3) it is a low temperature industrially feasible without significant increase of costs, and 4) the catalyst and mixture stability increase.

dx.doi.org/10.1021/ie2021398 | *Ind. Eng. Chem. Res.* 2012, 51, 8903−8912

During each single experiment, the liquid phase was sampled from the batch reactor and analyzed as follows: the water and H_2O_2 contents were determined by volumetric Karl Fischer and iodometric titration, respectively. The concentrations are given on weight basis. The selectivity is defined as $100[H_2O_2]/([H_2O_2]+[H_2O]_{prod})$; it is equal to the moles of H_2O_2 produced, divided by the moles of hydrogen consumed.

Catalyst and Catalyst Characterization Methods. The catalyst used was a 5% Pd/C commercial catalyst from Degussa (Evonik). The surface area and the pore size distribution were obtained from N_2 adsorption/desorption isotherms at −196 °C (using a Carlo Erba Sorptomatic 1900). Samples (300 mg) were outgassed at 300 °C for 2 h under vacuum. The surface area was calculated from the N_2 adsorption isotherm by the BET equation, and pore size distribution was determined by the BJH method. Total pore volume was taken at $P/P_0 = 0.99$.

CO chemisorption measurements were performed at 25 °C by a Micromeritics pulse flow system. Prior to the measurements, samples were subjected to a pretreatment involving exposure to hydrogen flow for 1 h at 25 °C, followed by He purge for 2 h at the same temperature of reduction.

XPS measurements were performed in a Perkin-Elmer 5400 ESCA spectrometer with monochromatized Al Kα radiation (photon energy 1486.6 eV) and a pass energy value of 35 eV. Samples were transferred to the XPS system in an ethanol solvent to protect them from oxidation in ambient air. A low energy electron gun (flood gun) was used to stabilize the charging that arises from loss of photoelectrons during X-ray bombardment. To calibrate the binding energy (BE) axis accurately, carbon 1s line at 284.6 eV was used as BE reference.[33] In the line fitting procedure, the intensity ratios of Pd 3d5/2:3d3/2 lines were kept fixed at their theoretical values (3:2) and a Doniach-Šunjić line shape[34] was used. The sensitivity factors used in determining the atomic concentration ratios for Pd 3d, C 1s, Cl 2p, and O 1s were 4.642, 0.296, 0.770, and 0.711, respectively.[33] FitXPS software by D. Adams, University of Aarhus, was used in the line fitting procedure. Pd 3d lines were found on a nonlinear background, and a parabolic background was used in the line fitting.

3. RESULTS AND DISCUSSION

Catalyst Characterization Results. The BET results revealed that the surface area was 792.8 m^2/g and the specific pore volume was 0.887 cm^3/g. The chemisorptions measurements revealed that the average particle size of Pd was 2.62 nm with a dispersion of 42.8%.

Regarding the XPS results, it is generally observed that Pd peaks for the Pd(3d5/2) and Pd(3d3/2) spin−orbit doublet reported for bulk Pd occur at about 334.9 and 340.1 eV, respectively. PdO peaks occur at about 336.5 and 341 eV. In our samples, however, the binding energies of the Pd(3d) peaks for Pd nanoparticles on C are about 1 eV higher and were located at 337.6 and 342.3 eV, respectively (Table 1) . The larger binding energies of the supported Pd have been reported previously. Our results, in fact, are very close to those reported by Campbell et al.,[35] who obtained the XPS of small Pd particles (2−10 nm) on an α-Al_2O_3 (0001) single crystal under different conditions. Also Liu et al.[13] reported a shift of 1 eV for palladium nanoparticles on silica. They also found that the binding energies of the Pd(3d) peaks increased about 1 eV compared to bulk palladium and suggested that the shift to higher binding energies for the Pd nanoparticles compared to the bulk Pd metal is mainly a result of final-state screening by conduction electrons. The catalyst presents an oxidized surface as explained. No changes occurred on the catalyst after a 4 h reaction (Table 2).

Table 2. XPS Results for the Catalyst Pd/C

catalyst	C ls (eV)	Pd $3d_{5/2}$ (eV)	0 ls (eV)	C12p (eV)
fresh	284.60	337.6	531.2 (34%)	198.6
			533.3 (26%)	
			534.9 (28%)	
			537.0 (11%)	
used	284.60	337.6	531.5 (45%)	198.6
			533.2 (21%)	
			534.7 (23%)	
			536.5 (11%)	

H_2O_2 Hydrogenation and Decomposition. Palladium based catalysts are well-known for being suitable for the direct synthesis of hydrogen peroxide. Unfortunately, they enhance H_2O_2 decomposition and hydrogenation too (reactions 3 and 4 of Scheme 1). To quantify the degree of H_2O_2 loss by decomposition and hydrogenation, kinetic experiments were carried out with the same catalyst and under the same operation conditions as the direct synthesis. The results in the batch reactor at different temperatures are shown in Figures 2

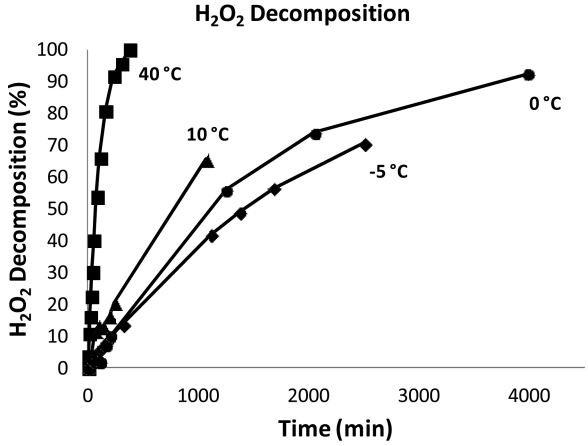

Figure 2. Decomposition of 0.5 wt.% of H_2O_2 in methanol at 18 bar at different temperatures: 40 °C (■), 10 °C (▲), 0 °C (●), −5 °C (♦).

and 3, as a percentage of the H_2O_2 loss. Qualitatively, both degradation paths (with/without H_2) were similarly affected by the temperature. At low temperatures, the decomposition was almost suppressed due to the low activity of palladium, and less degradation of H_2O_2 occurred. Figure 2 shows the kinetics of the hydrogen peroxide decomposition. At 40 °C, a fast H_2O_2 decomposition was observed, with a 50% loss after 1 h operation, and almost a total decomposition after 3 h of reaction. The decomposition experiments carried out at −5, 0, and 10 °C showed a similar trend (Figure 2). The H_2O_2 decomposition was around 10% after 1 h and between 12 and 18% after 4 h. Stirring speeds up to 1000 rpm did not decompose hydrogen peroxide in the solution as reported above. Figure 3 shows the hydrogenation kinetics at different temperatures. Even if the presence of H_2 enhanced the hydrogen peroxide degradation, the time scale of the experiments was much smaller compared to the decomposition experiments. Surprisingly, the temperature did not seem to

dx.doi.org/10.1021/ie2021398 | Ind. Eng. Chem. Res. 2012, 51, 8903−8912

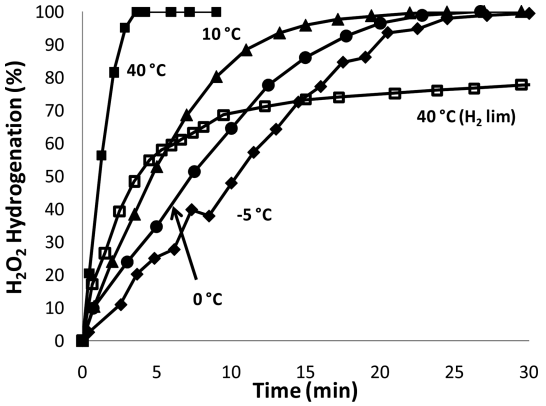

Figure 3. Hydrogenation (decomposition) of 0.5 wt.% of H_2O_2 in methanol at 18 bar. At different temperatures: 40 °C H_2 lim (◆), 40 °C (■), 10 °C (▲), 0 °C (●), −5 °C (♦).

have a large effect on the hydrogenation rate between −5, 0, 10, and 40 °C H_2 lim (i.e., hydrogen as limited reagent). Only the hydrogenation at 40 °C, with hydrogen peroxide as limited reagent, went really fast. At 10 and 40 °C H_2 lim (i.e., hydrogen as limited reagent), the hydrogenation rates seemed to be rather similar. After 15 min, the H_2O_2 degradation was almost 90% of the total hydrogen peroxide introduced. On the other hand, at −5 °C after 15 min, the hydrogen peroxide that remained in the solution was around 40% of the total amount introduced. The hydrogenation and decomposition reactions affected differently the direct synthesis. The decomposition at low temperatures did not largely affect the direct synthesis, whereas hydrogenation did. It seemed that the palladium catalyst was activated very fast by hydrogen at low temperatures, while during the decomposition experiments the catalyst was activated at high temperatures only. This implies that the hydrogenation was not affected in great extent by the temperature but by the hydrogen feeding into the reactor. The decomposition reaction was most probably controlled by kinetics while the hydrogenation was first kinetically controlled and when the hydrogen concentration was decreasing in the liquid phase, it entered into the mass transfer limited regime.

Hydrogenation at 40 °C H_2 lim was performed by using H_2 as a limiting reagent. The data collected by the Fugatron instrument gave important information about kinetic and mass transfer regimes during the reaction. After three minutes of reaction the hydrogen dissolved in the liquid phase reached a maximum (peak). After such peak (Figure A Supporting Information), the H_2O_2 degration rate starts to decrease. Eight minutes after the peak, hydrogen was completely consumed, and the hydrogenation of H_2O_2 becomes slower (Figure 3 and Figure A Supporting Information). In the absence of dissolved hydrogen, the only possible reaction was the H_2O_2 decomposition. In the first three minutes the hydrogenation reaction appears to be very fast; H_2O_2 decreased rapidly in the solution and the H_2 amount in the solution was quite high. This situation is a classical kinetically controlled regime. Between four and ten minutes, mass transfer begins to be of importance as hydrogen started to be the limiting reagent in the liquid phase. Hydrogen disappeared after ten minutes of reaction where mass transfer limitations become evident. After this time, H_2O_2 decreased slowly compared to the first minutes, because no more available hydrogen was present in the liquid phase and only the decomposition reaction took place. In the experiment at 0 °C, H_2O_2 was the limiting reagent. The slope of hydrogenation in this case was linear, and it was not characterized by different regimes (Figure 3). A comparison of the collected information gave the opportunity to define the mass transfer and kinetic regimes.

H_2O_2 Synthesis: Effect of Temperature. Kinetic experiments of the hydrogen peroxide direct synthesis were carried out by varying the temperature. The H_2:O_2 ratio was set to 1:10, i.e. hydrogen was the limiting reagent. In Figure 4 the

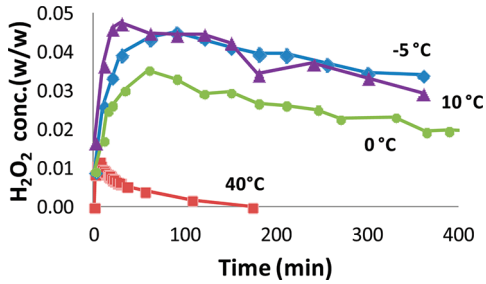

Figure 4. Production of H_2O_2 at 18 bar and different temperatures: 40 °C (■), 10 °C (▲), 0 °C (●), −5 °C (♦).

production of hydrogen peroxide is reported at 18 bar and temperatures between −5 and 40 °C. Water production measurements for the same experiments are reported in Figure 5. Overall, the water production during the experiments

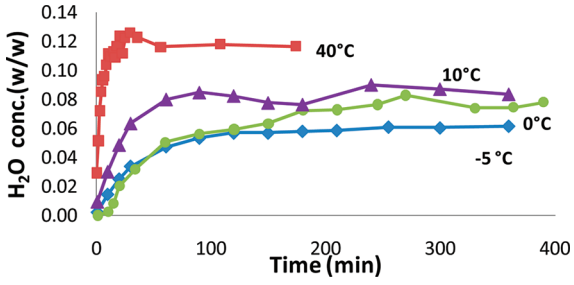

Figure 5. Production of H_2O at 18 bar and different temperatures: 40 °C (■), 10 °C (▲), 0 °C (●), −5 °C (♦).

increased constantly and, moreover, prevailed over the hydrogen peroxide formation, reaching higher concentrations than the peroxide. The H_2O_2 formation increased rapidly in the very beginning, reaching a maximum and gradually decreasing afterward. A complete consumption of H_2 corresponded to the maximum concentration of H_2O_2: after H_2 was no longer present in the liquid phase, the direct synthesis as well as the hydrogenation were suppressed. Thus, only the decomposition of H_2O_2 took place, resulting in a drop of the peroxide formation and consequently in a slower water production rate.

At 0 °C, the maximum H_2O_2 concentration was 0.02 wt.% after 60 min of reaction, and the maximum concentration of water reached 0.06 wt.% after 300 min. At 10 °C, the maximum H_2O_2 concentration was 0.03% wt. after 40 min and 0.07 wt % for water after 300 min. At −5 °C, the maximum hydrogen peroxide production was about 0.03 wt % after 70 min, and the maximum water production reached 0.05 wt % after 300 min. At 40 °C, the water formation was highly favored, as the H_2O_2 concentration only reached 0.015 wt %, while H_2O raised up to 0.13 wt % (Figures 4 and 5). The peak in H_2O_2 concentration was shifted with temperature: at 40 °C it appeared after 5 min of reaction, while at 10 °C the maximum of H_2O_2 production occurred after 40 min. When working at −5 °C, such peak

dx.doi.org/10.1021/ie2021398 | Ind. Eng. Chem. Res. 2012, 51, 8903−8912

appeared after 70 min of reaction (Figure 4). Such behavior is expected since at higher temperatures the solubility of hydrogen increases and reaction rates are faster as well.

Thinking about kinetics solely, at 40 °C a high production of hydrogen peroxide could be achieved. Unfortunately, due to the higher solubility of hydrogen in the liquid phase at higher temperatures, the consecutive reactions are favored (i.e., hydrogenation and decomposition) rendering the final hydrogen peroxide concentration in the liquid the lowest compared with lower temperatures (Figure 4). Comparing the experiments conducted at 10 and −5 °C, both achieved the same hydrogen peroxide production and the same selectivity (Figures 4 and 6). This could be explained with the following

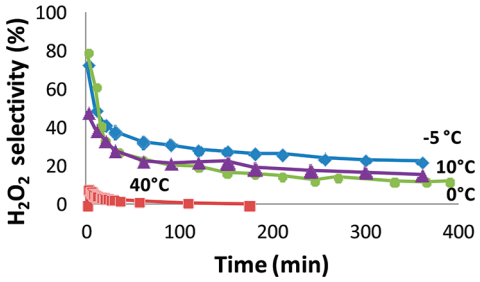

Figure 6. Selectivity toward hydrogen peroxide formation at 18 bar and different temperatures: 40 °C (■), 10 °C (▲), 0 °C (●), −5 °C (♦).

considerations: 1) hydrogenation and decomposition were slower at −5 °C compared to 10 °C; 2) the direct synthesis was faster at 10 °C due to the higher solubility of hydrogen compared to −5 °C. For such reasons a convenient combination between the three reactions involved in the system was found (i.e., direct synthesis, hydrogenation and decomposition) resulting in a similar overall reaction rate for H_2O_2 formation (Figures 4-6). Moreover, the maximum in the hydrogen peroxide production at −5 °C was reached 15 min later compared to the experiment conducted at 10 °C, which is in agreement with our considerations. In summary, the direct H_2O_2 direct synthesis reaction as well as decomposition and hydrogenation are faster at 10 °C compared to a temperature of −5 °C. A combination of the three reactions produces similar trends and similar values for the selectivity toward hydrogen peroxide.

The hydrogen peroxide selectivity data at different temperatures is presented in Figure 6. At temperatures equal or lower than 10 °C, the selectivity toward H_2O_2 was high at the beginning of the reaction and further decreased sharply during the first hour of reaction. Thereafter, only the decomposition reaction took place, and the final selectivity was found to be between 10 and 20%. Similar trends were observed at 40 °C, but the absolute values were much lower and the decrease on selectivity seemed somewhat faster. Taking into account the results of both the H_2O_2 production and selectivity it is reasonable to state that 1) the reaction of the direct synthesis of hydrogen peroxide is very fast at the beginning with a high selectivity; 2) hydrogenation and decomposition reactions increase as hydrogen peroxide is produced; 3) H_2O_2 production decreases and water formation is favored as hydrogen concentration in the liquid phase decreases; and 4) direct synthesis is highly unfavorable at higher temperatures, as the side reactions prevail over the H_2O_2 production.

A maximum selectivity of 80% at 0 °C was reached, compared to a maximum of 60% at −5 °C and 40% at 10 °C. That implies that without stabilizers in the media, both temperature and reaction time played an important role on the selectivity. Furthermore, a short contact time is necessary to achieve such extraordinarily high selectivity, even if this highest selectivity corresponded to low productivity rates.

H_2O_2 Synthesis: Hydrogen Feeding. The Fugatron instrument allowed us to measure the hydrogen dissolved in the liquid phase (Figure 7). The experiments were conducted at

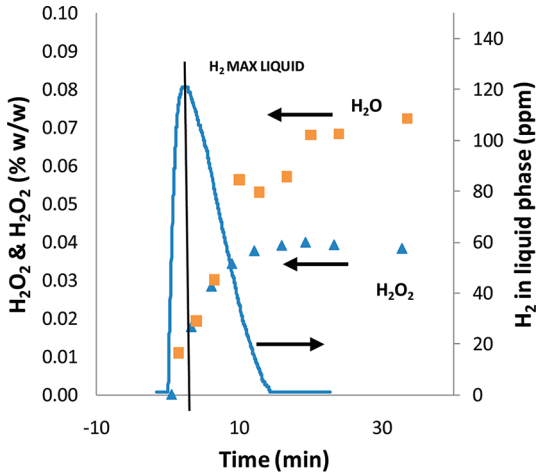

Figure 7. Hydrogen peroxide (▲) and water formation (■) at 18 bar and 10 °C depending on hydrogen solubility in the reaction medium (solid line).

10 bar and 10 °C. Gas and liquid feeding was done in the same way as in the former experiments. Three different experiments were conducted: 1) synthesis of hydrogen peroxide with one hydrogen filling at the beginning of the reaction; 2) synthesis of hydrogen peroxide with four hydrogen fillings along the reaction, after the totality of the hydrogen dissolved in the liquid phase was completely consumed; and 3) synthesis of hydrogen peroxide with four hydrogen fillings, as soon as the hydrogen concentration in the liquid phase started to decrease. Figure 7 shows a typical experiment of the direct synthesis, in which information about the amount of hydrogen dissolved in the liquid phase plus the hydrogen peroxide and water production are displayed. Hydrogen dissolved in the liquid phase was consumed rapidly as the narrow peak in Figure 7 shows. Additionally, this experiment showed how the hydrogen peroxide concentration started to decrease after hydrogen was no longer present in the liquid phase. The amount of hydrogen dissolved in the liquid reached a peak during the first minutes of the reaction, decreasing slowly afterward. The peak of H_2 in the liquid phase corresponded with the maximum in selectivity (i.e., max $H_2O_2/H_2O_2+H_2O$ ratio). After such peak, hydrogen decreased slowly. The increase of hydrogen in the liquid was faster then its decrease. As soon as hydrogen decreased in the liquid phase, the selectivity toward hydrogen peroxide was also reduced, and the formation of water prevailed. Additionally, as the hydrogen concentration in the liquid started to increase, the amount of water in the system increased drastically. After hydrogen was completely consumed from the liquid phase the concentration of hydrogen peroxide decreased slowly. These results were in line with our decomposition experiments presented in this work (Figure 2). A relationship between the

dx.doi.org/10.1021/ie2021398 | Ind. Eng. Chem. Res. 2012, 51, 8903−8912

amount of hydrogen in the liquid phase and the quantity of hydrogen peroxide produced could be found. It appears that there is an optimum amount of hydrogen in the liquid phase that enhances the selectivity of the direct synthesis reaction. Plausible hypotheses for this reaction are as follows: 1) before hydrogen was introduced oxygen covers catalyst surface;[13,15,17] 2) as soon as hydrogen was dissolved in the liquid phase, it reacted with oxygen on the catalyst surface;[15,17] 3) when hydrogen started to decrease some changes in catalyst surface happened;[13,15,17] and 4) probably the H_2/Pd ratio was changing and hydrogenation was favored compared to the direct synthesis reaction. In order to confirm these hypotheses, experiments refilling hydrogen were needed as well as measurements of hydrogen solubility.

The subsequent experiment was performed in order to find a relationship between the selectivity, the production rate, and the amount of hydrogen fed into the reactor (Figures 8 and 9).

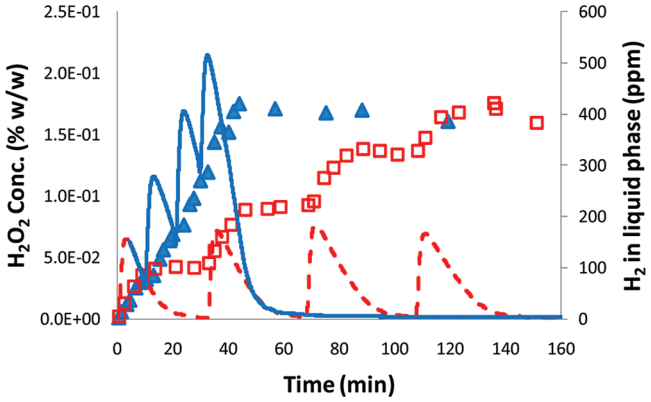

Figure 8. Production of H_2O_2 at 10 °C and 18 bar with different hydrogen feeding policies: 1) Hydrogen amount fed after its complete depletion in the liquid phase (solid line) and 2) hydrogen subsequently fed as it decreases in the liquid phase (dashed line). H_2O_2 production under feeding policy 1 (□) and under feeding policy 2 (▲).

The same amount of hydrogen was fed into the reactor straight after the gas dissolved in the liquid was completely consumed. Both the hydrogen peroxide and water concentrations

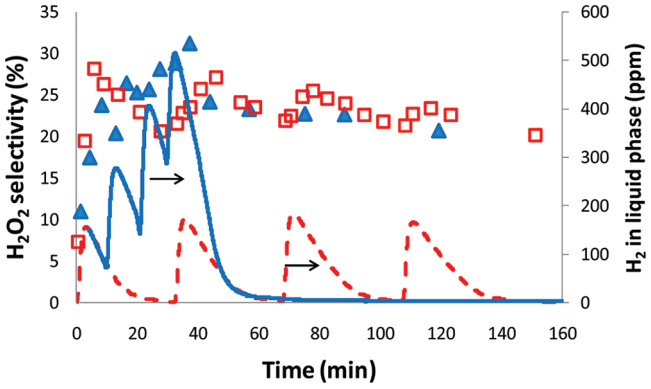

Figure 9. Selectivity of H_2O_2 at 10 °C and 18 bar with different hydrogen feeding policies: 1) Hydrogen amount fed after its complete depletion in the liquid phase (solid line) and 2) hydrogen subsequently fed as it decreases in the liquid phase (dashed line). H_2O_2 selectivity under feeding policy 1 (□) and under feeding policy 2 (▲).

increased during the reaction. The selectivity had different behavior though: every time that fresh hydrogen was fed into the reactor, the selectivity toward hydrogen peroxide increased; when hydrogen started to decrease, such selectivity decreased as well. The results prove that the amount of hydrogen plays an important role in the direct synthesis. A maximum selectivity toward hydrogen peroxide was found to be close to 30%. However, as hydrogen was consumed, this selectivity dropped to 20%. It was interesting to notice that when hydrogen was refilled into the reactor, the selectivity level of 27% was regained. This same result was reproduced with consecutive hydrogen loadings. Moreover, the hydrogen peroxide production increased with this hydrogen feeding policy (Figure 8). As hydrogen was already depleted from the liquid phase, the concentration of hydrogen peroxide remained stable, and, more importantly, no decomposition was detected as seen during former decomposition experiments (Figures 2 and 3). This experiment confirms all four hypotheses made above.

Regarding the importance of the H_2/Pd ratio, experiments were conducted avoiding the complete depletion of hydrogen in the liquid phase. In that sense, equal amounts of hydrogen were reloaded into the reactor after certain time after the H_2 peak was recorded with the Fugatron. Such subsequent hydrogen feeding policy demonstrated how a higher selectivity could be achieved compared to the former experiments when the hydrogen was refilled before its complete consumption. The selectivity toward hydrogen peroxide in this case reached a peak around 33%, compared to only 27% in the previous case, i.e., when hydrogen was completely consumed (Figure 9). Moreover, the hydrogen peroxide concentration increased constantly until soluble hydrogen was consumed. After this point, the concentration of H_2O_2 remained quite stable. It is interesting to notice that the hydrogen peroxide production was pretty much equal to the former experiments, but the selectivity reached a higher value (Figures 8 and 9). Hydrogen peroxide formed faster in such experiments due to the amount of hydrogen present in the liquid phase.

Comparing the two experiments performed with the hydrogen refilling, an obvious observation concerns the selectivity, which remained stable around a value of 20% after hydrogen depletion. Moreover, in both cases (Figure 8 and 9), the highest selectivity was reached during the first minutes of the reaction.

These results allow to arrive to the following considerations: 1) hydrogen dissolved in the liquid phase is consumed rapidly (during the first 30 min of reaction time); 2) when hydrogen was not present in the liquid phase, the hydrogen peroxide formed decreased slowly and so did the selectivity; 3) the hydrogen refilled in the reactor enhanced the selectivity; 4) hydrogen refilling before its complete depletion gave better results compared to the case when hydrogen was refilled after its complete consumption; and finally 5) hydrogen peroxide production could be increased by regulating the amount of hydrogen dissolved in the reaction medium.

Remarks on Conversion and Selectivity. Another general observation regards the correlation between selectivity and hydrogen conversion: low hydrogen conversions corresponded a high selectivity,[12,27,28,31,32] while a high conversion led to low selectivity.[15,23,29,30] In this work following the kinetics of hydrogen peroxide formation we saw that at the beginning of the reaction with low H_2 conversion selectivity was high, while when hydrogen was consumed (more than 40%) selectivity started to drop. With the refilling method was

dx.doi.org/10.1021/ie2021398 | Ind. Eng. Chem. Res. 2012, 51, 8903–8912

possible to see that there was the same trend of conversion vs selectivity. H_2O_2 formation and selectivity started to rise again when hydrogen was fed in the reactor, and when a specific amount of hydrogen was consumed (i.e., 40%) H_2O_2 formation and selectivity dropped again. It seems that keeping the hydrogen conversion below 100% (i.e., 60%) inside the reactor gives an enhancement on the selectivity. Most probably there is an effect of the hydrogen on the metal nanocluster surface that allows to reduce unwanted reactions like hydrogenation and decomposition. We want to underline that thanks to the measurements of the hydrogen dissolved in the liquid phase we were able to compare hydrogen solubilized in the liquid phase with the selectivity obtained finding that hydrogen consumption and selectivity are strictly interlinked. This correlation between conversion and selectivity can also be found in some of the works reported in Table 1.

In general, the final selectivity obtained in this work was lower than most of the studies reported in Table 1, but we remark that our aim was to study the H_2O_2 direct synthesis, decomposition, and hydrogenation only with respect to the temperature, the time, and in the absence of promoters and stabilizers. Usually in the literature most of the efforts are focused on the development of the catalyst,[2,12,15,23,29,31] and we were focusing on the reactor development trying to understand how it is possible to enhance hydrogen peroxide selectivity and productivity changing the operation conditions.

4. CONCLUSIONS

Hydrogen peroxide direct synthesis was studied deeply taking into account decomposition and hydrogenation reactions. Moreover a relationship between selectivity and the hydrogen dissolved in the liquid phase was found.

Temperatures between −5 and 10 °C did not decompose hydrogen peroxide in large amounts. Hydrogenation of H_2O_2 was fast, and its kinetics were similar in the range of 0 to 40 °C while at −5 °C showed to be slower than in the former cases. When trying the direct synthesis of hydrogen peroxide at high temperatures (i.e., 40 °C) without promoters, both decomposition and hydrogenation seemed too fast to allow a high production of hydrogen peroxide. Regarding hydrogenation and decomposition, experiments conducted at −5 and 10 °C showed similar production of H_2O_2. At −5 °C, hydrogenation was suppressed, while at 10 °C, the production of hydrogen peroxide was overcome by its hydrogenation. Experiments conducted at 0 °C showed that such temperature was not the best for hydrogen peroxide direct synthesis compared to −5 and 10 °C. The Fugatron instrument allowed monitoring hydrogen dissolved in the liquid phase during the experiments. Different policies of H_2 feeding gave the possibility to enhance the hydrogen peroxide production rate and selectivity. An enhanced selectivity was achieved by refilling hydrogen before its complete consumption. Experiments gave the further direction of investigation on the role of hydrogen dissolved in the liquid phase, in the direct synthesis reaction. Kinetic and reactor modeling will be performed with the obtained data in order to tune and engineer the reaction. Further kinetic analyses are needed to fully understand the reaction mechanism.

■ ASSOCIATED CONTENT

Supporting Information

Hydrogen in liquid phase vs hydrogenation of hydrogen peroxide is provided at 40 °C. This material is available free of charge via the Internet at http://pubs.acs.org.

■ AUTHOR INFORMATION

Corresponding Author

*E-mail: bpierdom@abo.fi.

Notes

The authors declare no competing financial interest.

■ ACKNOWLEDGMENTS

Pierdomenico Biasi and Nicola Gemo gratefully acknowledge the Process Chemistry Centre (PCC), Åbo Akademi, Finland and the Johan Gadolin Scholarship for financial support. This work is a part of the activities at the Åbo Akademi Process Chemistry Centre (PCC) within the Finnish Centre of Excellence Programmes (2000−2005 and 2006−2011) by the Academy of Finland. Nicola Gemo gratefully acknowledges the Cariparo Foundation for financial support.

■ REFERENCES

(1) Centi, G.; Perathoner, S.; Abate, S. *Modern Heterogeneous Oxidation Catalysis: Direct synthesis of hydrogen peroxide: recent advances*; Wiley-VCH: 2009; pp 253−287.

(2) Pashkova, A.; Dittmeyer, R.; Kaltenborn, N.; Richter, H. Experimental study of porous tubular catalytic membranes for direct synthesis of hydrogen peroxide. *Chem. Eng. J.* **2010**, *165*, 924−933.

(3) Piqueras, C. M.; García-Serna, J.; Cocero, M. J. Estimation of lower flammability limits in high-pressure systems. Application to the direct synthesis of hydrogen peroxide using supercritical and near-critical CO_2 and air as diluents. *J. Supercrit. Fluids* **2010**, *56*, 33−40.

(4) Voloshin, Y.; Lawal, A. Overall kinetics of hydrogen peroxide formation by direct combination of H_2 and O_2 in a microreactor. *Chem. Eng. Sci.* **2009**, *65*, 1028−1036.

(5) Campos-Martin, J. M.; Blanco-Brieva, G.; Fierro, J. L. G. Hydrogen peroxide synthesis: An outlook beyond the anthraquinone process. *Angew. Chem., Int. Ed.* **2006**, *45*, 6962−1984.

(6) Inoue, T.; Schmidt, M. A.; Jensen, K. F. Microfabricated multiphase reactors for the direct synthesis of hydrogen peroxide from hydrogen and oxygen. *Ind. Eng. Chem. Res.* **2007**, *46*, 1153−1160.

(7) Abate, S.; Centi, G.; Perathoner, S.; Melada, S.; Pinna, F.; Strukul, G. The issue of selectivity in the direct synthesis of H_2O_2 from H_2 and O_2: the role of the catalysts in relation to the kinetic of reaction. *Top. Catal.* **2006**, *38*, 181−193.

(8) Burch, R.; Ellis, P. R. An investigation of alternative catalytic approaches for the direct synthesis of hydrogen peroxide from hydrogen and oxygen. *Appl. Catal., B* **2003**, *42*, 203−211.

(9) Biasi, P.; Menegazzo, F.; Pinna, F.; Eränen, K.; Canu, P.; Salmi, T. O. Hydrogen Peroxide Direct Synthesis: Selectivity Enhancement in a Trickle Bed Reactor. *Ind. Eng. Chem. Res.* **2010**, *49*, 10627−10632.

(10) Biasi, P.; Menegazzo, F.; Pinna, F.; Eränen, K.; Salmi, T. O.; Canu, P. Continuous H_2O_2 direct synthesis over PdAu catalysts. *Chem. Eng. J.* **2011**, *176*−*177*, 172−177.

(11) Dissanayake, D. P.; Lunsford, J. H. Evidence for the Role of Colloidal Palladium in the Catalytic Formation of H_2O_2 from H_2 and O_2. *J. Catal.* **2002**, *206*, 173−176.

(12) Edwards, J. K.; Solsona, B.; Ntainjua, N. E.; Carley, A. F.; Herzing, A. A.; Kiely, C. J.; Hutchings, G. J. Switching Off Hydrogen Peroxide Hydrogenation in the Direct Synthesis Process. *Science* **2009**, *323*, 1037−1041.

(13) Liu, Q.; Gath, K. K.; Bauer, J. C.; Schaak, R. E.; Lunsford, J. H. Direct Synthesis of H_2O_2 from H_2 and O_2 over Pd/SiO_2 Catalyst in a H_2SO_4/Ethanol System. *Catal. Lett.* **2009**, *132*, 342−348.

(14) Melada, S.; Pinna, F.; Strukul, G.; Perathoner, S.; Centi, G. Direct synthesis of H_2O_2 on mono- and bimetallic catalytic membranes using methanol as reaction medium. *J. Catal.* **2006**, *237*, 213−219.
(15) Menegazzo, F.; Signoretto, M.; Manzoli, M.; Boccuzzi, F.; Cruciani, G.; Pinna, F.; Strukul, G. Influence of the preparation method on the morphological and composition properties of Pd−Au/ZrO_2 catalysts and their effect on the direct synthesis of hydrogen peroxide from hydrogen and oxygen. *J. Catal.* **2009**, *268*, 122−130.
(16) Ghedini, E.; Menegazzo, F.; Signoretto, M.; Manzoli, M.; Pinna, F.; Strukul, G. Mesoporous silica as supports for Pd catalyzed H_2O_2 direct synthesis: Effect of the textural properties of the support on the activity and selectivity. *J. Catal.* **2010**, *273*, 266−273.
(17) Melada, S.; Rioda, R.; Menegazzo, F.; Pinna, F.; Strukul, G. Direct synthesis of hydrogen peroxide on zirconia-supported catalysts under mild conditions. *J. Catal.* **2006**, *239*, 422−430.
(18) Piccinini, M.; Ntainjua, N. E.; Edwards, J. K.; Carley, A. F.; Moulijn, J. A.; Hutchings, G. J. Effect of the reaction conditions on the performance of Au-Pd/TiO_2 catalyst for the direct synthesis of hydrogen peroxide. *Phys. Chem. Chem. Phys.* **2010**, *12*, 2488−2492.
(19) Choudhary, V. R.; Jana, P. Direct oxidation of H-$_2$ to H_2O_2 over Br and F-promoted Pd/Al_2O_3 in aqueous acidic medium: Influence of the concentration of Br and F and the method of incorporation of the two halogens in the catalyst on their beneficial synergetic effect on the net H_2O_2 formation. *Appl. Catal., A* **2007**, *329*, 79−85.
(20) Choudhary, V. R.; Jana, P. Direct H_2-to-H_2O_2 oxidation over highly active/selective Br−F−Pd/Al_2O_3 catalyst in aqueous acidic medium: Influence of process conditions on the H_2O_2 formation. *Appl. Catal., A* **2009**, *352*, 35−42.
(21) Deguchi, T.; Iwamoto, M. Reaction mechanism of direct H_2O_2 synthesis from H_2 and O_2 over Pd/C catalyst in water with H^+ and Br^- ions. *J. Catal.* **2011**, *280*, 239−246.
(22) Liu, Q.; Lunsford, J. H. Controlling Factors in the Direct Formation of H_2O_2 from H_2 and O_2 over a Pd/SiO_2 Catalyst in Ethanol. *Appl. Catal., A* **2006**, *314*, 94−100.
(23) Menegazzo, F.; Burti, P.; Signoretto, M.; Manzoli, M.; Vankova, S.; Boccuzzi, F.; Pinna, F.; Strukul, G. Effect of the Addition of Au in Zirconia and Ceria Supported Pd Catalysts for the Direct Synthesis of Hydrogen Peroxide. *J. Catal.* **2008**, *257*, 369−381.
(24) Deguchi, T.; Iwamoto, M. Kinetics and Simulation Including Mass-Transfer Processes of Direct H_2O_2 Synthesis from H_2 and O_2 over Pd/C Catalyst in Water Containing H^+ and Br^- Ions. *Ind. Eng. Chem. Res.* **2011**, *50*, 4351−4358.
(25) Moreno, T.; García-Serna, J.; Cocero, M. J. Decomposition reaction of H_2O_2 over Pd/C catalyst in an aqueous medium at high pressure: Detailed kinetic study and modelling. *J. Supercrit. Fluids* **2011**, *57*, 227−235.
(26) Moreno, T.; Garcia-Serna, J.; Cocero, M. J. Direct synthesis of hydrogen peroxide in methanol and water using $scCO_2$ and N_2 as diluents. *Green Chem.* **2010**, *12*, 282−289.
(27) Voloshin, Y.; Halder, R.; Lawal, A. Kinetics of Hydrogen Peroxide Synthesis by Direct Combination of H_2 and O_2 in a Microreactor. *Catal. Today* **2007**, *125*, 40−47.
(28) Inoue, T.; Kikutani, Y.; Hamakawa, S.; Mawatari, K.; Mizukami, F.; Kitamori, T. Reactor design optimization for direct synthesis of hydrogen peroxide. *Chem. Eng. J.* **2010**, *160*, 909−914.
(29) Abate, S.; Lanzafame, P.; Perathoner, S.; Centi, G. SBA-15 as a support for palladium in the direct synthesis of H_2O_2 from H_2 and O_2. *Catal. Today* **2011**, *169*, 167−174.
(30) Abate, S.; Arrigo, R.; Schuster, M. E.; Perathoner, S.; Centi, G.; Villa, A.; Su, D.; Schlögl, R. Pd nanoparticles supported on N-doped nanocarbon for the direct synthesis of H_2O_2 from H_2 and O_2. *Catal. Today* **2010**, *157*, 280−285.
(31) Burato, C.; Campestrini, S.; Han, Y.-F.; Canton, P.; Centomo, P.; Canu, P.; Corain, B. Chemoselective and re-usable heterogeneous catalysts for the direct synthesis of hydrogen peroxide in the liquid phase under non-explosive conditions and in the absence of chemoselectivity enhancers. *Appl. Catal, A* **2009**, *358*, 224−231.
(32) Rueda, T. M.; Serna, J. G.; Alonso, M. J. C. Direct production of H_2O_2 from H_2 and O_2 in a biphasic $H_2O/scCO_2$ system over a Pd/C catalyst: Optimization of reaction conditions. *J. Supercrit. Fluids* **2012**, *61*, 119−125.
(33) Moulder, J. F.; Stickle, W. F.; Sobol, P. E.; Bomben, K. D. *Handbook of X-ray photoelectron spectroscopy, Perkin Elmer Corp.*; Physical Electronics Division: USA, 1992.
(34) Doniach, S.; Šunjić, M. Many-electron singularity in X-ray photoemission and X-ray line spectra from metals. *J. Phys. C: Solid State Phys.* **1970**, *3*, 285−291.
(35) Penner, S.; Bera, P.; Pedersen, S.; Ngo, L. T.; Harris, J. J. W.; Campbell, C. T. Interactions of O(2) with Pd nanoparticles on alpha-Al(2)O(3)(0001) at low and high O(2) pressures. *J. Phys. Chem. B* **2006**, *110*, 24577−24584.

III

Chemical Engineering Journal xxx (2012) xxx–xxx

Contents lists available at SciVerse ScienceDirect

Chemical Engineering Journal

journal homepage: www.elsevier.com/locate/cej

Mass transfer and kinetics of H_2O_2 direct synthesis in a batch slurry reactor

Nicola Gemo [a], Pierdomenico Biasi [b], Paolo Canu [a,*], Tapio O. Salmi [b]

[a] Dipartimento di Ingegneria Industriale, University of Padova, via Marzolo 9, 35131 Padova, Italy
[b] Process Chemistry Centre (PCC), Laboratory of Industrial Chemistry and Reaction Engineering, Åbo Akademi, Biskopsgatan 8, 20500 Turku, Finland

HIGHLIGHTS

- Modeling of H_2O_2 direct synthesis, decomposition and hydrogenation experiments.
- Gas to liquid and liquid to solid mass transfer limitation analysis.
- Estimation of activation energies and pre-exponential factors.

GRAPHICAL ABSTRACT

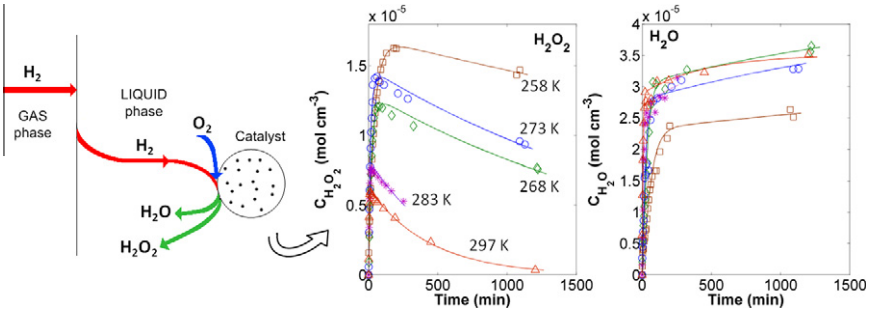

ARTICLE INFO

Article history:
Available online xxxx

Keywords:
Batch reactor modeling
Hydrogen peroxide
Direct synthesis
Green chemistry
Palladium

ABSTRACT

A model of a gas bubbling, batch slurry reactor for H_2O_2 direct synthesis is presented. Experimental measurements were carried out in the absence of halides and acids at temperatures between 258 and 297 K (pressures 14–20 bar, depending on temperature) with H_2 and O_2 diluted in CO_2 outside flammability limits (gas phase composition of CO_2, O_2 and H_2 was 77%, 21% and 2%, respectively). Kinetic experiments performed on a commercial 5% Pd/C catalyst (0.15 g in 400 ml methanolic solution) have been used to identify the intrinsic kinetics and assess the influence of mass transfer. The simplest rate equations compatible with the acknowledged reaction network has been included in a reactor model, which accounts for mass transfer resistances between gas and liquid and bulk of the liquid-catalyst surface.

The corresponding Arrhenius parameters were estimated from direct synthesis experiments for all the reactions. Comparable temperature dependence was observed for H_2O production, hydrogenation and decomposition (activation energies close to 45 kJ mol^{-1}), while H_2O_2 synthesis has a much lower activation energy (close to 24 kJ mol^{-1}), suggesting that a higher selectivity is achievable at low temperature. Decomposition had a very limited influence on the overall peroxide production rate, being quite slow (its rate is approx. 40% the direct synthesis rate at H_2 full conversion). Hydrogenation was the most rapid side reaction, depressing H_2O_2 production as H_2 conversion increased. Independent investigation on the H_2O_2 hydrogenation in the absence of O_2 highlighted significant difference in the kinetics, apparently due to a different oxidation state of the catalyst.

A sensitivity analysis on the mass transfer coefficients to allow for uncertainties in the correlations proved that no resistances in the liquid occur, while gas–liquid H_2 transfer rate may be limiting, although unlikely, requiring that literature coefficients overestimates the real transfer rate by an order of magnitude.

1. Introduction

Hydrogen peroxide is the simplest peroxide and is commercially available in aqueous solution over a wide concentration range. The main uses of hydrogen peroxide are in the preparation

* Corresponding author.
E-mail address: paolo.canu@unipd.it (P. Canu).

1385-8947/$ - see front matter © 2012 Elsevier B.V. All rights reserved.
http://dx.doi.org/10.1016/j.cej.2012.07.015

Nomenclature

A_R	pre-exponential factor of reaction R (same unit as rate constant)
a^{LG}	gas–liquid surface (cm^2)
a^{LS}	catalyst surface (cm^2)
C_i^L	concentration of species i in the bulk liquid (mol cm^{-3})
$C_i^{L,*}$	liquid equilibrium concentration of species i (mol cm^{-3})
C_i^S	concentration of species i in liquid at the catalyst surface (mol cm^{-3})
C_i^*	concentration of adsorbed species i (mol cm^{-2})
C^*	concentration of vacant active sites (mol cm^{-2})
C_{tot}^*	concentration of total active sites (mol cm^{-2})
d	impeller diameter (m)
d_b	bubble diameter (m)
d_{cat}	average catalyst particles diameter (mm)
D_{H_2}	effective diffusivity of H_2 ($m^2\ s^{-1}$)
$\wp_i$	diffusion coefficient of species i in the liquid phase ($m^2\ s^{-1}$)
Ea_R	activation energy of reaction R (kJ mol^{-1})
err	error function, as defined in Eq. (42)
h	impeller diameter (m)
K_i^L	gas–liquid mass transfer coefficient of species i, liquid side (cm s^{-1})
K_i^S	solid–liquid mass transfer coefficient of species i, liquid side (cm s^{-1})
H_i	equilibrium constant of species i
K_i	adsorption constant of species i ($cm^3\ mol^{-1}$)
k_i	irreversible rate constant of reaction i (units depend on reaction)
$k'_4 = k_{ds}$	apparent irreversible rate constant of direct synthesis reaction $\left(cm^6 mol^{-1} s^{-1} mol_{Pd}^{-1}\right)$
$k'_5 = k_{wf}$	apparent irreversible rate constant of water formation reaction ($cm^{9/2}\ mol^{-1/2}\ s^{-1}\ mol_{Pd}^{-1}$)
$k'_6 = k_d$	apparent irreversible rate constant of decomposition reaction ($cm^3\ s^{-1}\ mol_{Pd}^{-1}$)
$k'_7 = k_h$	apparent irreversible rate constant of hydrogenation reaction $\left(cm^6\ mol^{-1}\ s^{-1}\ mol_{Pd}^{-1}\right)$
m_j	slope of Arrhenius plot for the reaction j, Eqs. (44) and (45)
mol_{Pd}	quantity of palladium in each experiment (mol)
N	impeller speed (rps)
n_{exp}	number of isothermal experiments
$n_{H_2O}^{exp}$	number of experimental data of H_2O in each isothermal experiment
$n_{H_2O_2}^{exp}$	number of experimental data of H_2O_2 in each isothermal experiment
n_{H_2}	total amount of H_2 introduced in the reactor (mol)
q_j	intercept of Arrhenius plot for the reaction j, Eqs. (44) and (45)
P	power input under gassed conditions (W)
P_0	power input in un-aerated systems (W)
Q	recirculated gas flow rate ($m^3\ s^{-1}$)
R_{cat}	catalyst radius (cm)
R_j	rate of reaction j $\left(mol\ s^{-1}\ mol_{Pd}^{-1}\right)$
r_i	production rate of species i $\left(mol\ s^{-1}\ mol_{Pd}^{-1}\right)$
$s_{m,j}$	standard deviation of m_j (%)
$s_{q,j}$	standard deviation of q_j (%)
t	impeller blade thickness (m)
V^L	liquid volume (cm^3)
V^V	gas volume (cm^3)
w	parameter in Eq. (42)
z	reactor radius (m)

Greek letters

ε_{cat}	catalyst porosity
ϕ	gas hold-up
ϕ	Thiele modulus
κ_i	equilibrium rate constant of reaction i (units depend on reaction)
κ'_i	apparent equilibrium rate constant of reaction i (units depend on reaction)
μ^L	liquid viscosity (Pa s)
μ^G	gas viscosity (Pa s)
ξ	energy dissipation rate per unit mass (W kg^{-1})
ρ^L	liquid density (kg m^{-3})
ρ^G	gas density (kg m^{-3})
ρ_{cat}	catalyst density ($mol_{Pd}\ cm^{-3}$)
σ	interfacial tension (N m^{-1})

of other peroxides, as an oxidizing agent and to substitute chlorine in the waste treatment, textile industries and pulp and paper bleaching. The major manufacturing process (anthraquinone autoxidation) involves a catalytic hydrogenation, followed by an oxidation reaction to yield H_2O_2. Anthraquinone (Q) is used as a H_2 carrier.

Nowadays the interest on hydrogen peroxide direct synthesis (DS) is growing due to its constantly increasing demand. Moreover the possibility to couple the DS with already existent processes (i.e. synthesis of caprolactame and propene oxide) would allow reducing operations and transportations costs as well as the hazard of handling H_2O_2 solution.

The direct synthesis of hydrogen peroxide is a thermodynamically favored process, but selectivity and safety are still an obstacle to the industrial feasibility. The major limits of the DS process are selectivity (the same catalyst active for the DS is also promoting the consecutive reactions, i.e. decomposition and hydrogenation) and safety, because of the wide flammability limits of hydrogen. Lately the DS has attracted interests of both the Academia and Industries, trying to develop new catalyst concepts, reactor design and operation conditions [1,2]. Unfortunately, due to the interconnected reaction mechanism shown in Scheme 1 and the difficulty of analyzing the real mechanism of each reaction at the catalytic surface, the kinetic is still mostly empirical. In Scheme 1 all the reactions are catalyzed by Pd, and the contribution of each one differs with the reaction conditions (i.e. temperature, pressure, promoters, stabilizers, reactant medium, etc.).

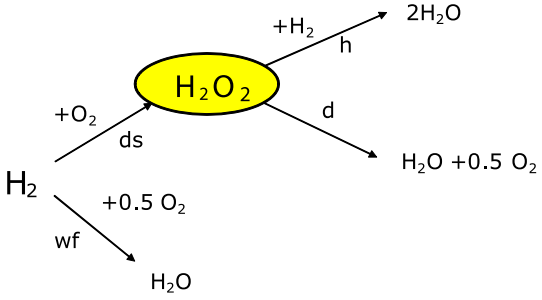

Scheme 1. Reactions involved in the direct synthesis of H_2O_2.

The four reactions involved are the direct formation of H_2O_2 (ds), the formation of H_2O (wf) and two consecutive reactions

Please cite this article in press as: N. Gemo et al., Mass transfer and kinetics of H_2O_2 direct synthesis in a batch slurry reactor, Chem. Eng. J. (2012), http://dx.doi.org/10.1016/j.cej.2012.07.015

consuming H_2O_2, i.e. decomposition (d) and hydrogenation (h). The unwanted reactions (wf, d and h) could be minimized acting on the operating conditions, in addition to designing a suitable catalyst, but kinetics and mass transfer limitation must be known. Most of the research on hydrogen peroxide DS concentrate on the catalyst design [3–8], where different metals or combination of metals and supports were studied to minimize the unwanted reactions. Results are difficult to compare mainly because of the different catalyst and reaction conditions involved. More recently contributions on the kinetics are growing in the Literature [9–13]. The main efforts were spent in rationalizing the effect of different reaction conditions on the catalyst and develop models to study the actual mechanism, for further optimization of selectivity and production rate. Recently kinetics has been studied with different approaches [13,12,9], Deguchi et al. [10], Moreno et al. [11].

Menegazzo et al. [13] correlated semi-batch reactor results (mono and bi-metallic Pd/Au catalysts over zirconia and ceria), with power law rates for the H_2O_2 formation, synthesis of water and reduction of H_2O_2, taking advantage of constant H_2 and O_2 concentration in the reaction environment. Depending on catalyst type and conditions, estimated kinetic constants were in the range 2.2–7.9 mol L^{-1} min^{-1}, 0.1–7.6 mol L^{-1} min^{-1} and 0.9–8.8 min^{-1} for direct synthesis, water formation and H_2O_2 hydrogenation, respectively. Note that the given kinetic parameters incorporate H_2 and O_2 liquid concentrations, considered constant in the work. Inoue et al. [12] formulated a power law kinetic constant for the DS using results from a microreactor with a commercial 5% Pd/C catalyst, calculating rate constants between 53.5 and 61.9 L^2 mol^{-1} s^{-1}, depending on operating conditions. Voloshin et al. [9], isolated and described in a microreactor the decomposition [14], reduction [15] (estimating an activation energy of 43.71 kJ mol^{-1}) and synthesis reactions [9] (calculated activation energy was 22.34 kJ mol^{-1}), also considering a Langmuir–Hinshelwood mechanism (over a Pd/Si catalyst); then the rate equations were coupled and implemented in a reactor model [16]. The isolation of the decomposition, H_2O_2 reduction and synthesis reactions was possible operating the microreactor in differential mode, where the conversion of the reactants was limited to 2%. Gas–liquid mass transfer parameters were measured studying the hydrogenation reaction over a range of velocities in order to model the reactor in the mass transfer regime. Deguchi et al. [10] tested a Pd/C catalyst in a semi-batch reactor and developed a Langmuir–Hinshelwood type mechanism taking into account also hydridohyroperoxy intermediate MHOOH for H_2O_2 formation; they also determined that the mass transfer was controlling their DS data. Deguchi et al. [10] was the only one taking into account the adsorption of the promoters in the kinetic study.

Moreno et al. [11] thoroughly discussed the effect of the promoters on the activation energy of the decomposition reaction in a semi-batch reactor at high pressure with a commercial Pd/C catalyst, estimating values in the range 15–83.87 kJ mol^{-1}, depending on the operating conditions and presence/absence of promoters. All the authors mentioned used stabilizers and promoters to reduce the effect of the consecutive reactions. The kinetic models cited above were all successful in describing their experimental data, although only a few accounted for mass transfer, suggesting a key role.

In this work we speculate theoretically on the kinetics and transport limitations using some knowledge developed in our previous works on hydrogen solubility [17] and kinetics experiments [18] performed without using promoters and stabilizers. We tried to understand the controlling factors that limits the hydrogen peroxide DS. The kinetic study was carried out both on the DS experiments and the decomposition and hydrogenation reactions, carried out in separate experiments. A multiphase reactor model was developed including the influence of transport limitations.

2. Experimental

The experiments were performed batchwise in a 600 ml unbaffled reactor with standard geometry (Buchi) and equipped with a self-sucking 6 blade impeller. Experimental apparatus and procedures are described elsewhere [18]. Shortly, 0.15 g of a 5% Pd/C catalyst were loaded in the reactor, that was then flushed four times with CO_2 to remove air and moisture. Carbon dioxide (18.4 bar) and oxygen (6 bar) were introduced in the vessel (298 K), followed by the injection of 400 ml of methanol. After pressure and temperature were stable at the desired values, hydrogen was fed as the limiting reagent. The reaction was assumed to start immediately after hydrogen loading. The gas mixture was carefully kept outside flammability limits (composition was 77%, 21% and 2% of CO_2, O_2 and H_2 respectively). A stirring rate of 1000 rpm was conservatively adopted to ensure a good mixing of the liquid phase, as verified in dedicated experiments. Hydrogenation and decomposition experiments were carried out following the same procedure, with N_2 replacing O_2 or H_2, respectively. The liquid phase was sampled at different times and water and H_2O_2 contents were determined by volumetric Karl Fischer and iodometric titration, respectively. The amount of liquid subtracted for each analysis was 0.7 ml, so that the total uptake never exceeded 8% of the initial liquid volume. Errors on H_2O_2 and H_2O measurements were estimated analyzing a methanol solution with a known water and hydrogen peroxide content (0.8% and 1.6% respectively), sampled from the reactor at experimental conditions. Estimated error on H_2O_2 was 0.8%, whereas on H_2O it was 2%.

3. Model

3.1. Chemical kinetics

Several surface mechanisms on palladium can give the overall process described in Scheme 1. Voloshin et al. [16] screened some mechanisms to describe kinetic data obtained from microstructured reactors and concluded that a Langmuir–Hinshelwood-type mechanism, with the surface reaction steps as rate determining ones, gave the best agreement with experimental data. Dissociative adsorption of the reactant species was also proposed by Deguchi et al. [10]. Some mechanistic studies have given information about the reaction mechanism. For instance, Dissanayake and Lunsford [19] proposed that the O–O bond does not dissociate during the H_2O_2 synthesis process and Sivadinarayana et al. [20] confirm the species HO^{2-} on a gold catalyst surface. However, it is clear that water formation requires the rupture of the O–O bond on the catalyst surface.

All the reactions involved in the series–parallel network (Scheme 1) are exothermic and thermodynamically favored [21] and Pd is known to promote all of them. Some basic assumptions are used here to describe the rate equations for the overall reactions in as simple as possible manner. The reaction mechanism proposed is summarized in Table 1.

The mechanism is based on the hypotheses that hydrogen and oxygen adsorb simultaneously and dissociatively on the metal catalyst surface, and surface hydroxyls are formed leading to the formation of hydrogen peroxide and water. The hydrogen peroxide decomposition and hydrogenation are described with the simplest possible mechanisms. Homogeneous reactions in the liquid phase are neglected, as experimentally demonstrated [18]. The adsorption and desorption steps are assumed to be rapid enough to reach quasi-equilibria, while the surface reaction steps IV, V, VI and VII are assumed to limit the rates.

For hydrogen and oxygen, the quasi-equilibrium hypothesis yields:

Please cite this article in press as: N. Gemo et al., Mass transfer and kinetics of H_2O_2 direct synthesis in a batch slurry reactor, Chem. Eng. J. (2012), http://dx.doi.org/10.1016/j.cej.2012.07.015

Table 1
Reaction steps, reaction routes and stoichiometric numbers ($\nu_{P1},\ldots,\nu_{P4}$).

	Step #	ν_{P1}	ν_{P2}	ν_{P3}	ν_{P4}
$H_2 + 2^* = 2H^*$	I	1	1	0	1
$O_2 + 2^* = 2O^*$	II	1	½	−1/2	0
$O^* + H^* = OH^* + ^*$	III	2	1	0	0
$OH^* + OH^* = HOOH^* + ^*$	IV	1	0	0	0
$OH^* + H^* = H_2O^* + ^*$	V	0	1	0	0
$HOOH^* + ^* = H_2O^* + O^*$	VI	0	0	1	0
$HOOH^* + 2H^* = 2H_2O^* + ^*$	VII	0	0	0	1
$HOOH^* = H_2O_2 + ^*$	VIII	1	0	−1	−1
$H_2O^* = H_2O + ^*$	IX	0	1	1	2

Route 1 (ν_{P1}): direct synthesis (ds) $H_2 + O_2 \rightarrow H_2O_2$.
Route 2 (ν_{P2}): water formation (wf) $H_2 + ½O_2 \rightarrow H_2O$.
Route 3 (ν_{P3}): decomposition (d) $H_2O_2 \rightarrow H_2O + ½\ O_2$.
Route 4 (ν_{P4}): hydrogenation (h) $H_2O_2 + H_2 \rightarrow H_2O$.
Rate limiting steps: IV, V, VI and VII.

$$K_{H_2} = \frac{C^{*2}_{H_2}}{C^S_{H_2} C^{*2}} \tag{1}$$

$$K_{O_2} = \frac{C^{*2}_{O_2}}{C^S_{O_2} C^{*2}} \tag{2}$$

from which the concentrations of the adsorbed species are obtained:

$$C^*_{H_2} = \left(K_{H_2} C^S_{H_2}\right)^{1/2} C^* \tag{3}$$

$$C^*_{O_2} = \left(K_{O_2} C^S_{O_2}\right)^{1/2} C^* \tag{4}$$

Application of the quasi-equilibrium hypothesis on the surface hydroxyls gives

$$K_{OH} = \frac{C^*_{OH} C^*}{C^*_O C^*_H} \tag{5}$$

which combined with the quasi-equilibria for adsorbed hydrogen and oxygen gives

$$C^*_{OH} = K_{OH}\left(K_{H_2} C^S_{H_2}\right)^{1/2}\left(K_{O_2} C^S_{O_2}\right)^{1/2} C^* \tag{6}$$

Analogously, the adsorption equilibria of hydrogen peroxide and water give the corresponding surface concentrations as described below:

$$C^*_{H_2O_2} = K_{H_2O_2} C^S_{H_2O_2} C^* \tag{7}$$

$$C^*_{H_2O} = K_{H_2O} C^S_{H_2O} C^* \tag{8}$$

The total site balance comprises all the adsorbed species (H^*, O^*, OH^*, $HOOH^*$, H_2O^*) and the vacant sites (*). After inserting all the quasi-equilibrium expressions into the balance equation, the fraction of vacant sites can be solved:

$$\frac{C^*}{C^*_{tot}} = \left(\left(K_{H_2} C^S_{H_2}\right)^{1/2} + \left(K_{O_2} C^S_{O_2}\right)^{1/2} + K_{OH}\left(K_{H_2} C^S_{H_2}\right)^{1/2}\left(K_{O_2} C^S_{O_2}\right)^{1/2} + K_{H_2O} C^S_{H_2O} + K_{H_2O_2} C^S_{H_2O_2} + 1\right)^{-1} = D^{-1} \tag{9}$$

where C^*_{tot} denotes the total concentration of surface sites. The rates of the rate-limiting steps can now be written as:

$$R_4 = k_4\left(C^{*2}_{OH} - C^*_{H_2O_2} C^* \Big/ \kappa_4\right) \tag{10}$$

$$R_5 = k_5\left(C^*_{OH} C^*_H - C^*_{H_2O} C^* \Big/ \kappa_5\right) \tag{11}$$

$$R_6 = k_6\left(C^*_{H_2O_2} C^* - C^*_{H_2O} C^*_O \Big/ \kappa_6\right) \tag{12}$$

$$R_7 = k_7\left(C^*_{H_2O_2} C^{*2}_{H_2} - C^{*2}_{H_2O} C^* \Big/ \kappa_7\right) \tag{13}$$

The concentrations of the surface species are expressed with the quasi-equilibria and the concentration of vacant sites. After inserting all these expressions, the rate equations can be rearranged. The constants can be merged, so that just a forward rate constant and an equilibrium constant is used for each step (the merged constants (k and κ') are products of surface rate and adsorption equilibrium constants):

$$R_4 = k'_4\left(C^S_{O_2} C^{S2}_{H_2} - C^S_{H_2O_2} \Big/ \kappa'_4\right) D^{-2} \tag{14}$$

$$R_5 = k'_5\left(C^S_{H_2} C^{S1/2}_{O_2} - C^S_{H_2O} \Big/ \kappa'_5\right) D^{-2} \tag{15}$$

$$R_6 = k'_6\left(C^S_{H_2O_2} - C^S_{H_2O} C^{S1/2}_{O_2} \Big/ \kappa'_6\right) D^{-2} \tag{16}$$

$$R_7 = k'_7\left(C^S_{H_2O_2} C^S_{H_2} - C^{S2}_{H_2O} \Big/ \kappa'_7\right) D^{-2} \tag{17}$$

Assuming that the steps are practically irreversible under the actual conditions and neglecting the adsorption contribution in the denominator because of low concentrations ($D = 1$), gives the simplest rate equations:

$$R_4 = R_{ds} = k_{ds} C^S_{O_2} C^{S2}_{H_2}, \quad k_{ds} = k'_4 \tag{18}$$

$$R_5 = R_{wf} = k_{wf} C^S_{H_2} C^{S1/2}_{O_2}, \quad k_{wf} = k'_5 \tag{19}$$

$$R_6 = R_d = k_d C^S_{H_2O_2}, \quad k_d = k'_6 \tag{20}$$

$$R_7 = R_h = k_h C^S_{H_2O_2} C^S_{H_2}, \quad k_h = k'_7 \tag{21}$$

with temperature dependent, Arrhenius-type kinetic constants:

$$k_i = A_i e^{-Ea_i/RT} \tag{22}$$

Pre-exponential factor (A_i) and activation energy (Ea_i) of each reaction are determined from our experimental data, as described below. The generation rates are formulated with the aid of the rate-limiting steps IV–VII. The following expressions are obtained:

$$r_{H_2O_2} = R_{ds} - R_d - R_h \tag{23}$$

$$r_{H_2O} = R_{wf} + R_d + 2R_h \tag{24}$$

$$r_{H_2} = -R_{ds} - R_{wf} - R_h \tag{25}$$

$$r_{O_2} = -R_{ds} - 0.5R_{wf} + 0.5R_d \tag{26}$$

3.2. Mass transfer

Mass transfer resistances are always involved in a multiphase reacting environment, hence, their role should be taken into account in a kinetic study. Here we consider two mass transfer resistances, dissolution of gases into the liquid phase and reactant transport in the liquid to the catalyst surface. For sake of clarity, a schematic representation is given in Fig. 1.

The gas phase is assumed well mixed so that the mass transfer between gas and liquid is controlled by the liquid side resistance (Fig. 1). At the gas–liquid interface, equilibrium holds. Vapor pressure of H_2O and H_2O_2 are neglected ($258 < T\,(K) < 297$) so that gradients occur only near the solid interface and species cumulate in the liquid phase.

Species fluxes are described in terms of mass transfer coefficients times concentration differences. Coefficients are calculated according to best available correlation for the reactor used, considering

Please cite this article in press as: N. Gemo et al., Mass transfer and kinetics of H_2O_2 direct synthesis in a batch slurry reactor, Chem. Eng. J. (2012), http://dx.doi.org/10.1016/j.cej.2012.07.015

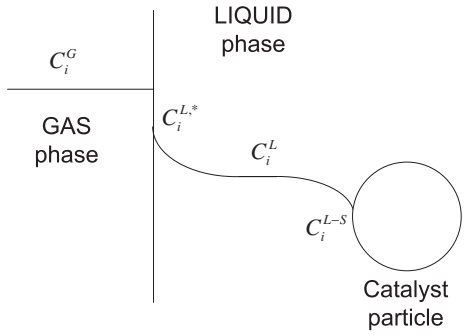

Fig. 1. Qualitative concentration profile of a reagent from the gas phase to the catalyst surface.

that gas is bubbling in the liquid and catalyst is in the form of fine powder, suspended in the liquid.

3.3. Gas–liquid mass transfer coefficients

The gas–liquid mass transfer coefficient depends on several factors (fluids considered, apparatus, agitation rate, temperature) and a suitable correlation for their estimation should be carefully chosen. The reactor used for the kinetics experiments was equipped with a self-suction turbine. Stirring causes a negative pressure at the impeller that indices suction of gas from the atmosphere above the liquid, through the hollow shaft, continuously yielding fine bubbles in the liquid phase. Therefore, the liquid mass transfer coefficients for O_2 and H_2 are estimated with a correlation for sparged stirred tank reactors [22]:

$$K_i^L a^L = \frac{2}{\sqrt{\pi}}\sqrt{\wp_i}\left(\frac{\xi\rho^L}{\mu^L}\right)^{\frac{1}{4}} a^L \tag{27}$$

Values of the diffusion coefficients ($\wp_i$) are calculated with the Wilke–Chang equation [23] assuming pure methanol, because it largely dominates the liquid composition. Assuming that energy at gas–liquid interface is consumed at the gas bubbles surface, the energy dissipation rate per unit mass (ξ) can be evaluated with the correlation proposed by Garcia-Ochoa et al. [24]:

$$\xi = \frac{P}{\rho^L(\pi/4)dh} \tag{28}$$

where the power input (P) is calculated as:

$$P = 0.783\left(\frac{P_0^2 \mathrm{Nd}^3}{Q^{0.56}}\right)^{0.459} \tag{29}$$

We used the gas flow rate recirculated through the hollow shaft for Q. The value of Q was $5\ \mathrm{cm^3\ s^{-1}}$, estimated with dedicated experiments. P_0 is the power consumption in an un-aerated system. Its values depends on the power number, N_p, that can be considered constant assuming turbulent regime [24]. According to the definition of the dimensionless power number, P_0 is given by:

$$N_p = \frac{P_0}{\rho^L N^3 d^5} \tag{30}$$

The power number depends on the impeller type and geometry and is estimated using the correlation proposed by Rutherford et al. [25]:

$$N_p = 6.405 - 55.673(t/d) \tag{31}$$

For the correct evaluation of the mass transfer resistance, also the gas–liquid interfacial area (a^L) has to be estimated. Assuming spherical bubbles, a^L can be calculated from the average bubble size, d_b, and the gas hold-up, ϕ, by the following correlations [24]:

$$a^L = \frac{6\phi}{d_b} \tag{32}$$

$$\frac{\phi}{1-\phi} = 0.5\frac{(Q/(\pi z^2))^{2/3}}{(9.81l)^{1/3}}\left(\frac{\rho^L}{\rho^L - \rho^G}\right) \tag{33}$$

where

$$l = 2\left(\frac{\sigma}{0.4\rho^L}\right)^{3/5}\left(\frac{(h/6)^{2/5}}{(\pi Nd)^{6/5}}\right)\left(\frac{\rho^L}{\rho^G}\right)^{0.1} \tag{34}$$

For Newtonian fluids, the estimation of the average bubble size (d_b) is given by [26]:

$$d_b = 0.7\frac{\sigma^{0.6}}{\left(10^6 P/V^L\right)^{0.4}\rho^{L0.2}}\left(\frac{\mu^L}{\mu^G}\right)^{0.1} \tag{35}$$

The density (ρ) and the viscosity (μ) of liquid and gas phases, as well as the interfacial tension (σ), required in Eqs. (10)–(18), are estimated with an equation of state [17] at experimental conditions.

3.4. Liquid–solid mass transfer coefficients

The catalyst effectiveness factor is initially considered equal to one because of the small particle size (the average diameter is 30 μm) and slow reaction rate, so that mass transfer limitation inside the catalyst is likely to be negligible. This assumption will be discuss later. The external mass transfer coefficients at the catalyst surface are evaluated assuming no relative velocity between the liquid and the catalyst. This assumption is justified because of the small dimension of the catalyst particles. In this condition the Sherwood number can be approximated to 2, and the K_i^S values are essentially the diffusion coefficients ($\wp_i$):

$$Sh = 2 = \frac{K_i^S d_{cat}}{\wp_i}10^5 \tag{36}$$

The liquid–solid interface area (a^s) is evaluated from the catalyst amount (0.15 g) and its specific surface area, according to BET measurements (Sorptomatic 1900, Carlo *Erba* Instruments) resulted in 855 $\mathrm{m^2\ g^{-1}}$, which implies $a^s = 128\ \mathrm{m^2}$.

3.5. Reactor model

The reactor and operating procedures have been described elsewhere [18]. Shortly, it is a batch, slurry reactor with a gas entraining stirrer that continuously creates gas bubbles in the bulk of the liquid, drawing gas from the atmosphere above the liquid. The species mass balances have been written in each phase, i.e. gas and liquid, the solid being assumed non-porous reduce to a flux balance at its interface. Balances are based on the following assumptions:

(a) both liquid and gas phase are well mixed;
(b) carbon dioxide and methanol are not involved in any reaction;
(c) any increment of liquid volume due to the accumulation of H_2O_2 and H_2O is neglected, while the change caused by sampling is taken into account;
(d) species cannot accumulate on the catalyst surface, nor in the liquid boundary layer surrounding the catalyst particles.

According to these assumptions, the mass balances in the gas and liquid phases can be written as:

$$V^G \frac{dC_i^G}{dt} = a^{LG} K_i^L \left(C_i^L - C_i^{L,*} \right) \quad i = H_2, O_2 \tag{37}$$

$$V^L \frac{dC_i^L}{dt} = a^{LG} K_i^L (C_i^{L,*} - C_i^L) - a^{LS} K_i^S \left(C_i^L - C_i^S \right)$$
$$i = H_2, O_2, H_2O_2, H_2O$$

At the catalyst surface interface the material balances under assumption (d) becomes:

$$0 = a^{LS} K_i^S (C_i^S - C_i^L) - r_i \cdot mol_{Pd} \quad i = H_2, O_2, H_2O_2, H_2O \tag{39}$$

where the production rates r_i appears, which are functions of the species concentration facing the catalyst surface, C_i^S. At the gas–liquid interface equilibrium holds:

$$C_i^{L,*} = H_i C_i^G \tag{40}$$

The equilibrium constants H_i depends on total composition, pressure and temperatures. H_i values are only needed for oxygen and hydrogen, due to assumptions (b) and (c), and are estimated from an equation of state [17] tuned on specific experimental data.

The proposed model is given by a total of ten equations: two ODEs for the gas phase, four ODES for the liquid phase and four algebraic equations for the catalyst surface, resulting in a low index ADEs system. Its integrations yields the evolution in time of the concentration of reactants (i.e. H_2 and O_2) in the gas and liquid phases and at the catalyst surface (six unknown functions), and the concentration of H_2O_2 and H_2O in the liquid phase and at the catalytic surface (four unknowns).

According to the experimental procedure [18], the following ten initial conditions are assumed:

$$\begin{aligned}
&\text{(a) } C_{O_2}^G\Big|_{t=0} = C_{O_2}^{G,0} \qquad \text{(e) } C_{H_2}^L\Big|_{t=0} = C_{H_2O_2}^L\Big|_{t=0} = 0 \\
&\text{(b) } C_{H_2}^G\Big|_{t=0} = \frac{n_{H_2}}{V^L} \qquad \text{(f) } C_{O_2}^S\Big|_{t=0} = C_{O_2}^{L,0} \\
&\text{(c) } C_{O_2}^L\Big|_{t=0} = C_{O_2}^{L,0} \qquad \text{(g) } C_{H_2O}^S\Big|_{t=0} = C_{H_2O}^{L,0} \\
&\text{(d) } C_{H_2O}^L\Big|_{t=0} = C_{H_2O}^{L,0} \qquad \text{(h) } C_{H_2}^S\Big|_{t=0} = C_{H_2O_2}^S\Big|_{t=0} = 0
\end{aligned} \tag{41}$$

Primarily, hydrogen (the limiting reagent) was introduced after all the other species, when stable values of pressure and temperature were reached inside the reactor (filled with O_2, CO_2 and methanol). Since the H_2 feeding was fast compared to the reaction time [18], hydrogen is assumed not to dissolve in the liquid phase while introduced (conditions 41b and 41e). Initial compositions of the gas and liquid phases were evaluated with an equation of state [17]. The initial concentration of water in the reaction medium (condition 41d) was measured [18] prior the introduction of hydrogen.

The material balances Eqs. (37)–(39), together with initial conditions (41) have been efficiently solved using Matlab's ode15s ADEs solver, also suitable for stiff equations, being based on a multistep, variable order method based on the numerical differentiation formulas.

3.6. Kinetics identification

The kinetic model has been formulated above. To complete its definition, values of the activation energy and the pre-exponential factor of the reactions involved in the catalytic process must be calculated. They have been determined by a sequence of isothermal experimental data fitting, providing the four irreversible reaction rate constants k_{ds}, k_{wf}, k_d and k_h at the given temperature. Then an Arrhenius plot is assembled for each reaction, and the relative activation energy and pre-exponential factors determined by fitting $k(T)$.

To fit the experimental data, the following error function was used for each experiment (i.e. a given temperature):

$$err = \frac{\sqrt{\sum_{i=1}^{n_{H_2O_2}^{exp}} \left| C_{H_2O_2,i}^{S,Exp} - C_{H_2O_2,i}^{S,Calc} \right|^2}}{\frac{1}{n_{H_2O_2}^{exp}} \sum_{i=1}^{n_{H_2O_2}^{exp}} C_{H_2O_2,i}^{S,Exp}} + w \frac{\sqrt{\sum_{i=1}^{n_{H_2O}^{exp}} \left| C_{H_2O,i}^{S,Exp} - C_{H_2O,i}^{S,Calc} \right|^2}}{\frac{1}{n_{H_2O}^{exp}} \sum_{i=1}^{n_{H_2O}^{exp}} C_{H_2O,i}^{S,Exp}} \tag{42}$$

Note that errors between experimental and calculated concentrations have been rescaled. In pure decomposition and hydrogenation experiments, where water concentration was not measured, we set the parameter $w = 0$; in all other cases, $w = 1$. A Nelder–Mead simplex algorithm with positivity constraints on the parameters (fminsearchbnd function) is used to minimize the error by adjusting the four parameters of the model (k_{ds} k_{wf}, k_d and k_h).

The results were critically analyzed by preparing sensitivity plots, in which the objective function was plotted as a function of a single parameters at a time, while the other parameter values were kept fixed, which gave the objective function minimum. The correlation between the parameters are visualized evaluating a contour plots for each pair, that is plotting couples of parameter values that result in the same value of the error function (42), with the other parameters kept constant.

The goodness of the fit in each experiment is measured with the squared correlation between predicted and experimental concentrations:

$$r_{H_2O_2}^2 = 1 - \frac{\sum_{i=1}^{n_{H_2O_2}^{exp}} \left| C_{H_2O_2,i}^{S,Exp} - C_{H_2O_2,i}^{S,Calc} \right|^2}{\sum_{i=1}^{n_{H_2O_2}^{exp}} \left(C_{H_2O_2,i}^{S,Exp} - \frac{1}{n_{H_2O_2}^{exp}} \sum_{k=1}^{n_{H_2O_2}^{exp}} C_{H_2O_2,k}^{S,Exp} \right)^2} \tag{43}$$

Whenever experimental concentrations of H_2O are available, Eq. (43) is also used to check the fit to those data.

The slope and the intercept of the Arrhenius plots are fitted in a least-square sense using linear fitting. The errors on activation energy and pre-exponential factors of each reaction are calculated [27] as standard deviations of slope (m_j) and intercept (q_j) of the fitted lines, respectively:

$$s_{m,j} = \frac{1}{m_j} \sqrt{\frac{n_{exp} \sum_{i=1}^{n_{exp}} \left| \ln(k_{j,i}) - \left(m_j \frac{1}{T_i} + q_j \right) \right|^2}{(n_{exp} - 2) \left(n_{exp} \sum_{i=1}^{n_{exp}} \left(\frac{1}{T_i} \right)^2 - \left(\sum_{i=1}^{n_{exp}} \frac{1}{T_i} \right)^2 \right)}} \cdot 100 \tag{44}$$

$$s_{q,j} = s_{m,j} \frac{m_j}{q_j} \sqrt{\frac{\sum_{i=1}^{n_{exp}} \left(\frac{1}{T_i} \right)^2}{n_{exp}}} \tag{45}$$

The goodness of the fitting to the Arrhenius plot is also checked by the degree of explanation (r^2, analogous of Eq. (43)).

4. Results and discussion

The kinetics has been formulated above; assuming pseudo-elementary reactions, the partial reaction orders have been taken from the stoichiometry. Experimental data were then used to estimate the parameters in the Arrhenius constant for each step in the mechanism. Experiments of direct synthesis, H_2O_2 decomposition and hydrogenation have been analyzed independently.

4.1. Direct synthesis experiments

Fig. 2 shows the whole set of experimental data used. H_2O and H_2O_2 mol concentration in the liquid have been collected along the time in isothermal, batch experiments, at different temperatures. A

minimum of 30 samples was collected at each temperature; a total of 174 data was used for the regression of the eight parameters, i.e. activation energy and pre-exponential factors. Each isothermal run has been simulated and a set of k's estimated, for each step in the mechanism; results are reported in Table 2, along with the coefficients of determination r^2 measuring the agreement of model predictions with both H_2O_2 and H_2O concentration profiles, qualitatively shown in Fig. 2.

The model is always in very good agreement with experimental results, with r^2 values for H_2O_2 very close to 1. Experimental measurements of H_2O are less precise, due to the different analytical procedure, slightly decreasing the goodness of fit.

With the calculated isothermal rate constants the assumption of unitary effectiveness factor can be checled. The Thiele modulus, ϕ, is estimated as [28]:

$$\phi = \frac{R_{cat}}{3}\sqrt{\frac{\left(k_{ds}C^s_{O_2} + k_{wf}(C^s_{O_2})^{1/2} + k_h C^s_{H_2O_2}\right)\rho_{cat}}{10^4 D_{H_2}}} \quad (46)$$

where D_{H_2} (effective diffusivity of H_2) is computed as $D_{H_2} = \varepsilon^2_{cat}\wp_{H_2}$, where $\varepsilon_{cat} = 0.6$ is the porosity of the catalyst. The effectiveness factor is calculated as follows:

$$\eta = \frac{1}{\phi}\left(\coth 3\phi - \frac{1}{3\phi}\right) \quad (47)$$

For a typical particle size $R_{cat} = 15$ μm and at the highest temperature (i.e. highest reaction rates), ϕ is in the order of 10^{-3} and $\eta \approx 1$, so that recalculation of the mass transfer coefficients and rate constants is unnecessary.

The kinetic constants calculated at each temperature are collected in Fig. 3 in the form of Arrhenius plots, and the resulting activation energies and pre-exponential factor are reported in Table 3.

The temperature dependence of water formation, decomposition and hydrogenation are all comparable (activation energies close to 45 kJ mol^{-1}). However, the kinetics of these reactions is quite different. Table 2 shows that k values can differ by orders of magnitude, but they are not really comparable, because refer to different overall reaction orders. The most appropriate comparison must inspect the values of the reaction rates during the course of each experiments, as shown in Fig. 4.

Each reaction rate has been related to the one of direct synthesis, R_{wf}/R_{ds}, R_d/R_{ds} and R_h/R_{ds}. Both decomposition and hydrogenation rates are null at the beginning, requiring the presence of the peroxide (i.e. they are reactions consecutive to the direct synthesis). Their rates increase during the reactions course, at a different pace. Decomposition reaction is very slow compared to the direct synthesis and becomes important only at a high H_2 conversion, when the direct synthesis reaction slows down. A strong effect of the temperature is also observed on this reaction, where lower temperature is confirmed to stabilize the H_2O_2 produced. The preferred path of H_2O_2 degradation is the hydrogenation reaction: its rate rapidly increases as H_2O_2 becomes available, limiting the H_2O_2 production. However this reaction is always slower than the direct synthesis ($R_h/R_{ds} < 1$) and it can be limited by decreasing the temperature, up to $R_h/R_{ds} < 0.5$ at 258 K. Unfortunately, the R_{wf}/R_{ds} is always significant because the formation of water really competes with the direct synthesis, prevailing ($R_{wf}/R_{ds} > 1$) at higher temperature, whereas lower temperature favors the direct synthesis ($R_{wf}/R_{ds} < 1$). This explains the increased selectivity at lower temperature reported in the Literature, including our previous work [18]. At a given temperature, the rate of H_2O formation remains very close to that of the direct synthesis (constant R_{wf}/R_{ds}) except for a short initial transient favoring the direct synthesis.

Due to the intrinsic nature of the interconnected reaction mechanism, a correlation between the estimates of reaction rate constants has to be expected. A quantitative evaluation is given in Fig. 5 as contour plots for the parameter estimates, at $T = 268$ K. A small correlation is indicated by contours approaching circles.

A strong correlation is observed between most reaction constants, and remarkably among direct H_2O_2 synthesis and the other reactions. The lowest correlation occurs between decomposition and water formation, as expected. The same analysis was carried out for all isothermal data with similar results. In order to improve or double check our estimates and suppress the correlation among the parameters, we studied the decomposition and hydrogenation rate constants independently, with dedicated experiments.

4.2. Decomposition experiments

Rate expression (20) was used to fit the H_2O_2 concentration profiles during decomposition experiments, to isolate this step. At each temperature a minimum of 10 samples was collected; a total of 45 data was used to calculate the two parameters, i.e. activation energy and pre-exponential factor. Since in these experiments H_2 was replaced with N_2, calculations were carried out neglecting rate expressions (18) and (19) and hydrogen mass balance (Eq. (25)). Fig. 6 shows the results, both as measured and calculated isothermal data of H_2O_2 concentration as a function of time, and in terms of Arrhenius plot.

Predictions are in good agreement (r^2 very close to 1) with experimental observations at any temperature considered, confirming that decomposition is a first order reaction with respect to H_2O_2 concentration. The calculated reaction rate constants are

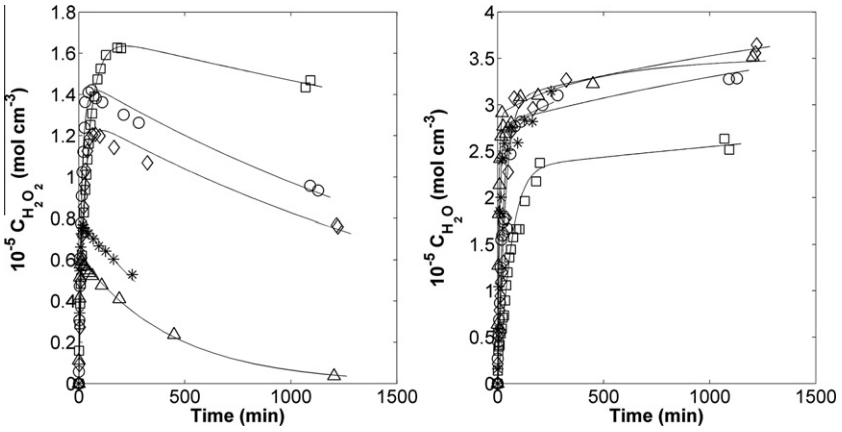

Fig. 2. H_2O_2 direct synthesis experiments in the batch reactor: □, 258 K; ◇, 268 K; ○, 273; *, 283 K; △, 297 K; solid line, model.

Table 2
Isothermal reaction rate constants and *r*-square value on H_2O_2 and H_2O.

T (K)	$k_{ds}/10^7$ $\left(cm^6\ mol^{-1}\ s^{-1}\ mol_{Pd}^{-1}\right)$	$k_{wf}/10^5$ $\left(cm^{9/2}\ mol^{-1/2}\ s^{-1}\ mol_{Pd}^{-1}\right)$	k_d $\left(cm^3\ s^{-1}\ mol_{Pd}^{-1}\right)$	$k_h/10$ $\left(cm^6\ mol^{-1}\ s^{-1} mol_{Pd}^{-1}\right)^8$	$r^2H_2O_2$ (−)	r^2H_2O (−)
297	26.42	48.78	221	35.20	0.9897	0.9777
283	17.68	19.84	227	17.39	0.9846	0.9790
273	12.17	7.18	48	5.68	0.9929	0.9525
268	8.00	6.18	52	4.46	0.9920	0.9738
258	6.67	3.27	17	2.30	0.9913	0.9716

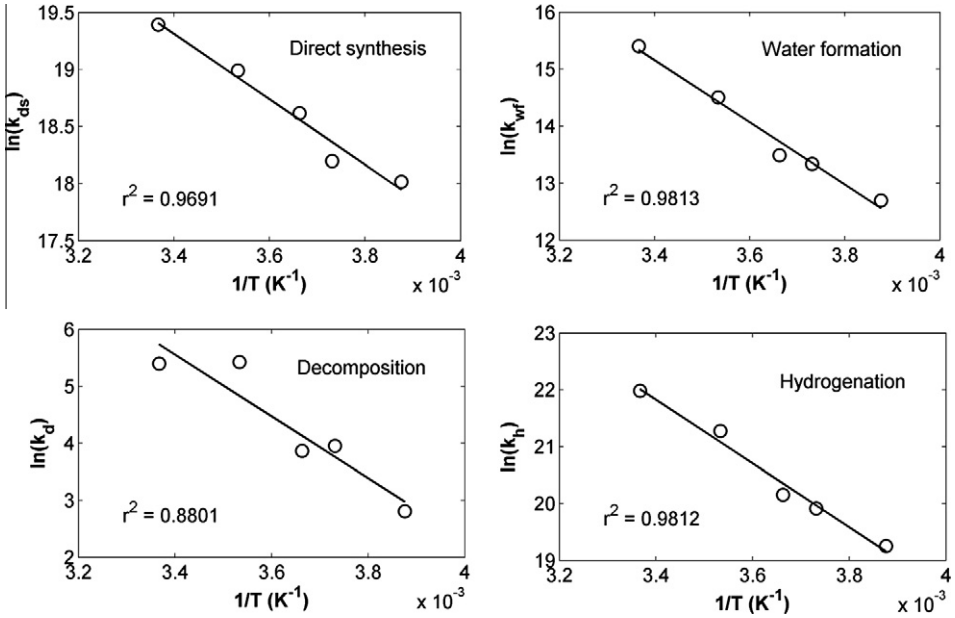

Fig. 3. Arrhenius plots for the kinetic constants of each individual step in the mechanism.

Table 3
Arrhenius constants for the rate Eqs. (1)–(4) (direct synthesis experiments).

	Pre-exponential factor (see Table 2 for units)	Activation energy (kJ mol^{-1})
Direct synthesis	$4.18 \pm 0.15 \times 10^{12}$	23.84 ± 2.45
Water formation	$4.27 \pm 0.20 \times 10^{14}$	45.31 ± 3.61
Decomposition	$2.61 \pm 0.45 \times 10^{10}$	45.06 ± 9.60
Hydrogenation	$5.65 \pm 0.22 \times 10^{17}$	46.58 ± 3.72

shown in Fig. 6b and the corresponding kinetic parameters are reported in Table 4.

A comparison of the Arrhenius constants obtained by fitting all the rate constant in Eqs. (18)–(21) together, using the direct synthesis experimental data, shows that the activation energy for k_d obtained here for the decomposition reaction (50.43 kJ mol^{-1}) compares well with the above value (45.06 kJ mol^{-1}, Table 3), being that their confidence intervals overlap substantially. A higher deviation is observed in the pre-exponential factors. However, the deviation on the isothermal kinetic constants k_d is less than 10% ($T < 273$ K), confirming the results reported in Table 3.

4.3. Hydrogenation experiments

H_2O_2 hydrogenation experiments were carried out collecting a minimum of 10 samples; a total of 36 data was used to calculate the two parameters, i.e. activation energy and pre-exponential factor. The experiments were performed substituting O_2 with N_2. Hence, direct synthesis and water formation reactions do not occur. Accordingly, when regressing these data the mass balance of O_2 (Eq. (26)) and rates (18) and (19) are ignored. Decomposition rate constants are not regressed this time and the parameters previously obtained (Table 4) are introduced in the model and kept fixed. Only rate expression (21) is considered and isothermal hydrogenation reaction constants regressed. The deviation between experimental H_2O_2 concentration measured during pure hydrogenation and the best fit predictions is rather high, as shown in Fig. 7a.

Apparently, the kinetic model in this case is not adequate. The decay of H_2O_2 concentration in time is only approximately exponential, as clearly perceivable from Fig. 7a. In the first minutes of reaction, and more clearly at lower temperature, the H_2O_2 concentration decreases more slowly than later on. At higher H_2 conversion, the decay is very rapid, in a way that a second-order rate equation, linearly proportional to each reagent concentration, cannot fit. Consequently, the model switch from under- to over-estimation of the measured H_2O_2 concentration, when approx. 70% of the introduced H_2O_2 is consumed. The effect of temperature, within the approximation discussed above, is well described by a linear Arrhenius plot, shown in Fig. 7b. The calculated activation energy and pre-exponential factor are respectively 17.85 ± 1.00 kJ mol^{-1} and $7.47 \pm 0.11 \times 10^{12}$ $cm^6 mol^{-1} s^{-1} mol_{Pd}^{-1}$. However, the k_h values are much higher compared to the ones reported in Fig. 3, also reflected in a significantly lower activation energy. We explain both results, a 2-steps H_2O_2 consumption and its higher rate, in terms of differences in the catalyst oxidation state. Synthesis and hydrogenation experiments use a different experimental condition: the former are carried out in large excess of O_2, the latter does not include any O_2, but H_2 is the only reactant present. Accordingly, the

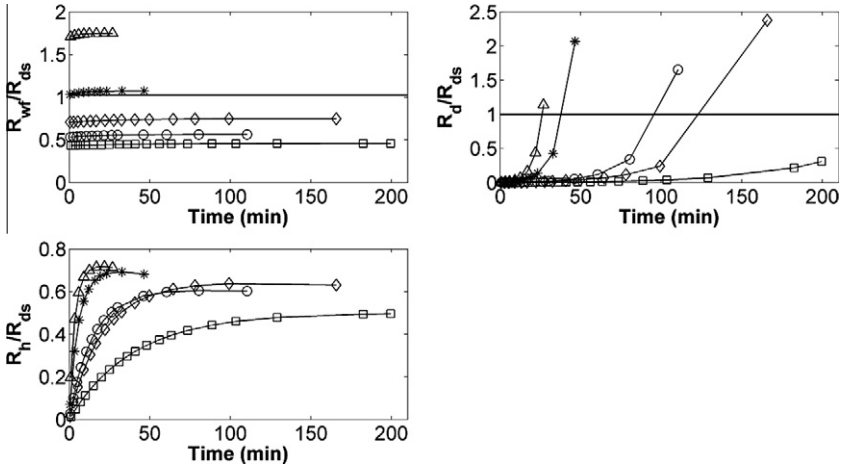

Fig. 4. Ratio of each reaction rate to the direct synthesis during the reaction course. △, 297 K; *, 283 K; ○, 273 K; ◇, 268; □, 258 K.

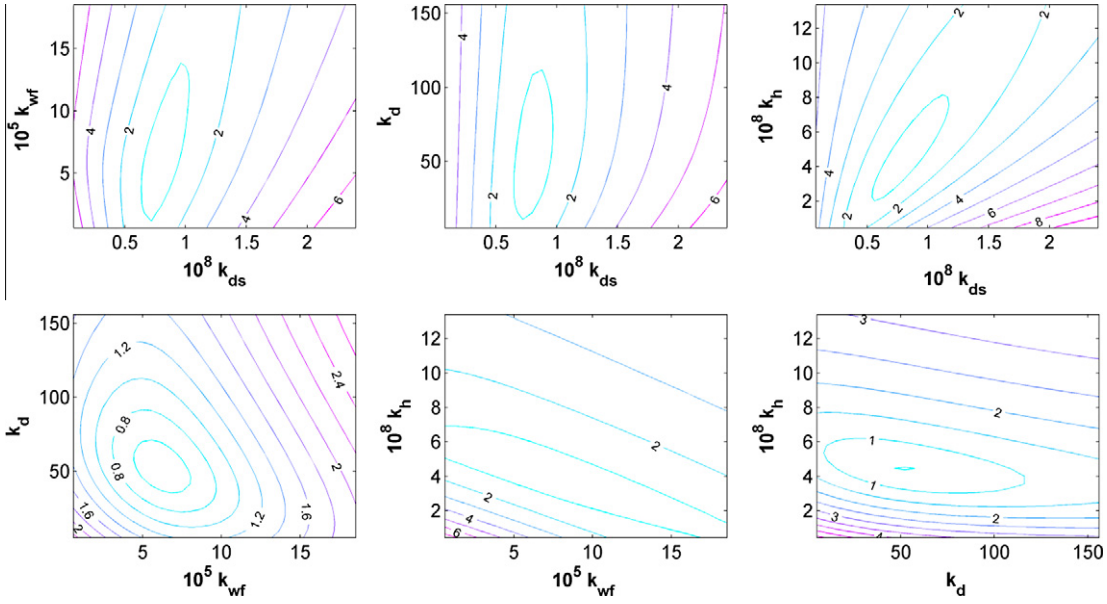

Fig. 5. Contour plots of regressed kinetic parameters (T = 268 K).

Table 4
Arrhenius constants for rate Eq. (3) (decomposition experiments).

Pre-exponential factor ($cm^3\ s^{-1}$)	Activation energy ($kJ\ mol^{-1}$)
$3.11 \pm 0.21 \times 10^{11}$	50.43 ± 4.28

active metal on the catalyst can be mostly oxidized in excess of O_2 (synthesis conditions), and reduced in excess of H_2 (hydrogenation conditions). The reduced form of the catalyst can be more effective for the hydrogenation reaction, enhancing its rate, consistently with literature observations [21,12] that the production of hydrogen peroxide is favoured by the oxidized form of Pd. In addition, the H_2O_2 hydrogenation on reduced Pd may occur with a non-elementary mechanism, involving a complex model also accounting for competitive adsorption of H_2 and O_2. According to the discussion above, we rely on the kinetic model and values of Table 2 to describe the reaction network at synthesis (i.e. O_2 dominated) conditions. Further, we question the significance of independently estimating the H_2O_2 hydrogenation kinetics in case the catalyst is vulnerable to oxidation/reduction at conditions of the experiments, which is quite common. Also, in case of non-elementary mechanism, a competitive adsorption on the catalyst sites between H_2 and O_2 is expected in the synthesis experiments, which is not the case for hydrogenation experiments.

Unfortunately, the kinetic parameters determined here are difficult to compare numerically with other studies in the Literature, because of the different rate laws, catalysts, and assumptions in describing the reacting environment. Menegazzo et al. [13] studied the kinetics on a bimetallic Pd/Au catalyst, in a semi-batch reactor (batch liquid phase and flowing gas), at ambient conditions. Being the concentration of H_2 and O_2 constant (albeit not specified), they were included in the kinetic parameters, making a quantitative comparison with our results quite difficult. In addition, material balances differ in the stoichiometry and reaction orders as well. Voloshin et al. [15] measured the kinetics of H_2O_2 hydrogenation reaction over a Pd/SiO catalyst in a microreactor; they determined an activation energy of 43.71 $kJ\ mol^{-1}$, close to our estimate using synthesis experiments (46.58 $kJ\ mol^{-1}$), but not the pure hydrogenation ones, as discussed above. In another study [9], the same Authors reported the activation energy for the direct synthesis as

Please cite this article in press as: N. Gemo et al., Mass transfer and kinetics of H_2O_2 direct synthesis in a batch slurry reactor, Chem. Eng. J. (2012), http://dx.doi.org/10.1016/j.cej.2012.07.015

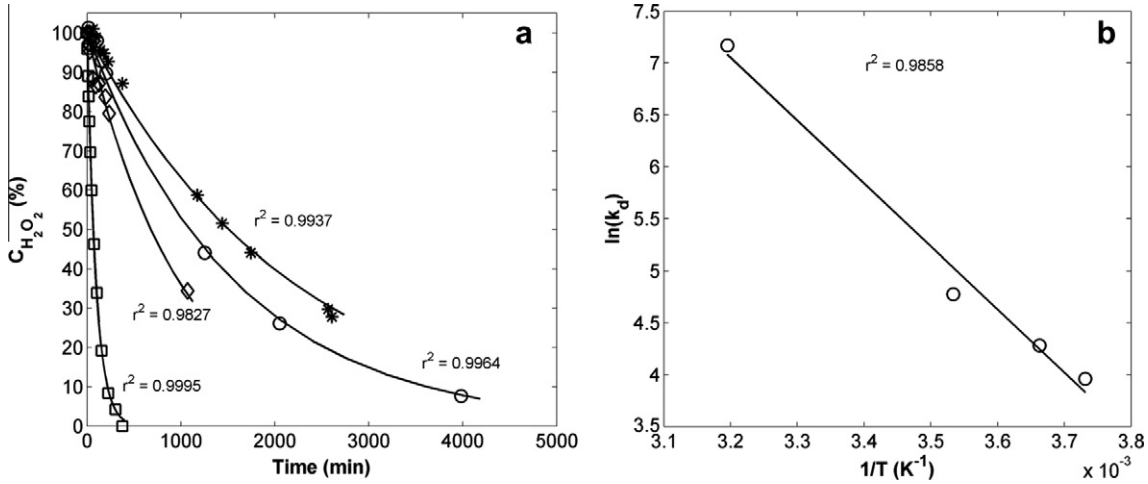

Fig. 6. H_2O_2 decomposition experiments in a batch reactor: (a) normalized experimental and calculated H_2O_2 concentration and *r*-square values: □, 313 K; ◇, 283; ○, 273 K; *, 268 K; solid line, model. (b) Arrhenius plot for k_d.

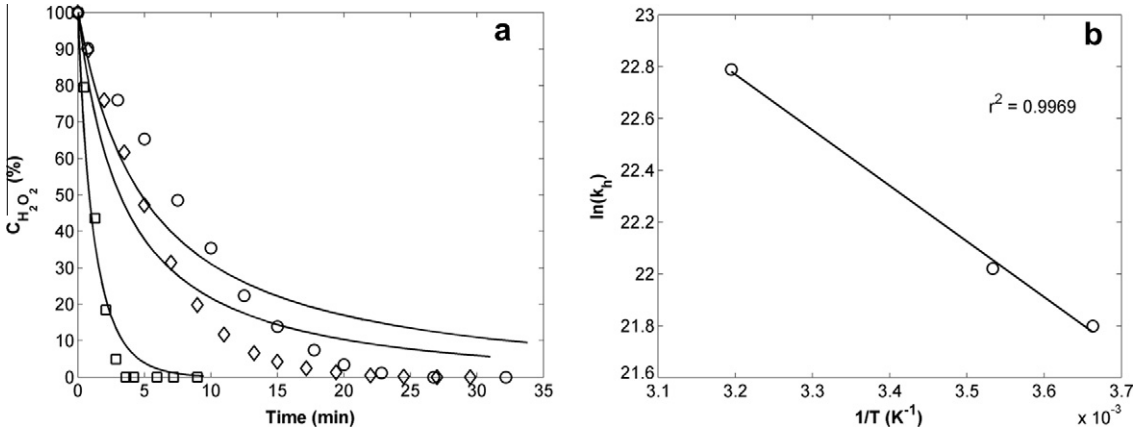

Fig. 7. H_2O_2 hydrogenation experiments in batch reactor: (a) normalized experimental and calculated H_2O_2 concentration: □, 313 K; ◇, 283; ○, 273 K; solid line, model. (b) Arrhenius plot.

well, in a similar apparatus; they found 22.34 kJ mol^{-1}, a value that compare well to 23.84 kJ mol^{-1} that we calculated here.

5. Parametric sensitivity on mass transfer coefficients

Values of $K_i^L a^L$ (mass transfer between gas and liquid) for H_2 was calculate in the range 960–1880 h^{-1}, at 258 and 297 K, respectively. Similar values were obtain for O_2. Our calculations compare well with 1080 h^{-1} measured by Meyberg et al. [29] for H_2 in liquid alkyne in a similar apparatus. Deguchi et al. [30] observed smaller values for H_2 dissolution in water at 303 K in a 300 ml flask equipped with a magnetic stirrer (149–560 h^{-1} varying the stirring speed from 1000 to 1350 rpm). Andersson et al. [31] performed H_2 dissolution experiments in anthraquinones at different temperatures in a two liters autoclave with two turbine impeller, reporting a $K_i^L a^L$ value of 1400 h^{-1} at 298 K. The deviations observed among these works are likely due to differences in the geometry of the equipment used, stirring and operative conditions adopted.

The coefficients of mass transfer resistance at the catalyst surface, K_i^S, estimated by Eq. (36), are in the range 1.4×10^{-2}–3.5×10^{-2} cm s^{-1} at 258 K and 297 K, respectively, for all components.

Since we tried to predict the mass transfer rates a priori, using the best available correlations, we expect that the chemical kinetics was properly identified, with the results given in Table 3. Would the mass transfer actually control the process, or part of it, we should expect the chemical kinetics to be inaccurately determined. We actually used this reasoning to evaluate the extent of mass transfer control at our experimental conditions. The values of $K_i^L a^L$ and K_i^S, first calculated by Eqs. (27)–(36), have been increased or decreased by up to one order of magnitude and the kinetic parameters (activation energy and pre-exponential factors) re-estimated. Different simulations were carried out changing each individual mass transfer coefficients, one at a time. As expected, no influence on the kinetic parameters was observed varying $K_i^L a^L$ and K_i^S values of O_2, H_2O_2 and H_2O, the only critical species being hydrogen, the limiting reagent in all the performed experiments. Further, decomposition reaction is not affected by hydrogen concentration because of its rate law expression, and it is excluded from this analysis. The sensitivities of the reaction rate constants k to $K_{H_2}^L a^L$ are shown in Fig. 8.

Decreasing H_2 mass transfer coefficients from gas to liquid affects the estimated rate constants of any reaction; the reduced H_2 transfer rate to the liquid phase (and hence to the catalyst) must be balanced by the increased reaction kinetics. Interestingly, limitations in the H_2 mass transfer rate cause an apparent increase in the estimated activation energy, as can be observed in Fig. 9, recalling the importance of accounting for mass transfer to properly identify the kinetics.

However, some mass transfer effect was only evident at temperatures above 283 K, by artificially lowering $K_{H_2}^L a^L$ at least by

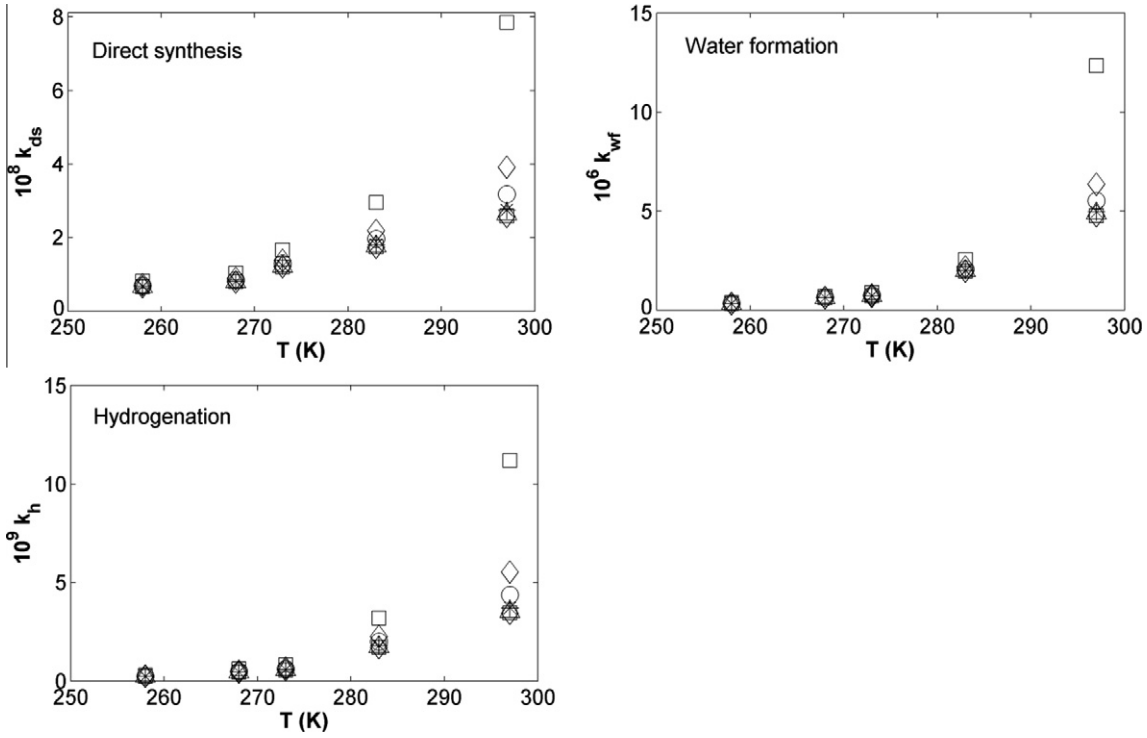

Fig. 8. Effect of $K^L_{H_2} a^L$ on the reaction rate constants of direct synthesis, water formation and hydrogenation. The value given by correlation 10 has been multiplied by: 0.0035 (□), 0.08 (◇), 0.15 (○), 0.5 (*), 1 (△), 5 (+), 10 (x).

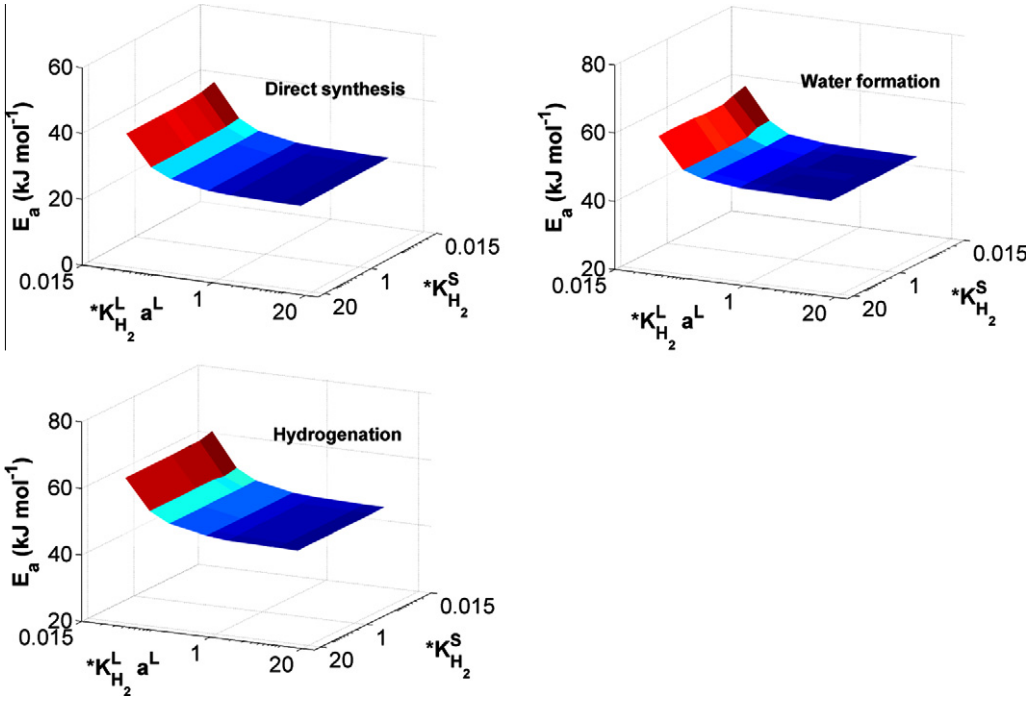

Fig. 9. Effect of $K^L_{H_2} a^L$ and $K^S_{H_2}$ on the activation energy of direct synthesis, hydrogenation and hydrogenation reactions.

one order of magnitude (form 1880 h^{-1} to 140 h^{-1}). Accordingly, we conclude that limitations due to the dissolution rate of hydrogen can be excluded at the experimental conditions, even accounting for uncertainties in the correlations, that could not be as high as 1 order of magnitude.

Fig. 10 shows the effect of the mass transfer rate from the liquid to the solid surface ($K^S_{H_2}$) on the reaction rate constants of direct synthesis, water formation and hydrogenation.

At the highest temperature (i.e. 297 K), where the effect is expected to be more evident, $K^S_{H_2}$ were varied from 3.01×10^{-4} cm s^{-1} to 8.61×10^{-2} cm s^{-1}. As can be seen, predicted values of reaction rate constants do not significantly change, even varying the resistance by two orders of magnitude. Accordingly, the activation energy of the three reaction remains constant (Fig. 9). This proves that any restriction due to the mass transfer limitation to the catalyst surface is negligible at the experimental conditions.

Please cite this article in press as: N. Gemo et al., Mass transfer and kinetics of H_2O_2 direct synthesis in a batch slurry reactor, Chem. Eng. J. (2012), http://dx.doi.org/10.1016/j.cej.2012.07.015

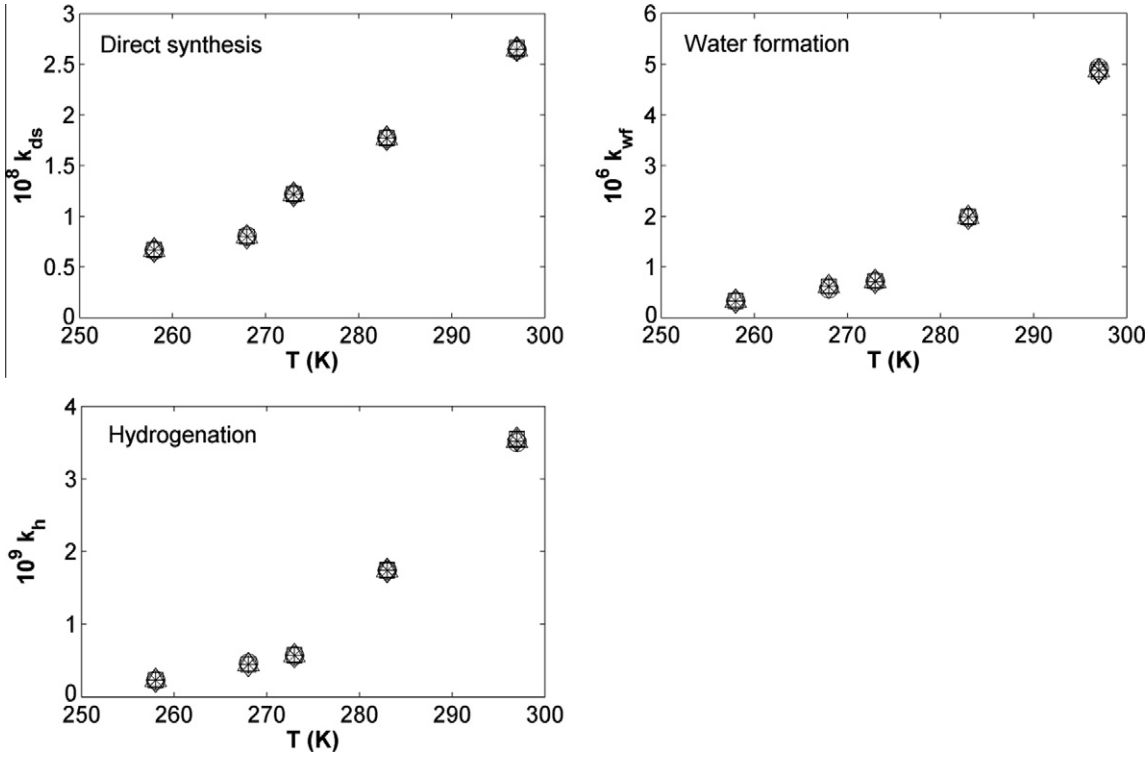

Fig. 10. Effect of $K^S_{H_2}$ on the reaction rate constants of direct synthesis, water formation and hydrogenation. The value given by correlation 19 has been multiplied by: 0.0035 (□), 0.08 (◇), 0.15 (○), 0.5 (*), 1 (△), 5 (+), 10 (x).

6. Conclusions

Direct synthesis of H_2O_2 is mainly limited by the identification of a selective catalyst, but fully exploiting the potential of the most promising ones requires knowledge of the reaction kinetics. Among the many studies on commercial and innovative catalysts, we perceived controversial indications about the role of mass transfer in either limiting the conversion or affecting the selectivity. Due to the parallel and consecutive structure of the mechanism, simple method based on a single reaction cannot be used to easily assess the mass transfer contribution. In addition, without any information about the controlling regime, a kinetic study is inevitably connected to an appropriate account of the transport limitations. In the present study we formulated a model of a gas bubbling, batch slurry reactor for H_2O_2 direct synthesis. Direct synthesis data were collected at temperatures in the range 258–297 K and pressure between 14 and 20 bar (depending on the temperature) using a commercial 5% Pd on carbon catalyst (0.15 g) in a methanolic solution (400 ml). The reagents H_2 and O_2 were diluted with CO_2 outside flammability limits. Our experimental measurements, carried out batchwise in the absence of halides and acids, have been used to identify the intrinsic kinetics and assess the influence of mass transfer. The simplest rate equations compatible with the acknowledged reaction network has been included in a reactor model accounting for mass transfer resistance between gas and liquid and bulk of the liquid-catalyst surface.

The corresponding Arrhenius parameters were estimated from direct synthesis experiments for all the reactions. Comparable activation energies close to 45 kJ mol^{-1} were observed for H_2O production, hydrogenation and decomposition, while H_2O_2 synthesis had a different temperature dependence (23 kJ mol^{-1}), suggesting that a higher selectivity is achievable at low temperature. Decomposition had a very limited influence on the overall peroxide production rate, with $R_d/R_{ds} > 0.5$ only at high H_2 conversion, when the direct synthesis reaction slows down. Hydrogenation was the preferred path of H_2O_2 degradation as its reaction rate rapidly increased with H_2 conversion. Water formation was always significant, prevailing ($R_{wf}/R_{ds} > 1$) at higher temperature, whereas lower temperature favors the direct synthesis ($R_{wf}/R_{ds} < 1$). Independent investigations on decomposition in the absence of H_2 confirmed the results, whereas H_2O_2 hydrogenation experiments (carried out in the absence of O_2) highlighted significant difference in the kinetics, apparently due to a different oxidation state of the catalyst.

A sensitivity analysis on the mass transfer coefficients to allow for uncertainties in the correlations proved that no resistances in the liquid occur, while gas–liquid H_2 transfer rate may be limiting, although unlikely, requiring that literature coefficients overestimates the real transfer rate by an order of magnitude.

Acknowledgments

Nicola Gemo gratefully acknowledges the Cariparo Foundation and the Johan Gadolin Scholarship for financial support. Nicola Gemo and Pierdomenico Biasi gratefully acknowledge the PCC (Process Chemistry Centre) and Åbo Akademi, Finland, for financial support. Pierdomenico Biasi gratefully acknowledges the Otto A. Malm Foundation for financial support. This work is a part of the activities at the Åbo Akademi Process Chemistry Centre (PCC) within the Finnish Centre of Excellence Programmes (2000–2005 and 2006–2011) by the Academy of Finland.

References

[1] P. Biasi, F. Menegazzo, F. Pinna, K. Eränen, P. Canu, T.O. Salmi, Hydrogen peroxide direct synthesis: selectivity enhancement in a trickle bed reactor, Ind. Eng. Chem. Res. 49 (2010) 10627–10632.
[2] P. Biasi, F. Menegazzo, F. Pinna, K. Eränen, T.O. Salmi, P. Canu, Continuous H_2O_2 direct synthesis over PdAu catalysts, Chem. Eng. J. 176–177 (2011) 172–177.
[3] E. Ntainjua, J.K. Edwards, A.F. Carley, J.A. Lopez-Sanchez, J.A. Moulijn, A.A. Herzing, C.J. Kiely, G.J. Hutchings, The role of the support in achieving high selectivity in the direct formation of hydrogen peroxide, Green Chem. 10 (2008) 1162–1169.

[4] G. Li, J. Edwards, A.F. Carley, G.J. Hutchings, Direct synthesis of hydrogen peroxide from H_2 and O_2 and in situ oxidation using zeolite-supported catalysts, Catal. Commun. 8 (2007) 247–250.
[5] F. Menegazzo, M. Signoretto, M. Manzoli, F. Boccuzzi, G. Cruciani, F. Pinna, G. Strukul, Influence of the preparation method on the morphological and composition properties of Pd–Au/ZrO_2 catalysts and their effect on the direct synthesis of hydrogen peroxide from hydrogen and oxygen, J. Catal. 268 (2009) 122–130.
[6] E. Ghedini, F. Menegazzo, M. Signoretto, M. Manzoli, F. Pinna, G. Strukul, Mesoporous silica as supports for Pd-catalyzed H_2O_2 direct synthesis: effect of the textural properties of the support on the activity and selectivity, J. Catal. 273 (2010) 266–273.
[7] S. Melada, F. Pinna, G. Strukul, S. Perathoner, G. Centi, Direct synthesis of H_2O on monometallic and bimetallic catalytic membranes using methanol as reaction medium, J. Catal. 237 (2006) 213–219.
[8] S. Melada, F. Pinna, G. Strukul, S. Perathoner, G. Centi, Palladium-modified catalytic membranes for the direct synthesis of H_2O_2: preparation and performance in aqueous solution, J. Catal. 235 (2005) 241–248.
[9] Y. Voloshin, R. Halder, A. Lawal, Kinetics of hydrogen peroxide synthesis by direct combination of H_2 and O_2 in a microreactor, Catal. Today 125 (2007) 40–47.
[10] T. Deguchi, M. Iwamoto, Reaction mechanism of direct H_2O_2 synthesis from H_2 and O_2 over Pd/C catalyst in water with H^+ and Br^- ions, J. Catal. 280 (2011) 239–246.
[11] Teresa Moreno, Juan García-Serna, María José Cocero, Decomposition reaction of H_2O_2 over Pd/C catalyst in an aqueous medium at high pressure: detailed kinetic study and modelling, J. Supercrit. Fluids 57 (2011) 227–235.
[12] T. Inoue, M.A. Schmidt, K.F. Jensen, Microfabricated multiphase reactors for the direct synthesis of hydrogen peroxide from hydrogen and oxygen, Ind. Eng. Chem. Res. 46 (2007) 1153–1160.
[13] F. Menegazzo, P. Burti, M. Signoreto, M. Manzoli, S. Vankova, F. Boccuzzi, F. Pinna, G. Strukul, Effect of the addition of Au in zirconia and ceria supported Pd catalysts for the direct synthesis of hydrogen peroxide, J. Catal. 257 (2008) 369–381.
[14] Y. Voloshin, J. Manganaro, A. Lawal, Kinetics and mechanism of decomposition of hydrogen peroxide over Pd/SiO_2 catalyst, Ind. Eng. Chem. Res. 47 (2008) 8119–8125.
[15] Y. Voloshin, A. Lawal, Kinetics of hydrogen peroxide reduction by hydrogen in a microreactor, Appl. Catal. A: Gen. 353 (2009) 9–16.
[16] Y. Voloshin, A. Lawal, Overall kinetics of hydrogen peroxide formation by direct combination of H_2 and O_2 in a microreactor, Chem. Eng. Sci. 65 (2010) 1028–1036.
[17] N. Gemo, P. Biasi, T.O. Salmi, P. Canu, H_2 solubility in methanol in the presence of CO_2 and O_2, J. Chem. Thermodyn. 54 (2012) 1–9.
[18] P. Biasi, N. Gemo, J.R. Hernández Carucci, K. Eränen, P. Canu, T.O. Salmi, Kinetics and Mechanism of H_2O_2 Direct Synthesis over a Pd/C Catalyst in a Batch Reactor. Ind. Chem. Eng. Res. 51 (2012) 8903-8912.
[19] D.P. Dissanayake, J.H. Lunsford, The direct formation of H_2O_2 from H_2 and O_2 over colloidal palladium, J. Catal. 214 (2003) 113–120.
[20] C. Sivadinarayana, T.V. Choudhary, L.L. Daemen, J. Eckert, D.W. Goodman, The nature of the surface species formed on Au/TiO_2 during the reaction of H_2 and O_2: an inelastic neutron scattering study, J. Am. Chem. Soc. 126 (2004) 38–39.
[21] J.H. Lunsford, The direct formation of H_2O_2 from H_2 and O_2 over palladium catalysts, J. Catal. 216 (2003) 455–460.
[22] Y. Kawase, M. Moo-Young, Volumetric mass transfer coefficients in aerated stirred tank reactors with Newtonian and non-newtonian media, Chem. Eng. Res. Des. 66 (1988) 284–288.
[23] C.R. Wilke, P. Chang, Correlation of diffusion coefficients in dilute solutions, AIChE J. 1 (1955) 264–270.
[24] F. Garcia-Ochoa, E. Gomez, Theoretical prediction of gas–liquid mass transfer coefficient, specific area and hold-up in sparged stirred tanks, Chem. Eng. Sci. 59 (2004) 2489–2501.
[25] K. Rutherford, S.M.S. Mahmoudi, K.C. Lee, M. Yianneskis, The influence of Rushton impeller blade and disk thickness on the mixing characteristics of stirred vessels, Trans IChemE, Part A – Chem. Eng. Res. Des. 74 (1996) 369–378.
[26] S.M. Bhavaraju, T.W.F. Russell, H.W. Blanch, The design of sparged devices for viscous liquid systems, AIChE J. 24 (1978) 454–466.
[27] L.A. Currie, G.S. Svehla, Nomenclature for the presentation of results of chemical analysis, Pure Appl. Chem. 66 (3) (1994) 595–608.
[28] E.L. Cussler, Diffusion: mass transfer in fluid systems, 3rd ed., Cambridge University Press, Cambridge, 2007.
[29] M. Meyberg, F. Roessler, In situ measurement of steady-state hydrogen concentrations during a hydrogenation reaction in a gas-inducing stirred slurry reactor, Ind. Eng. Chem. Res. 44 (2005) 9705–9711.
[30] T. Deguchi, M. Iwamoto, Kinetics and simulation including mass-transfer processes of direct H_2O_2 synthesis from H_2 and O_2 over Pd/C catalyst in water containing H^+ and Br^- ions, Ind. Eng. Chem. Res. 50 (2011) 4351–4358.
[31] B. Andersson, T. Berglin, On the theory and use of a new fast-response dissolved hydrogen probe for hydrogen transfer studies, Chem. Eng. J. 24 (1982) 201–212.

Please cite this article in press as: N. Gemo et al., Mass transfer and kinetics of H_2O_2 direct synthesis in a batch slurry reactor, Chem. Eng. J. (2012), http://dx.doi.org/10.1016/j.cej.2012.07.015

IV

Reactivity aspects of SBA15-based doped supported catalysts: H_2O_2 direct synthesis and disproportionation reactions

Nicola Gemo[1,‡], Pierdomenico Biasi[2,,‡],Paolo Canu[1], Federica Menegazzo[3], Francesco Pinna[3], Ajaikumar Samikannu[4], Krisztián Kordás[4], Tapio O. Salmi[2], Jyri-Pekka Mikkola[2,4]*

[1]Dipartimento di Ingegneria Industriale University of Padova, via Marzolo 9, 35131, PADOVA, Italy

[2]Department of Chemical Engineering, Process Chemistry Centre (PCC), Laboratory of Industrial Chemistry and Reaction Engineering Åbo Akademi University, Biskopsgatan 8, ÅBO-TURKU, 20500, Finland

[3]Department of Molecular Science and Nanosystems, Ca' Foscari Venice University and Consortium INSTM UdR Ve, Dorsoduro 2137, Venezia, Italy;

[4]Department of Chemistry, Chemical-Biochemical Centre (KBC), Technical Chemistry, Umeå University, UMEÅ, SE-90187, Sweden

[*]*To whom correspondence should be addressed. E-mail:* bpierdom@abo.fi, Jyri-Pekka.Mikkola@chem.umu.se

[‡] *The first two authors contributed equally to the present work*

1. Abstract

Pd and PdAu catalysts supported on SBA15 and SiO_2 were prepared and investigated for H_2O_2 direct synthesis in a batch autoclave (10°C and 17.5 bar) and in the absence of halides and acids. The SiO_2 supported catalysts exhibited inferior performances compared to the mesoporous ordered-SBA15. A good control of both the catalysts dispersion and nanoparticle stability was achieved using SBA15. Catalysts were doped with bromine, a promoter in the H_2O_2 direct synthesis. Productivity and selectivity decreased when bromine was incorporated in the catalysts, thus indicating a possible poisoning due to the grafting process. A synergetic effect between Pd and Au was observed both in presence and absence of bromopropylsilane grafting on the catalyst surface. Three modifiers of the SBA15 support (Al, CeO_2 and Ti) were chosen to elucidate the influence of the surface properties on metal dispersion and catalytic performance. Higher productivity and selectivity were achieved incorporating Al into the SBA15 framework, whereas neither Ti nor CeO_2 improved H_2O_2 yields. The enhanced performance observed for the PdAu/Al-SBA15 catalysts was attributed to the increased number of Brønsted acid sites. A modification of this catalyst with bromine was confirmed to impair both productivity and selectivity, possibly due to the broader particle size distribution and the poor stability of the metal nanoparticles, as demonstrate by Transmission Electron Microscopy (TEM) images. H_2O_2 disproportionation was also investigated. A much slower reaction rate was observed compared to the H_2O_2 production, suggesting that the major contributor in the process of H_2O_2 destruction must be connected to the hydrogenation reaction.

Hydrogen peroxide, direct synthesis, SBA15, silica, palladium

2. Introduction

The global demand of hydrogen peroxide is increasing due to its recent usage in new large scale oxidation processes, such as the epoxidation of propylene to propylene oxide[1] and the synthesis of caprolactam (Sumitomo)[2] Since the early 90's, many research groups have tried to develop new alternatives for the production of this peroxide[3-5]. The most attractive one is the direct synthesis (DS process), due to its atom-efficient nature and the costs savings that can be achieved[3]. Basically, hydrogen and oxygen are dissolved in a proper reaction medium (i.e. alcoholic solution or water) and react over a solid catalyst. This three phase system has been under intensive study during the last thirty years both by industries as well as academia[3, 4, 6-15]. The main obstacles to industrial feasibility are selectivity and safety issues[4]. The reaction pathway for the direct synthesis of hydrogen peroxide is depicted in Scheme 1.

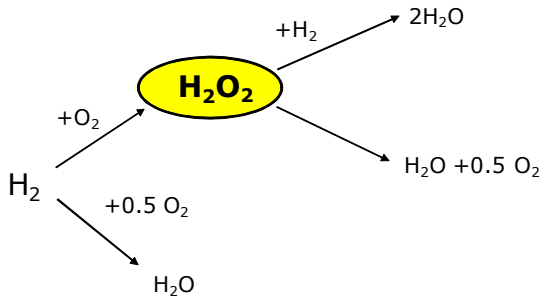

Scheme 1. Reactions involved in the direct synthesis of H_2O_2.

Two consecutive (hydrogenation and disproportionation) and one parallel reaction (H_2O formation) competing with the formation of the hydrogen peroxide are involved. Recent progress in terms of kinetic studies[16-21] aim at elucidating the specific role of each of these reactions. However, the results are often difficult to compare because of the different approaches, reactors and reaction conditions adopted. In the present study, we focused on identifying a suitable support to limit the undesired reactions. Monometallic (Pd)[17, 22-25] and bi-metallic (Pd and Au)[26, 27] catalysts with different surface properties were

synthesized and investigated for H_2O_2 direct synthesis in the absence of halides and acids at identical reaction conditions, to facilitate a consistent comparison. Kinetic studies were carried out in a batch, laboratory scale slurry autoclave with H_2 as the limiting reagent. SBA15 mesoporous material was chosen as support because of its interesting characteristics: it has a high specific surface area, it promotes a high dispersion and stability of metal nanoparticles[28-30] and it also acts as a template to control the nanocluster size. A good control of the catalysts dispersion is fundamental: very small metal nanoclusters are not desired because of their O-O bond breaking aptitude, hence leading to H_2O formation[11], whereas low dispersion catalysts are less active[30]. On the other hand, an acidic environment is known to promote the peroxide formation[3, 4, 31, 32]. Consequently, three modifications of the parent SBA15 support material (incorporation of Al, CeO2 and Ti) were chosen to elucidate the influence of surface properties (such as Brønsted and Lewis acidity) on the metal dispersion and the overall performance observed upon H_2O_2 direct synthesis. Halide ions are also known to increase the selectivity towards H_2O_2, especially bromide[26, 33-35], but their presence in the solution is undesired. Hence, Br-doped catalysts were obtained by grafting bromine on SBA15-based catalysts, so that presence of the free ions in the solution was avoided. The performances of these SBA15 supported catalysts were also compared to unordered, classic silica[11]. After complete conversion of H_2, the disproportionation reaction was also investigated.

3. Materials

SiO_2 (Akzo), tetraethyl orthosilicate (purity ≥ 99.0%), poloxamer (pluronic P-123), hydrochloric acid (37%), urea (purity ≥ 98%), aluminium isopropoxide, titanium tetraisopropoxide and $PdCl_2$ (all purchased from Sigma-Aldrich) were used for the catalyst preparations as received, as well as $Ce(NO_3)_3.6H_2O$ (purity 99.5%, Alfa Aesar), ammonia solution (25%, Fisher Scientific) and $HAuCl_4$ (ABCR).

Methanol was the reaction medium (J.T. Baker 99,99% purity). H_2, O_2 and CO_2 were used in the direct synthesis experiments as received (AGA 99.999% mol/mol purity).

4. Catalysts preparation

A total of eleven catalysts were synthesized according to the following procedures.

4.1 Preparation of the supports

Preparation of SBA15 and M-SBA15 (M = Al and Ti) by hydrothermal method

Mesoporous silica SBA15 was synthesized according to a modification of the procedure reported by Zhao et al.[36]. In a typical synthesis, 10 g of the structure directing agent, a triblock copolymer Pluronic P-123 (poly(ethylene oxide)-poly(propylene oxide)-poly(ethylene oxide), EO_{20}-PO_{20}-$EO_{20,}$ M_n ~5,800) was dissolved in a polypropylene bottle using 75 ml of distilled water, followed by an addition 300 ml of 2M of hydrochloric acid and stirred at 40ºC for 2 h. Then, 21.25g of the silica source, tetraethyl orthosilicate (TEOS) was slowly added to the above mixture, stirred for 24 h at 40ºC and aged for 48 h at 90 ºC under static conditions. The resultant solid product was filtered, washed thoroughly with deionized water to reach neutral pH, dried at 90 ºC in an oven and, finally, the organic template in the synthesized material was removed by calcination under air flow at 550ºC for 6 h.

Metal substituted M-SBA15 with Si/M ratio of 25 (where M= Al and Ti) were synthesized by hydrothermal incorporation method using tetraethyl orthosilicate (TEOS), aluminium isopropoxide and titanium tetraisopropoxide as the sources of Si, Al and Ti, respectively. These materials were obtained following the procedure described for SBA15, expect that the addition of tetraethyl orthosilicate (TEOS) was followed by the addition of an appropriate amount of metal precursors (dissolved in ethanol).

Preparation of CeO_2-SBA15

CeO_2 modified SBA15 was prepared by means of deposition-precipitation method. About 6 gram of the calcined SBA15 was dispersed in 300 ml of urea (0.372M). Under stirring, an appropriate amount of $Ce(NO_3)3.6H_2O$ (dissolved in deionized water) was added to the above suspension to yield a theoretical loading of 20 wt.% CeO_2. The temperature of the suspension was raised to 70 °C and stirred for 5 h enabled slow disproportionation of the urea to ammonia, increasing the pH and, consequently, giving a slow precipitation of metal precursors. The pH of the suspension was then increased to 9 by addition of 25% aqueous ammonia to ensure complete precipitation. After stirring for 1 h, the solids were recovered by filtration and washed thoroughly with deionized water. Finally, the solids were dried overnight in an oven at 100 °C and calcined in a furnace under normal air at 500 °C for 5 hours.

4.2 Metal loading

Br-modified PdAu/ and Pd/SBA15 catalysts

PdAu/SBA15 catalyst was synthesized supporting Pd and Au (1:4 mole ratio) on SBA15 by wet impregnation method. $HAuCl_4 \cdot H_2O$ and $PdCl_2$ were used as precursors, added to the solution at the same time. The impregnated catalyst was dried at 100°C overnight and then reduced at 300°C for 8 hours with a 30 ml/min flow of hydrogen. The furnace was allowed to cool down to room temperature and the catalyst was passivated for 24 h under a 2 vol% O_2/N_2 mixture. The final metal content observed was 0.3 wt% of Pd and 2.2 wt% of Au, respectively.

A bromopropyl-PdAu/SBA15 (Br-PdAu/SBA15) catalyst was obtained grafting the reduced form of this catalyst with 3-bromopropyl-trimethoxy-silane. The catalyst was suspended in

dry toluene. Then the 3-bromopropyl-trimethoxy-silane (5 mmol per gram of catalyst) was slowly added to the suspension. The mixture was fluxed at 80 °C in inert atmosphere for 24 h. After completion, the catalyst was washed with an excess of dry toluene and dried at 100°C for 24 h in air. The synthesis and the grafting process of the Pd/SBA15 (2.5 wt.%) and Br-Pd/SBA15 (0.3 wt.5) catalysts were carried out following the same procedure, but impregnating the support with Pd only. PdAu-Br/SBA15 (0.3 wt% Pd and 2.2 wt% Au) was prepared reversing the order of the described procedures, first grafting the support and then impregnating the active metals.

PdAu/M-SBA15 (M = Al, Ti and CeO_2)

The active metals were supported on M-SBA15 (M = Al, Ti and CeO_2) by impregnation method using aqueous methanol solutions. About 2.0 grams of the pre-dried M-SBA15 support was dispersed in 30 ml of methanol. Then, the required amount of metal precursors ($HAuCl_4$ and $PdCl_2$) were dissolved separately in water (1M HCl in the case of $PdCl_2$) and added simultaneously to the above stirred suspension of the support. Stirring was continued for 5 hours. The solid product was recovered by evaporation of the solvent under reduced pressure using a rotary evaporator and dried overnight in an oven at 100 °C. Finally, the material was calcined at 400 °C for 3 h in air and reduced at 300 °C for 3 h in 30 ml/min H_2 flow. The active metal content of the catalysts were 0.19 wt.% and 1 wt.% for Au and Pd, respectively.

Br-PdAu/Al-SBA15

About 1.0 gram of the above prepared PdAu/Al-SBA15 was dispersed in 20 ml of dry methanol. An appropriate amount of ammonium bromide (5mmol per gram of catalyst) was dissolved in 5 ml of methanol and added to the stirred suspension of the base-catalyst. Stirring was continued for 2 h. The solid product was recovered by evaporation of the solvent under

reduced pressure using rotary evaporator and dried in an oven at 80 °C. Finally, the material was calcined at 400 °C for 1 h under nitrogen atmosphere (flow 30 ml/min) and reduced at 300 °C flowing hydrogen (30 ml/min) for 3 h. (NOTE: Care must be taken while adding methanol to the reduced form of the catalyst due to a possibility of explosion. Self ignition of the catalyst was observed in our laboratory during this procedure).

Pd/Si and PdAu/Si

A commercial SiO_2 (Akzo, 329 m^2/g of surface area) was used as received for samples synthesis. It was impregnated by incipient wetness with H_2PdCl_4 and/or $HAuCl_4$ aqueous solutions (addition of the two precursor solutions was simultaneous for the bimetallic catalyst) to give the desired metal loading (0.5 wt.% Pd for Pd/Si and 1.5 wt% Pd and Au for PdAu/Si). Samples were finally calcined at 500 °C in flowing air for 3 hours.

5. Experimental section

A recent study highlighted how carbon dioxide can reduce the flammability region of the hydrogen/oxygen mixture[37]. Moreover, CO_2 is also known to enhance H_2 solubility in many solvents[38-40]. For these particular reasons, in this study CO_2 was chosen as a dilutant for the H_2/O_2 mixture residing outside the flammability limits. The experiments were performed in a 600 ml laboratory-scale batch reactor, described elsewhere[23]. Briefly, after the introduction of the catalyst (0.15 g), CO_2 (18.4 bar at 23°C) and O_2 (up to 24.7 bar at 23°C) were introduced into the reactor, followed by methanol (400 ml). The temperature was decreased to 10°C and stirring (1000 rpm) for 30 min allowed to reach the equilibrium (17.5 bar). Hydrogen (0.0183 mol) was fed as the limiting reagent from a dedicated vessel. The reaction started immediately after H_2 was introduced to the reaction zone and the stirring turned on. Several liquid samples were withdrawn through a GC-valve during each experiment. H_2O_2 concentration was determined by iodometric titration whereas H_2O content

was measured by Karl-Fischer analysis. The selectivity and H_2 conversion were calculated as follows: H_2O_2 selectivity = (moles H_2O_2 produced) / (moles H_2O + H_2O_2 produced) x 100; H_2 conversion = (moles H_2O + H_2O_2 produced) / (moles H_2 introduced) x 100. Specific H_2O_2 productivity was calculated as: (moles H_2O_2 produced) / (time · moles of active metal).

N_2 adsorption measurements were performed with a Carlo Erba Sorptomatic 1900. Specific surface area was evaluated according to the BET equation, whereas pore size distribution of the bulk supports was estimated according to Dollimore/Heal method.

The nature of the acid sites of the catalysts was determined by Fourier transform infrared (FT-IR) spectroscopy of adsorbed pyridine. The analysis were carried out according to literature procedure[41]. Lewis and Brønsted acid sites were calculated from the IR band area at 1450 and 1545 cm^{-1}, respectively. The integrated molar extinction coefficients were assumed as 1.67 cm/μmol for Brønsted acidity and 2.22 cm/μmol for Lewis acidity. Particle size and structure was assessed by energy-filtered transmission electron microscopy (EFTEM, LEO 912 OMEGA, LaB6 filament, 120 kV).

TGA measurements were carried out on the grafted catalysts. Weight loss was due to the loss of the organic part carrying the bromine. Hence, bromine content was estimated from the weight loss upon heating. The bromine content of the catalysts obtained grafting the support after active metals deposition was 4.5 wt.%. The catalyst obtained with the reversed procedure, i.e. grafting the support before the deposition of the active metals (PdAu-Br/SBA15), revealed a lower bromine content (2.8 wt.%).

6. Results and discussion

Table 1 summarizes H_2O_2 productivity, selectivity and H_2 conversion after 15 min of reaction for all the catalysts. For selected catalysts, acid sites concentration of the support is also reported.

Table 1. H_2O_2 synthesis with SBA15 and Si supported catalysts: acidity, H_2 conversion after 15 min of reaction, productivity and selectivity (after 15 min of reaction and at complete H_2 conversion). Conditions: T = 10 °C, P = 17.5 bar.

#	Catalyst	Productivity H_2O_2 ($mol_{H_2O_2}/mol_{metal}$ h)		Selectivity (%)		H_2 conversion @ 15 min (%)	Complete H_2 conversion (min)	Acidity (µmol/g)	
		@ 15 min	@ complete H_2 conversion	@ 15 min	@ complete H_2 conversion			Lewis	Brønsted
1	Pd/SBA15	359	311	20	20	99	20	/	/
2	PdAu/SBA15	634	326	28	24	65	41	/	/
3	Br-Pd/SBA15	39	/	/	/	/	/	/	/
4	Br-PdAu/SBA15	192	/	24	/	13	/	/	/
5	PdAu-Br/SBA15	0	0	0	0	/	/	/	/
6	Pd/Si	850	234	17	15	51	85	/	/
7	PdAu/Si	183	77	8	8	77	57	/	/
8	PdAu/CeO2-SBA15	399	314	16	14	48	34	39	0
9	PdAu/Ti-SBA15	538	463	13	12	77	18	16	0
10	PdAu/Al-SBA15	870	422	30	24	67	37	22	8
11	Br-PdAu/Al-SBA15	76	/	20	/	11	/	9	0

It is important to compare the different catalysts in similar reaction conditions, that is before H_2 was completely consumed. We observed that 15 min were enough to obtain a significant quantity of H_2O_2 with H_2 still present in the liquid phase. Thus, the catalysts were compared while the direct synthesis of H_2O_2 was still increasing. For sake of completeness, selectivity and H_2O_2 productivity values at complete H_2 consumption are also included. The selectivity measured at different H_2 conversions are quite close, whereas the H_2O_2 productivity spread displays bigger differences. However, caution should be taken comparing the productivity at complete H_2 conversion, as it occurs at different reaction time. The selectivities reported in Table 1 are generally lower compared to the values obtained by other authors with nominally similar catalysts[11, 29, 30, 42]. However, in these papers an acidic medium was adopted to stabilize the peroxide formed, hence drastically increasing the selectivity. In our study the presence of promoters and stabilizers was deliberately avoided to focus on the catalysts performance solely. Experimental results are discussed below.

6.1 Non-ordered and ordered mesoporous Si-based catalysts: Au and incorporated-bromine effect

We investigated the role of Au and incorporated-bromine over five different SBA15-based catalysts. Selectivity, H_2 conversion and H_2O_2 productivity after 15 min of reaction are reported in Table 1, entries 1 to 5.

Figure 1 illustrates H_2O_2 concentration as a function of time observed with these catalysts.

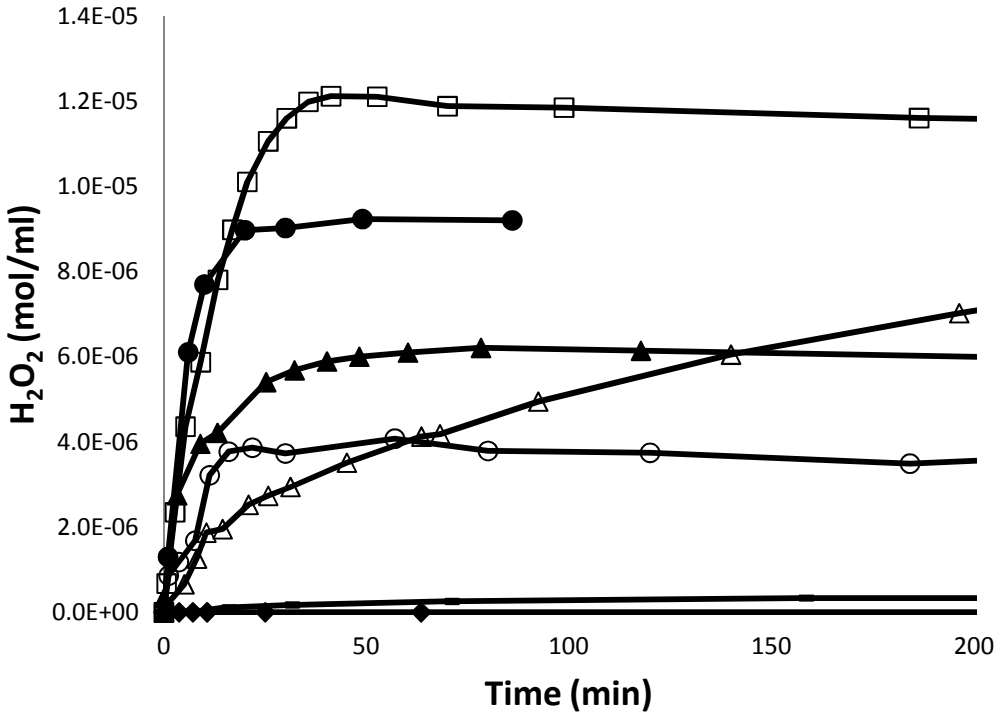

Figure 1. H_2O_2 concentration in batch reactor: PdAu/SBA15 (□), Br-PdAu/SBA15 (△), Pd/SBA15 (●), Br-Pd/SBA15 (-), PdAu-Br/SBA15 (♦), Pd/Si (▲), PdAu/Si (○). Conditions: T = 10 °C, P = 17.5 bar

Typically, H_2O_2 formation increased rapidly in the beginning, reaching a maximum and gradually decreasing afterwards. The exceptions were Br-PdAu/SBA15, Br-Pd/SBA15 and PdAu-Br/SBA15, showing low or negligible activity (Table 1). The H_2O_2 concentration profile is closely related to the H_2 consumption, as discussed in the next section.

Among the synthesized catalysts, PdAu/SBA15 was the most active one. Figure 1 clearly distinguishes the differences in mono- and bimetallic catalysts, where the latter ones always show a much higher H_2O_2 productivity upon short contact time. Monometallic Pd/SBA15 catalyst had a productivity 50% reduced compared to the bimetallic PdAu/SBA15. Its grafted parent (Br-Pd/SBA15) demonstrated a poor H_2O_2 productivity also, i.e. five times lower

compared to the bimetallic Br-PdAu/SBA15. Upon testing the monometallic Br-Pd/SBA15 catalyst, H_2O concentration was within the measurement error and, consequently, H_2 conversion and selectivity could not be calculated. The comparison of mono- and bimetallic catalysts (either grafted or not) confirms the synergetic effect between Pd and Au reported in the literature[26, 27].The grafting process had a two-fold effect on the bimetallic catalyst, clearly seen when comparing the performance of the PdAu/SBA15 and Br-PdAu/SBA15. The selectivity was reduced by 15% in the presence of bromine attached on the catalyst. Moreover, the productivity was three times lower over Br-PdAu/SBA15 and also the H_2 conversion was reduced by a factor of 80%. The grafting process could induce poisoning of the catalyst by pore blocking (bromoalkyl species) and/or causing migration and sintering of the metal nanocluster outside the mesoporous of the support, as shown by the TEM images discussed below. Neither H_2O_2 nor H_2O were observed when the SBA15 was grafted before Pd and Au deposition. The reduction performed at 300 °C after the grafting process could induce a partial disproportionation of the bromopropyl groups, leading to coke formation and poisoning of the catalyst. Thermogravimetric Analysis (TGA) measurements confirmed this hypothesis. Weight loss upon heating of the catalyst reduced after Br grafting was 37% lower compared to the catalysts obtained with the reverse procedure, i.e. grafting the catalysts after active metals deposition, suggesting that partial decomposition of the organic chains occurred during reduction of the PdAu-Br/SBA15 catalyst.

Performances of SBA15-based catalysts were also compared to non-ordered SiO_2-based catalysts, Figure 1 and Table 1, entries 6 to 7, respectively. The synergetic effect of Pd and Au observed with SBA15 supported catalysts was not observed when using silica as support. Compared to the PdAu/Si, the monometallic Pd/Si catalyst displayed both higher selectivity and productivity, though at lower H_2 conversion. However, the performance of these catalysts

was generally lower than that shown by the non-grafted SBA15 supported one, confirming the advantage of using an ordered mesoporous support.

6.2 Al, Ti and CeO_2-SBA15 modified catalysts

Starting from the consolidated knowledge that an acid environment favors the H_2O_2 direct synthesis[3, 4, 31, 32], the catalyst displaying the best performance (PdAu/SBA15) was further modified. Three different surface modifiers were chosen: incorporation of Al into the framework is known to give Brønsted acidity[43], CeO_2 adds Lewis acidity[44, 45] while Ti gives mild oxidizing property[46, 47]. H_2O_2 concentrations obtained in batch experiments with PdAu/M-SBA15 (M = Al, Ti and CeO_2) are reported in Figure 2.

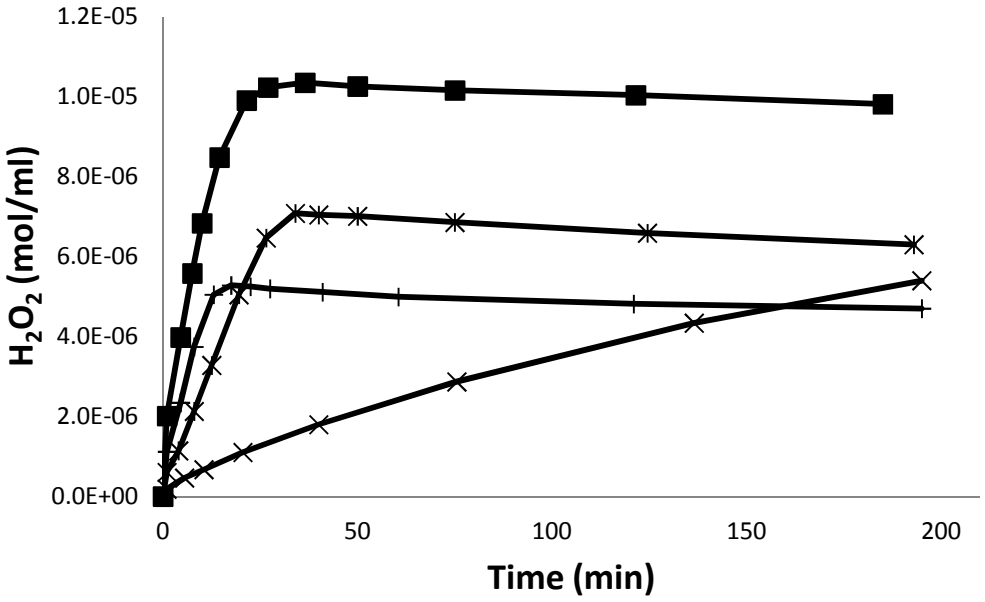

Figure 2. H_2O_2 concentration in batch reactor: PdAu/Al-SBA15 (■), PdAu/CeO_2-SBA15 (*), PdAu/Ti-SBA15 (+), Br-PdAu/Al-SBA15 (x). Conditions: T = 10 °C, P = 17.5 bar.

Again, H_2O_2 concentration goes through a maximum and then slowly decreases, except for Br-PdAu/Al-SBA15 catalyst, that demonstrates a lower reaction rate. The performance of these catalysts are reported in Table 1, entries 8 to 11. Modifying the support with Al gave the

best results, both in terms of productivity and selectivity. Compared with the corresponding unmodified catalyst (Table 1, entry PdAu/SBA15), the productivity was increased by 37% with comparable selectivity and H_2 conversion. Modification of the support with CeO_2 or Ti impaired the catalytic performances, decreasing both selectivity and productivity values. A catalytic test was also carried out with the best catalyst (PdAu/Al-SBA15) modified by an addition of bromine (Br-PdAu/Al-SBA15). Bromine was grafted after the deposition of the active metals on the support, whereas the reverse procedure revealed the deactivation of the catalyst (Table 1). However, doping the catalyst decreased the selectivity and resulted in a drop of productivity by one order of magnitude (entry Br-PdAu/Al-SBA15,Table 1), confirming the poisoning already observed with the unmodified SBA15-based catalysts. Different surface analysis techniques were carried out on the catalysts to explain these results.

Figure 3 shows TEM images of PdAu/M-SBA15 (M = Al, Ti and CeO_2) catalysts, before and after use.

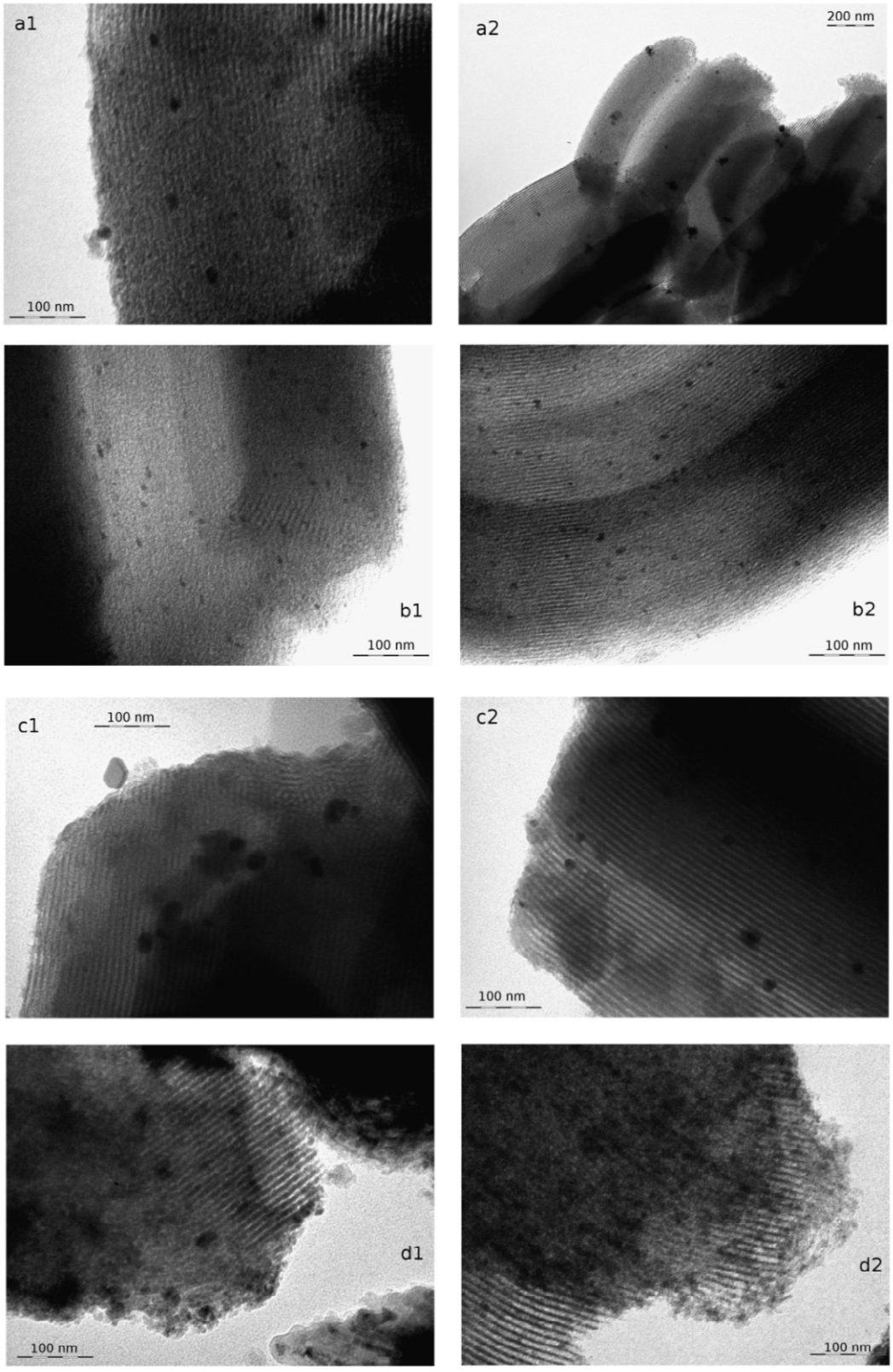

Figure 3. TEM images of SBA15 modified catalysts: a) PdAu/Ti-SBA15, b) PdAu/Al-SBA15, c) Br-PdAu/Al-SBA15, d) PdAu/CeO_2-SBA15; 1) fresh catalyst (left), 2) used catalyst (right).

Pore size diameters of the bulk support were estimated from TEM images, and the calculations suggested that approx. 6 nm is a realistic estimate for all of the catalysts. This result was confirmed by nitrogen physisorption measurements as well (Dollimore/Heal method). This also compares well with values reported in the literature[28, 29, 36]. The analyses were repeated before and after the reaction. No significant changes were found, confirming the stability of the support during the reaction. Particle size distributions of the bimetallic (PdAu) nanoclusters obtained from the TEM images on fresh and spent catalysts are summarized in Figure 4.

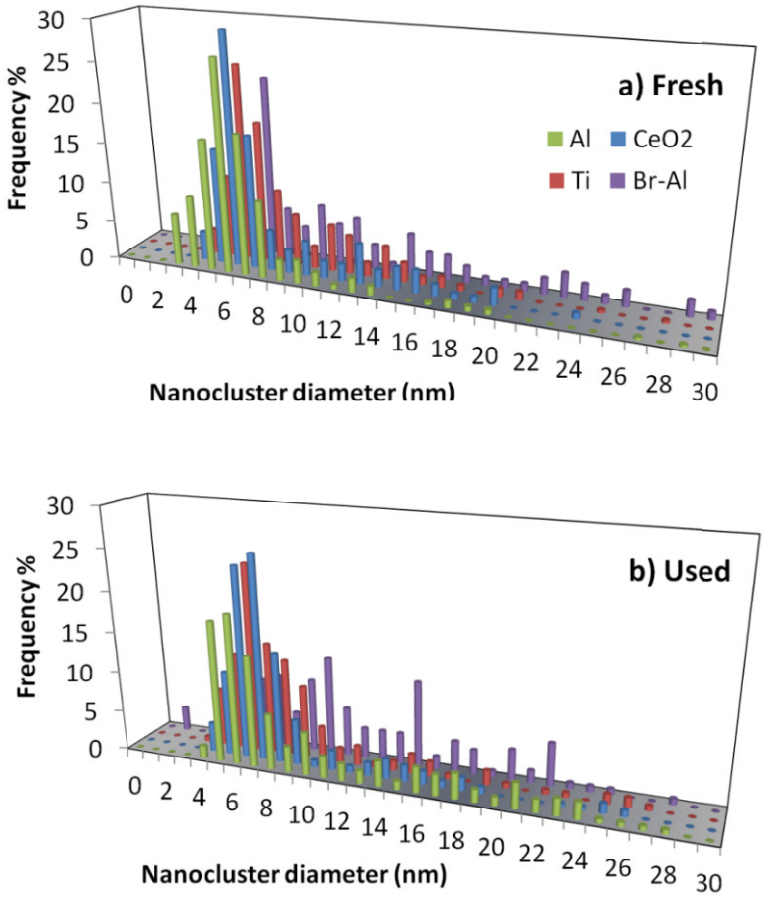

Figure 4. Particle size distribution of modified SBA15-based catalyst (the modifier is indicated in the legend): a) fresh catalyst; b) spent catalyst.

All except the Br-PdAu/Al-SBA15 catalysts demonstrated comparable particle size distributions where most of the nanoclusters had a diameter close to that of the support pores (i.e. 6-7 nm) and only occasionally showing diameters up to 25 nm. This confirms that a good control of the nanocluster size was achieved using SBA15 as support. The particle size distributions were almost unchanged in the spent catalysts (Figure 4b), confirming the stability of the metal nanoclusters at reaction conditions. A comparison of PdAu/Al-SBA15 with Br-PdAu/Al-SBA15 (Figure 4a) clearly demonstrated that a broader particle size distribution was obtained after bromine doping (clusters between 6 and 22 nm). The metal nanoparticles possibly migrated on the catalyst surface and agglomerate into larger clusters upon bromine modification. The bromine also caused a noticeable sintering of metal nanoclusters after use, as shown in Figure 4b. The broader nanocluster size distribution and the poorer stability of the metal nanoclusters are deemed responsible for the lower activity of the bromine containing catalyst. Compared to the other catalysts, TEM images of the PdAu/CeO_2-SBA15 (Figure 3d) revealed a more homogeneous surface, where the support channels are less clearly distinguishable. This difference in the surface structure is possibly due the presence of CeO_2. All SBA15-based catalysts were prepared via a direct synthesis method[36], except CeO_2 modification, carried out by a post-synthesis method. The high CeO_2 loading (20 wt%) may have caused partial pore blocking. To verify this hypothesis, nitrogen physisorption (BET method) measurements were carried out on the catalysts. The specific surface area of the PdAu/M-SBA15 (M = Al and Ti) catalysts resulted in 600 m^2/g. Only the CeO_2-modified catalyst had a lower area of 430 m^2/g, confirming partial pore blocking caused by the CeO_2 doping. The decreased available surface area can also be responsible for the lower activity of this particular catalyst (Table 1).

FT-IR spectroscopy by means of pyridine adsorption was performed on these catalysts to characterize the Lewis and Brønsted acidity present. IR spectra were recorded at 250, 350 and

450 °C, respectively. Adsorbed pyridine was detected only at 250 °C. No peaks were observed at higher temperatures. Measured acid sites concentrations are reported in Table 1 (entries 8 to 11). The presence of Brønsted and/or Lewis acid sites was confirmed in the modified supports. The enhanced performance of the PdAu/Al-SBA15 catalyst can be explained by the presence of Brønsted acid sites: hydrogenation of H_2O_2 is suppressed when the peroxide is surrounded by protons[4, 31], and hence the increased Brønsted acidity as a result of increased Al (modifier) enhanced the peroxide productivity.

6.3 H_2 conversion and disproportionation reaction

H_2 conversion has a key role on the H_2O_2 concentration profiles shown in Figure 1and Figure 2. The moment of complete H_2 conversion is particularly important, implying a significant change in the ongoing reactions: initially, H_2 is present and all the reactions (see Scheme 1) occur simultaneously. After complete H_2 conversion, disproportionation is the only possible reaction. Interestingly, complete H_2 conversion was found to occur simultaneously to the peroxide peak (Figure 1 and Figure 2), meaning that the experimental data collected afterwards are representative only of the disproportionation reaction. It has to be mentioned that Br-Pd/SBA15, PdAu-Br/SBA15, Br-PdAu/SBA15 and Br-PdAu/Al-SBA15 catalysts demonstrated a low productivity (Figure 1and Table 1) and did not reach complete H_2 conversion within experimental time. Hence these catalysts are excluded from this discussion. In general, it is apparent that the H_2O_2 disproportionation occurs at a different time scale compared to the other reactions: H_2O_2 concentration is rapidly increased in less than 50 min, while the subsequent disproportionation took several hours. Thus, the major step for the peroxide destruction is to be assigned to the hydrogenation reaction, regardless the support and the active metal content of the catalyst**.** Assuming disproportionation is a first order

reaction with respect to H_2O_2, its rate constant (k_d) can be estimated with the experimental data collected after H_2O_2 peak by integration of Equation 1:

$$\frac{d[H_2O_2]}{dt} = k_d \cdot [H_2O_2] \cdot \frac{n_{metal}}{V_L} \qquad 1$$

Note that the decomposition kinetic constant is scaled to the total moles of metal on the catalyst (n_{metal}).

Figure 5 depicts the experimental disproportionation data collected after complete H_2 consumption along with their fit, for a few catalysts. k_d values estimated accordingly are reported in Table 2.

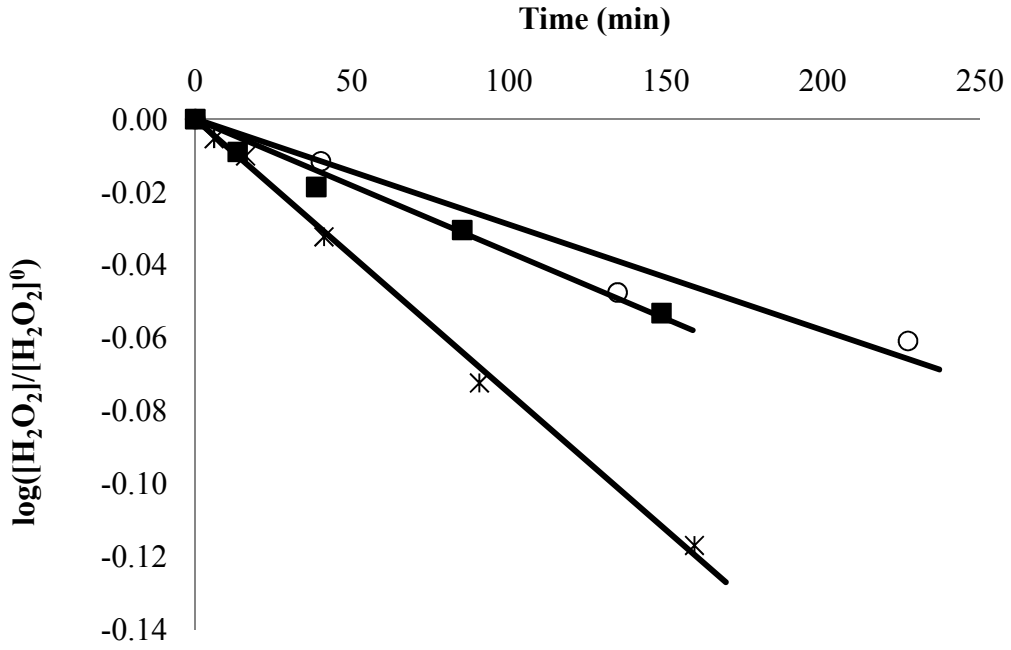

Figure 5. Elaboration of disproportionation data (i.e. collected after complete H_2 conversion) according to Eq. 1: PdAu/Si (○), PdAu/Al-SBA15 (■), PdAu/CeO_2-SBA15 (*); solid line, model.

Table 2. Disproportionation rate constants based on Eq. 1

Catalyst	k_d $l\,\mathrm{min}^{-1}\,n_{metal}^{-1}$
PdAu/Si	3.7
Pd/SBA15	4.6
PdAu/SBA15	4.3
PdAu/Al-SBA15	9.4
Pd/Si	18.1
PdAu/CeO_2-SBA15	19.6
PdAu/Ti-SBA15	19.6

Values in the range 4-20 $l\,\mathrm{min}^{-1}\,n_{metal}^{-1}$ were obtained. Three groups of catalysts are recognized: PdAu/Si, Pd/SBA15 and PdAu/SBA15 with $k_d \sim 4$ $l\,\mathrm{min}^{-1}\,n_{metal}^{-1}$, PdAu/Al-SBA15 with $k_d \sim 9$ $l\,\mathrm{min}^{-1}\,n_{metal}^{-1}$ and Pd/Si, PdAu/CeO_2-SBA15 and PdAu/Ti-SBA15 $k_d \sim$ 18-20 $l\,\mathrm{min}^{-1}\,n_{metal}^{-1}$. For sake of clarity, one representative catalyst per group is depicted in Figure 5. A good linear relationship was obtained, confirming that the disproportionation is a first order reaction with respect to H_2O_2. Calculated rates are close to the values reported by Moreno et al.[18] (3.5 $l\,\mathrm{min}^{-1}\,n_{metal}^{-1}$) and Lunsford et al.[48] (53 $l\,\mathrm{min}^{-1}\,n_{metal}^{-1}$), though in these papers different reactors and reaction conditions were adopted. Modifying the SBA15 support with Ti and CeO_2 resulted in an enhancement (approx. x 5) of the disproportionation rate with respect to the unmodified catalysts (PdAu/SBA15). This enhancement could be responsible for the decreased selectivity and productivity observed for these catalysts (Table 1). Modification with Al doubled the disproportionation rate but also enhanced the peroxide productivity (Table 1), suggesting that the direct formation of H_2O and H_2O_2 hydrogenation were successfully decreased by the Al (modifier), likely due to the increased Brønsted acidity[31]. The PdAu/Si catalyst had the lowest disproportionation rate, but also the lowest selectivity, which implies a high hydrogenation and water production activity.

7. Conclusions

Pd and PdAu catalysts supported on mesoporous ordered SBA15 and doped M-SBA15 (M = Al, Ti and CeO_2) were synthesized. All samples were tested for the direct synthesis and disproportionation of hydrogen peroxide. A good metal dispersion was achieved using SBA15 as support, with the majority of the metal nanoparticles in the range 5-7 nm. TEM images also confirmed that both the support structure and the metal nanoparticles size were almost unchanged before and after the reaction, revealing the stability of these catalysts at experimental conditions. Two techniques were applied for the incorporation of bromine onto the catalyst surface. Grafting of the metal containing catalysts and grafting the support before the deposition of active metal, respectively.

A synergetic effect between Pd and Au was observed when comparing mono- and bimetallic SBA15-based catalysts, both grafted and unmodified. However, the selectivity decreased when bromine was incorporated in the catalysts. Possibly the introduction of relatively bulky bromoalkyl–species caused the blocking/poisoning of the catalyst, especially when performed on the support before the active metal deposition. Ordered mesoporous SBA15 catalysts were compared to unordered SiO_2 based catalysts under identical experimental conditions. The performance of the latter catalysts was inferior compared to the SBA15-based ones, confirming the advantage of using an ordered mesoporous support. The catalyst showing the best performance (PdAu/SBA15) was modified to gain more surface acidity. Higher productivity and slightly higher selectivity were achieved incorporating Al into the framework, whereas the other modifiers (i.e. Ti and CeO_2) did not improve H_2O_2 productivity. The improved performance of the PdAu/Al-SBA15 catalysts were attributed to the increased number of Brønsted acid sites including Al into the support framework. Modification of this catalyst with bromine was confirmed to impair both productivity and

selectivity, possibly due to the broader particle size distribution and the poor stability of the metal nanoparticles.

After complete H_2 conversion, the disproportionation reaction was also investigated. Assuming a first order reaction rate, disproportionation kinetic constants were calculated from the experimental data. The values calculated were in the range of 4-20 $l\,\mathrm{min}^{-1}\,n_{metal}^{-1}$. It was apparent that this reaction had a remarkably slower time scale compared to the H_2O_2 formation, suggesting that the peroxide destruction mainly occurs upon the hydrogenation step, regardless of the support and the active metal content of the catalyst.

Acknowledgments: N. Gemo gratefully acknowledges the Cariparo Foundation and the Johan Gadolin Scholarship for financial support. P. Biasigratefully acknowledges the Otto A. Malm Foundation for financial support. F. Menegazzo thanks INSTM (Florence) for postdoctoral fellowship. This work is part of the activities at the Åbo Akademi Process Chemistry Centre (PCC) within the Finnish Centre of Excellence Programmes (2000–2005 and 2006–2011) by the Academy of Finland. In Sweden, the Bio4Energy programme and Kempe Foundations are acknowledged.

References

[1] Blanco-Brieva G, Capel-Sanchez M, de Frutos MP, Padilla-Polo A, Campos-Martin J, Fierro JLG (2008) Industrial and Engineering Chemistry Research 47:8011-8015.

[2] Metzger J (2012) Sustainable Industrial Chemistry - Principles, Tools and Industrial Examples. By F. Cavani, G. Centi, S. Perathoner, F. Trifiró. Chemie Ingenieur Technik 84:764-764.

[3] Campos-Martin JM, Blanco-Brieva G, Fierro JLG (2006) Angewandte Chemie International Edition 45:6962-6984.

[4] Samanta C (2008) Applied Catalysis A: General 350:133-149.

[5] G. Centi, S. Perathoner and S. Abate, in: Modern Heterogeneous Oxidation CatalysisAnonymous (Wiley-VCH Verlag GmbH & Co. KGaA, 2009).

[6] Ntainjua N. E, Edwards JK, Carley AF, Lopez-Sanchez JA, Moulijn JA, Herzing AA, Kiely CJ, Hutchings GJ (2008) Green Chemistry 10:1162-1169.

[7] Menegazzo F, Signoretto M, Manzoli M, Boccuzzi F, Cruciani G, Pinna F, Strukul G (2009) Journal of Catalysis 268:122-130.

[8] Li G, Edwards J, Carley AF, Hutchings GJ (2007) Catalysis Communications 8:247-250.

[9] Biasi P, Menegazzo F, Pinna F, Eränen K, Canu P, Salmi TO (2010) Industrial and Engineering Chemistry Research 49:10627-10632.

[10] Biasi P, Menegazzo F, Pinna F, Eränen K, Salmi TO, Canu P (2011) Chemical Engineering Journal 176-177:172-177.

[11] Menegazzo F, Signoretto M, Frison G, Pinna F, Strukul G, Manzoli M, Boccuzzi F (2012) Journal of Catalysis 290:143-150.

[12] Samanta C, Choudhary VR (2007) Applied Catalysis A: General 330:23-32.

[13] Abate S, Centi G, Melada S, Perathoner S, Pinna F, Strukul G (2005) Catalysis Today 104:323-328.

[14] Moreno T, García-Serna J, Cocero MJ (2010) Green Chemistry 12:282-289.

[15] Lunsford JH (2003) Journal of Catalysis 216:455-460.

[16] Voloshin Y, Halder R, Lawal A (2007) Catalysis Today 125:40-47.

[17] Deguchi T, Iwamoto M (2011) Journal of Catalysis 280:239-246.

[18] Moreno T, García-Serna J, Cocero MJ (2011) Journal of Supercritical Fluids 57:227-235.

[19] Inoue T, Schmidt MA, Jensen KF (2007) Industrial and Engineering Chemistry Research 46:1153-1160.

[20] Menegazzo F, Burti P, Signoretto M, Manzoli M, Vankova S, Boccuzzi F, Pinna F, Strukul G (2008) Journal of Catalysis 257:369-381.

[21] Gemo N, Biasi P, Canu P, Salmi TO (2012) Chemical Engineering Journal 207–208:539-551.

[22] Choudhary VR, Samanta C (2006) Journal of Catalysis 238:28-38.

[23] Biasi P, Gemo N, Hernández Carucci JR, Eränen K, Canu P, Salmi TO (2012) Industrial and Engineering Chemistry Research 51:8903-8912.

[24] Moreno T, García-Serna J, Plucinski P, Sánchez-Montero MJ, Cocero MJ (2010) Applied Catalysis A: General 386:28-33.

[25] Chinta S, Lunsford JH (2004) Journal of Catalysis 225:249-255.

[26] Landon P, Collier PJ, Carley AF, Chadwick D, Papworth AJ, Burrows A, Kiely CJ, Hutchings GJ (2003) Physical Chemistry Chemical Physics 5:1917-1923.

[27] Edwards JK, Carley AF, Herzing AA, Kiely CJ, Hutchings GJ (2008) Faraday Discussions 138:225-239.

[28] Abate S, Perathoner S, Centi G (2012) Catalysis Today 179:170-177.

[29] Abate S, Lanzafame P, Perathoner S, Centi G (2011) Catalysis Today 169:167-174.

[30] Ghedini E, Menegazzo F, Signoretto M, Manzoli M, Pinna F, Strukul G (2010) Journal of Catalysis 273:266-273.

[31] Park S, Lee J, Song JH, Kim TJ, Chung Y, Oh S, Song IK (2012) Journal of Molecular Catalysis A: Chemical 363–364:230-236.

[32] Han Y, Lunsford JH (2005) Journal of Catalysis 230:313-316.

[33] Samanta C, Choudhary VR (2007) Catalysis Communications 8:73-79.

[34] Melada S, Rioda R, Menegazzo F, Pinna F, Strukul G (2006) Journal of Catalysis 239:422-430.

[35] Choudhary VR, Samanta C, Gaikwad AG (2004) Chemical Communications:2054-2055.

[36] Zhao D, Huo Q, Feng J, Chmelka BF, Stucky GD (1998) Journal of the American Chemical Society 120:6024-6036.

[37] Piqueras CM, García-Serna J, Cocero MJ (2011) Journal of Supercritical Fluids 56:33-40.

[38] Gemo N, Biasi P, Salmi TO, Canu P (2012) The Journal of Chemical Thermodynamics 54:1-9.

[39] Lopez-Castillo Z, Aki SNVK, Stadtherr MA, Brennecke JF (2008) Industrial and Engineering Chemistry Research 47:570-576.

[40] Xie X, Brown JS, Bush D, Eckert CA (2005) Journal of Chemical & Engineering Data 50:780-783.

[41] Emeis CA (1993) Journal of Catalysis 141:347-354.

[42] Lee H, Kim S, Lee D, Lee K (2011) Catalysis Communications 12:968-971.

[43] Koekkoek AJJ, van Veen JAR, Gerrtisen PB, Giltay P, Magusin PCMM, Hensen EJM (2012) Microporous and Mesoporous Materials 151:34-43.

[44] Akondi AM, Trivedi R, Sreedhar B, Kantam ML, Bhargava S (2012) Catalysis Today 198:35-44.

[45] Timofeeva MN, Jhung SH, Hwang YK, Kim DK, Panchenko VN, Melgunov MS, Chesalov YA, Chang J- (2007) Applied Catalysis A: General 317:1-10.

[46] Chen S, Tang C, Lee J, Jang L, Tatsumi T, Cheng S (2011) Journal of Materials Chemistry 21:2255-2265.

[47] Trukhan NN, Romannikov VN, Shmakov AN, Vanina MP, Paukshtis EA, Bukhtiyarov VI, Kriventsov VV, Danilov IY, Kholdeeva OA (2003) Microporous and Mesoporous Materials 59:73-84.

[48] Liu Q, Lunsford JH (2006) Journal of Catalysis 239:237-243.